Permeability, Resistivity and Strength of Fouled Railroad Ballast

By: AJ Rahman

B.S., University of Kansas, Lawrence, Spring 2013

Submitted to the Department of Civil, Environmental, and Architectural Engineering and the Graduate Faculty of the University of Kansas in partial fulfillment of the requirements for the degree of Master of Science

_____

Chairperson Dr. Robert L. Parsons

Committee members

_____

Dr. Jie Han

_____

Dr. Thomas Glavinich

The Thesis Committee for AJ Rahman certifies that this is the approved version of the following thesis:

Permeability, Resistivity and Strength of Fouled Railroad Ballast

Date approved: 5/7/2013

_____

Chairperson Dr. Robert L. Parsons

Table of Contents

List of Figures

List of Tables

List of Abbreviations

Ground Penetrating Radar (GPR)

Liquid Limit (LL)

Mid-America Transportation Center (MATC)

Percentage Void Contamination (PVC)

Time Domain Reflectometry (TDR)

Acknowledgments

The author thanks the Mid-America Transportation Center (MATC) for providing financial support for the research described in this report, and Mr. Hank Lees of BNSF for providing material and technical support for this research. We also thank the many individuals who contributed to the completion of this research, including, Mr. Johnathon Crank, Miss. Jennifer Penfield, Mr. Jitendra Thakur, Mr. Deep Khatri, Mr. Raju Acharya and especially Mr. Jim Weaver and Mr. Matthew Maksimowicz for their help in with the physical testing.

Abstract

Ballasted tracks are the most common tracks used in the railroad industry and are designed to provide a stable, safe, and efficient rail foundation. A ballasted track consists of superstructure (ties, fasteners, and rails) and substructure (ballast, sub-ballast, and subgrade layers). The main functions of ballast are to support the superstructure by distributing the loads from the moving train, and to provide lateral resistance to tie movement and drainage. However, ballast deterioration and fouling are major issues in the railroad industry, and can be caused by repeated loadings, which lead to crushing ballast that is in contact with ties. Upward migration of subgrade particles into the ballast layer can increase fouling in the ballast and decrease drainage through the ballast layer. There is a need for methods to easily and inexpensively identify areas that have fouled ballast. The objective of this preliminary study was to evaluate the potential for estimating the level of fouling in a ballast layer by soil resistivity and permeability tests to be followed by a second study. A test box was designed and fabricated at the lab at the University of Kansas to perform the constant head permeability test and soil resistivity tests. Constant head tests were conducted to determine the coefficient of permeability of fouled ballast for different fouling percentages. Soil resistivity tests were also conducted using the Wenner method (4 points method) to determine the resistivity of ballast for different fouling ratios. The tests showed a relationship between the fouling ratio and ballast resistivity. The resistance of the ballast layer decreased as the fouling ratio increased due to the presence of water. Fouled material retained water and filled the voids between the ballast particles, and therefore decreased resistivity in the ballast layer. The permeability (hydraulic conductivity) also decreased as the fouling ratio increased due to the presence of fine particles between the ballast particles; therefore, permeability and resistivity were also correlated. The strength properties of clean and fouled

ballast were also evaluated using large direct shear box and modified direct shear box (extension in height for the large direct shear box). Three type of fouling materials were tested (crushed ballast fines, clay and coal dust) at different fouling ratios by dry weight of ballast. Test results showed that as fouling ratio increased, strength of ballast decreased for both set of tests (large direct shear and modified direct shear). Moreover, samples fouled with coal dust with more than 10% showed a significant decrease in strength properties. Also, samples fouled with clay showed a significant strength reduction at about 40% fouling. A large scale sample of heavily fouled ballast was constructed and tested under wet conditions. The four point Wenner method was used to measure resistivity at depths of eighteen inches, twelve inches and six inches. The results show that as the depth increased, resistivity increased. The higher resistivites at greater depths were interpreted to be representative of drier material, while the near suface material had a lower resistivity due to the addition of water to the surface.

Chapter 1 Introduction

A rail track structure is designed to provide a stable, safe, and efficient path for trains to operate at high speeds while transporting substantial loads. Ballasted track is the most common type of rail structure used throughout the world due to its relatively low cost of construction and maintenance (Indraratna 2006). A ballasted track system usually consists of a superstructure (ties, fasteners and rails), and substructure (ballast, sub-ballast and subgrade layers, (Indraratna 2011). Ballast consists of uniformly graded coarse aggregate placed between the cross ties and subgrade (Huang 2009). The main functions of railroad ballast are to support the superstructure by distributing the loads from the moving train to provide lateral resistance, and to facilitate drainage. The physical properties of high quality ballast can be classified by its angularity of particles, high toughness, high resistance to weathering, rough surface, high specific gravity, and shear strength (Huang 2009).

Ballast deterioration and fouling are major issues in the railroad industry, and can be caused from repeated dynamic loading, vibration, temperature, and the presence of water. Fouling is caused by breakage of the ballast aggregate, spillage of coal dust from moving trains, and the migration of subgrade particles. As the fouling ratio in the ballast and sub-ballast layers increases, more water is retained by the fouled layers, resulting in track instability due to the buildup of pore water pressure, as well as alignment problems. Detection of the fouling ratio in ballast has been a challenging task for maintenance units, especially if the drainage capacity varies significantly beneath the track with location. Track maintenance divisions need to have a system for scheduling maintenance when needed in order to maintain safe operation and traffic flow.

The objective of this study was to obtain a proper understanding of the fouling of ballast caused by various types of fines, and its implications on track drainage, which can affect track maintenance operations. Additionally, this study sought to determine the feasibility of evaluating the fouling ratio in railroad ballast by measuring the resistivity in the ballast and sub-ballast layer and finding a correlation between ballast permeability and resistivity. Also, determine the strength properties of fouled ballast at different fouling ratios. Tests included three main sources of fouling: internal ballast crushing, fine particles migrating from subgrade and coal dust. A relationship between the resistivity of ballast and fouling ratio was observed.

Chapter 2 Literature Review

2.1 Effects of Fouled Ballast

As ballast ages, it becomes progressively fouled with fine material filling the voids between coarse particles. Several research studies report that around 70% of fouling material results from ballast aggregate breakage (Huang 2009). Selig and Waters showed that about 76% of ballast fouling is caused by ballast breakdown, 13% by infiltration from sub-ballast, 7% by infiltration from the ballast surface, 3% from subgrade intrusion, and 1% is related to tie wear (Selig 1994).

Raymond reported that the liquid limit (LL) of fine particles in the ballast layer should be less than 35 to function as a drainable layer; also showing that aggregate breakdown is mainly influenced by the physical properties of the mineral aggregate (Raymond 1978).

According to (Indraratna 2011), under saturated conditions water and fine particles mix to form slurry and will migrate to the sub-ballast and ballast layer. This migration can fill voids within coarse aggregates and decrease drainage, which may lead to ballast degradation and may cause serviceability problems with the superstructure. Ballast is designed to be a free drainage material with particle sizes ranging from 0.5 to 2.5 inches; however, the infiltration of fouling material reduces the void spaces and restricts drainage. Specifications for the gradation of ballast require a uniform gradation with a uniformity coefficient between 1.5 and 3. Fouling materials can have variable specific gravity, void ratio, and gradation, which will result in changing the characteristics of the ballast layer (Huang 2009). In a study conducted by Wallace, an increase in the percentage of fines resulted in a decrease in hydraulic conductivity and decreased the drainage capacity of ballast; the results of the study showed that sand did not impact the

permeability of ballast significantly; however, clay and silt caused a significant reduction on permeability of ballast (Wallace 2003). When ballast is not functioning correctly the strength of the track structure may be inadequate and thus track stability may become compromised. The ballast particles must resist the vertical forces applied on the track and provide lateral stability, and the load is transferred by the inter-particle contact between adjacent ballast particles. However, fouling material fills up the voids between particles which can reduce strength and hydraulic conductivity of the ballast layer. The fouling material can reduce the friction angle at inter-particle contact points which reduces the strength and can cause instability of track structure. Furthermore, past studies on the effects of fouled ballast on drainage showed that drainage is significantly reduced when the fouling index is 30 or greater. The author suggested using new technologies to evaluate the ballast condition to reduce the risk of sudden failure (Sussmann 2012).

Moreover, a study conducted by Chiang showed that ballast settlement increased with the percentage fouling in ballast (Chiang 1989). Han and Selig conducted a similar study where the results showed that the degree of ballast fouling had a significant impact on ballast settlement (Han 1997). A study was presented by the University of Illinois with an assessment of the effects of different fouling agents on railroad ballast strength. A set of strength tests using the large direct shear box was conducted to investigate the strength of clean and fouled ballast by different agents at various level of fouling. The shear strength properties were related to field ballast fouling levels to better understand the impact of fouling on track stability. Results of large direct shear tests showed a trend of decreasing strength with samples fouled with 32% clay and 40% of mineral filler. Coal dust was particularly problematic with concentrations of more than 15 percent causing a significant reduction in strength (Huang 2009).

2.2 Soil Resistivity

Resistance is the ratio of applied voltage to the resulting current flow. Resistivity is the resistance of a conductor, which depends on its atomic structure and behavior of the material. The commonly used symbol for resistivity is ρ, and is usually measured in ohm-cm. the resistivity is defined by the following relationship:

$$\rho = (R \times A)/L \qquad (2.1)$$

where,

R is resistance in ohms,

A is cross section area in $cm,^2$

and L is length of conductor in cm.

A material with high resistivity is considered to be a bad conductor. Sand, loam, and crushed stone aggregate have high resistance and are considered to be bad conductors. However, when water is present, the resistivity decreases and the soil or aggregate will become a conductor, though still considered to be a poor conductor compared to metals. The resistivity of soil will be governed by the quantity of water held in the soil. In other words, conductivity of the soil would be a function of the water retained within the soil.

The main factors which determine resistivity are (Tagg 1964):

1- Type of soil

2- Chemical composition of salts dissolved in the contained water

3- Moisture content

4- Temperature

5- Grain size of the material and distribution of grain size

6- Closeness of packing and pressure

Table 2.1 Typical resistivity values of some soils (Tagg 1964)

Type of Soil	**Resistivity in ohm-cm**
Loams, garden soil	500 - 5000
Clays	800 – 5000
Clay, sand and gravel mixtures	4000 - 25,000
Sand and gravel	6000 - 10,000
Slates, shale, sandstone	1000 - 50,000
Crystalline rocks	20,000 - 1,000,000

There are several types of soil resistivity measurements that can be used in the field and also for laboratory testing (soil box testing). According to Tagg, the Wenner-four probe (point) method is considered to be the most accurate method, although 2 point and 3 point methods may also be used. The configuration of the Wenner-four probe method consists of four probes placed at equal distances from each other. A current is sent through the two outer electrodes (probes) and the voltage is measured between the two inner probes (Tagg 1964). The soil resistance is determined using Ohm's law, R = V/I. The following formula is used to determine soil resistivity in accordance with the Wenner-four probe method:

$$\rho = 2\pi \times R \times D \qquad (2.2)$$

where,

R= resistance in ohms and D = Distance between probes in cm (AEMC 2012).

Two other soil resistivity measurement methods which can be used to determine the soil resistivity using AEMC equipment are the two point method and three point method. The two point method measures the resistance between two points. The 3 point method (Fall-of-Potential) is used to measure resistance to ground of auxiliary electrodes and grids. The measurement of ground resistance can only be obtained with specially designed test equipment. Most equipment uses the Fall-of-Potential voltage of alternating current circulating around auxiliary electrodes and a ground electrode under test (AEMC 2012).

(Siddiqui 2012) presented correlations of electrical resistivity with soil strength properties such as internal angle of friction. The study was conducted using field electrical resistivity survey and laboratory electrical resistivity measurements. Electrical resistivity measurements were retrieved from boreholes in the field and samples were obtained from the field at different depths were tested in laboratory. Several laboratory tests were conducted on the field samples such as moisture content, unit weight, direct shear and electrical resistivity. Field data and laboratory data were analyzed and results showed strong correlation between electrical resistivity and angle of internal friction. According to the author, as the angle of internal friction increases, electrical resistivity increases (Siddiqui 2012).

2.3 Railroad Ballast Fouling Detection

In order to evaluate the need for maintenance to assure continued safe operations and to prevent any structure instability or drainage problems, several methods have been introduced to evaluate the percentage fouling of ballast. Selig and Waters proposed two methods to quantify the level of ballast fouling. The first method is the fouling index, which is the sum of the percent by weight of the ballast sample passing the 4.75 mm sieve plus the percent passing the 0.075 mm sieve. The second method is the fouling ratio, which is the ratio of the dry weight of the material passing the 9.5 mm sieve to the dry weight of total sample (Selig 1994). Feldman and Nissen developed the percentage void contamination (PVC) parameter to show the effect of void decrease in ballast as the ratio between the total volume of re-compacted fouling material (passing the 9.5 mm sieve) and the void volume between re-compacted ballast aggregates. This method determines the percentage of voids occupied by fouling material, but the gradation of fouling particles cannot be taken into account (Han 1997). Another method proposed by Indraratna is called relative ballast fouling ratio. It is a ratio between the solid volumes of fouling particles passing a 9.5 mm sieve and ballast particles being retained on a 9.5 mm sieve (Tagg 1964).

Traditionally, a destructive drilling method is used to evaluate the condition of ballast; however, this method is time consuming (Han 1997). Ground penetrating radar (GPR) has been used in the past for ballast evaluation. According to (Roberts and Rudy 2006), GPR has been utilized as a non-disturbing evaluation tool to evaluate railroad ballast and fouling level. GPR data is obtained on railroad ballast using 2 GHz horn antennas, and provides data that show significant energy scattering from the void space in the clean ballast. The data from fouled ballast produce less scattering energy due to fewer void spaces in ballast layer (Han 1997). The

GPR method has proven to be applicable for determining the percentage fouling in the ballast and sub-ballast layer; however, more data and ground properties are required to evaluate the limitations of this methodology (Han 1997). GPR is effective, according to many previous studies, for evaluating ballast conditions. According to Leng and Al Qadi, there are limitations that may result in undetected fouling (AEMC 2012). First, the dielectric constant of the railroad ballast is unknown in many evaluation cases. Another limitation with the GPR method is that the signal reflection can only detect an interface where there is a significant difference in dielectric contrast properties, even though the gradation of ballast changes with depth and there may not be a clear interface between fouled and clean ballast. Therefore, GPR may not be able to detect fouled ballast under certain conditions, which may lead to unreliable results (AEMC 2012).

Moreover, as the fouling level increases in a ballast layer, the reflection becomes less defined and data will be difficult to interpret. Overall, GPR studies illustrate the difficulty of data interpretation and the data are sensitive to the water content in fouled ballast (Ebrahimi 2008).

Another study conducted by (Ebrahimi 2008) contained adscription of a method for detecting and quantifying the fouling content by electromagnetic surveys and visual observation through boreholes. A small scale study was conducted using time domain reflectometry (TDR) to evaluate the change of electromagnetic parameters in detecting fouling content. The study focused on characterizing the EM parameters of two main sources of fouled ballast, deteriorated ballast and coal dust, using the TDR methodology to assess the percentage fouling and moisture content. The test results showed that an increase in water content of the fouling material from 5 to 10% increased the electrical conductivity of ballast from 10 to 24mS/m. Ebrahimi's study also showed that the fouling content and water content increased the plastic deformation of the track (Ebrahimi 2008).

(Anbazhagan 2011) attempted to identify ballast fouling in the field using a multichannel analysis of subsurface wave (MASW) on a model track and a field track. The tests were performed on clean and fouled ballast and track subsurface. Results of the study show that shear wave velocity (SWV) increases when fouling increases until it reaches a maximum level before decreasing. He observed that SWV reached a maximum at 15% fouling with coal dust and 25% fouling with clay. Fouled ballast with coal dust reaches the critical fouling point before clayey sand fouled ballast. Since fouling of ballast reduces the drainage, a plot of permeability and SWV with fouling ratios shows that for fouling percentages above the critical fouling point, drainage capacity decreases significantly below acceptable limits (Anbazhagan 2011).

Chapter 3 Material Testing

This chapter contains descriptions of the railroad ballast, crushed ballast, clay and coal dust, and the methods used to characterize them. The proposed tests ensure that the material meet the requirements to be used in the field.

3.1 Material

The railroad ballast material was provided by BNSF and was excavated from track undergoing maintenance in Gardner, Kansas. The coal dust was also provided by BNSF from undercut material from line milepost 61.This material was characterized during a previous project (Jowkar 2013). Several tests were conducted to determine the properties of ballast, crushed ballast, clay and coal dust in the soils lab at the University of Kansas.

3.1.1 Gradation of Ballast

The ballast coarse aggregates were separated by conducting a sieve analysis test, where the distribution of particle size was determined. Ballast aggregates were sieved with a sieve shaker provided by BNSF, as shown in figure 3.1. Separation was achieved from retained particles of different sieve sizes starting at 2.5 in. opening and ending at 0.5. in. The results of this test were plotted on a graph as shown in figure 3.2, and the following parameters were determined: the maximum size, minimum size, coefficient of curvature, and coefficient of uniformity of ballast aggregates. The results were used to determine compliance of the particle size distribution with applicable specifications requirements provided by BNSF (table 3.1).

Figure 3.1 Sieve shaker (Jowkar 2013)

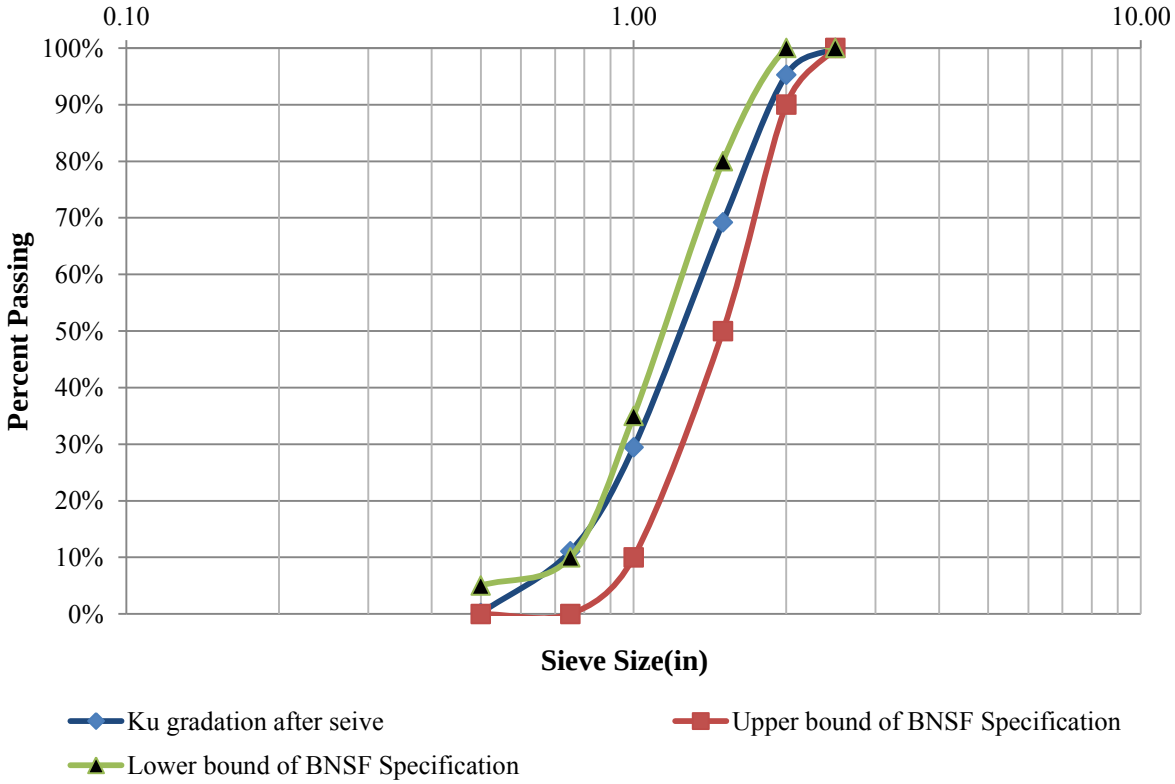

Figure 3.2 Gradation curves of the ballast aggregates (Jowkar 2013)

Table 3.1 BNSF specification limits class 1 (Jowkar 2013)

Sieve Analysis (ASTM C 136)	
Sieve Size	**BNSF Specification Limits (Class 1)**
2.5"	100
2"	90-100
1.5"	50-80
1"	10-35
0.75"	0-10
0.5”	0-5

3.1.2 Gradation of Crushed Ballast Fines

The ballast fine aggregates were separated by sieve analysis, where the distribution of particle size was determined by sieving. This test separated the particles by their size. Separation was achieved for retained particles of different sieve sizes starting at 4.75 mm opening and ending at 0.075 mm, in accordance with ASTM D5444-08. The results of this test are plotted in figure 3.3. The maximum size, mean size, coefficient of curvature, and coefficient of uniformity of crushed ballast particles were found to be 9.5 mm, 1.7 mm, 0.959, and 7.19, respectively.

Table 3.2 Gradation data for crushed ballast fines

Sieve No.	Size Opening (mm)	Mass Clean Sieve, Ms (g)	Mass Sieve and Soil, Mss (g)	Mass Retained, Mn (g)	% of mass retained	Cumulative % Retained	% Finer
4	4.75	498.77	734.87	236.1	18.4	18.4	**81.6**
8	2.36	477.94	736.24	258.3	20.1	38.5	**61.5**
16	1.18	442	726.56	284.56	22.1	60.6	**39.4**
30	0.6	400.56	626.53	225.97	17.6	78.2	**21.8**
50	0.3	368.33	533.3	164.97	12.8	91.0	**9.0**
100	0.15	341	411.8	70.8	5.5	96.6	**3.4**
200	0.075	326.24	352.4	26.16	2.0	98.6	**1.4**
Pan		496.07	512.87	16.8	1.4	100.0	**0.0**

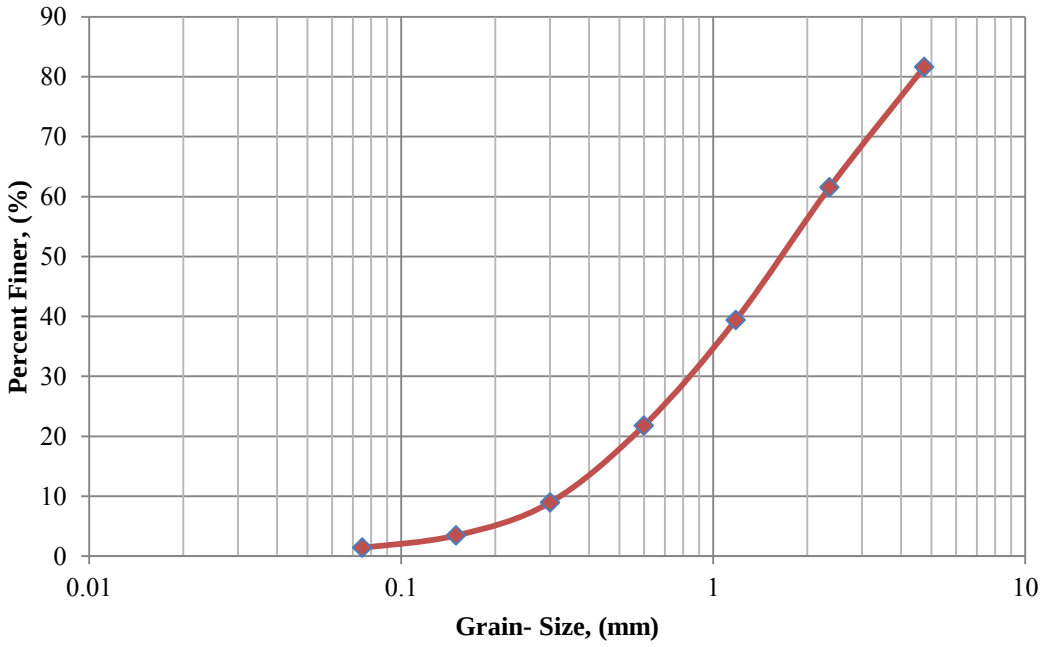

Figure 3.3 Gradation curve of the crushed ballast fines

3.1.3 Gradation of Clay

The grain size distribution of the clay used as fouling material was determined by hydrometer analysis in accordance with ASTM D22.2703-1. The grain size distribution chart of the clay is shown in figure 3.4.

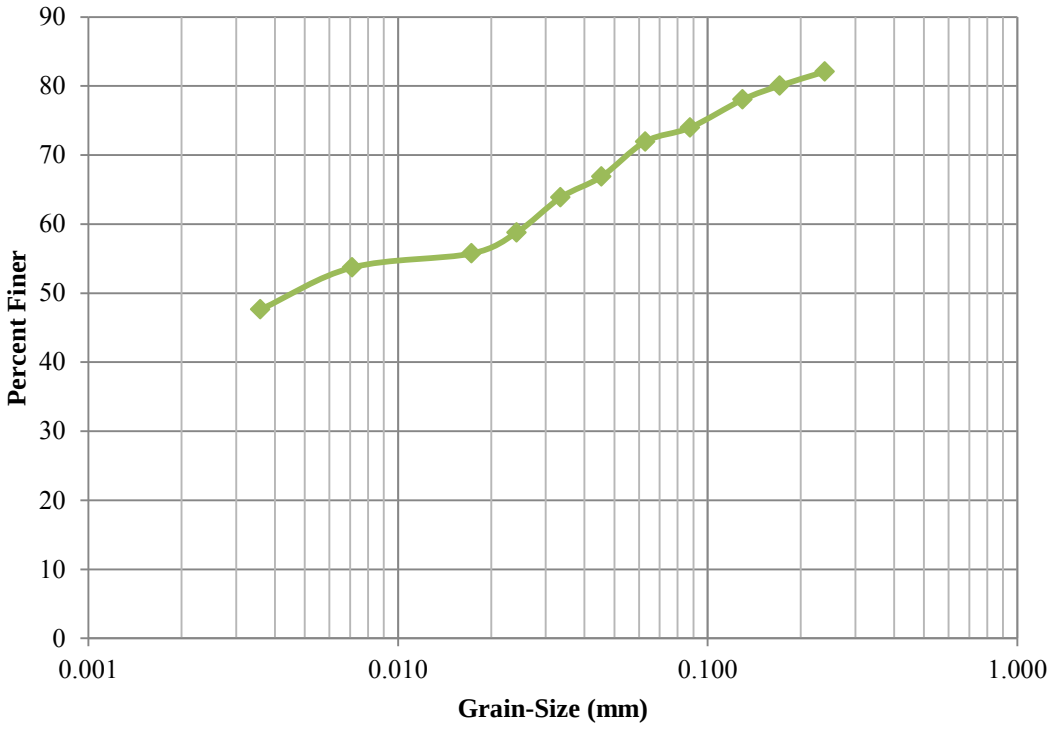

Figure 3.4 Gradation curve of clay

3.1.4 Gradation of Coal Dust

The grain size distribution of the coal dust used as fouling material was determined by sieve analysis in accordance with ASTM D22.2703-1. The grain size distribution chart of the coal dust is shown in figure 3.5.

Table 3.3 Gradation data for coal dust

Sieve No.	Size Opening (mm)	Mass Clean Sieve, Ms (g)	Mass Sieve and Soil, Mss (g)	Mass Retained, Mn (g)	% of mass retained	Cumulative % Retained	% Finer
4	4.75	498	502	4	0.48	0.5	**99.5**
8	2.36	478	534	56	6.71	7.2	**92.8**
16	1.18	442	696	254	30.4	37.6	**62.4**
30	0.6	414	628	214	25.6	63.3	**36.7**
50	0.3	364	512	148	17.7	81.1	**18.9**
100	0.15	340	420	80	9.60	90.6	**9.4**
200	0.075	322	360	38	4.56	95.2	**4.8**
Pan		354	394	40	4.80	100.0	**0.0**

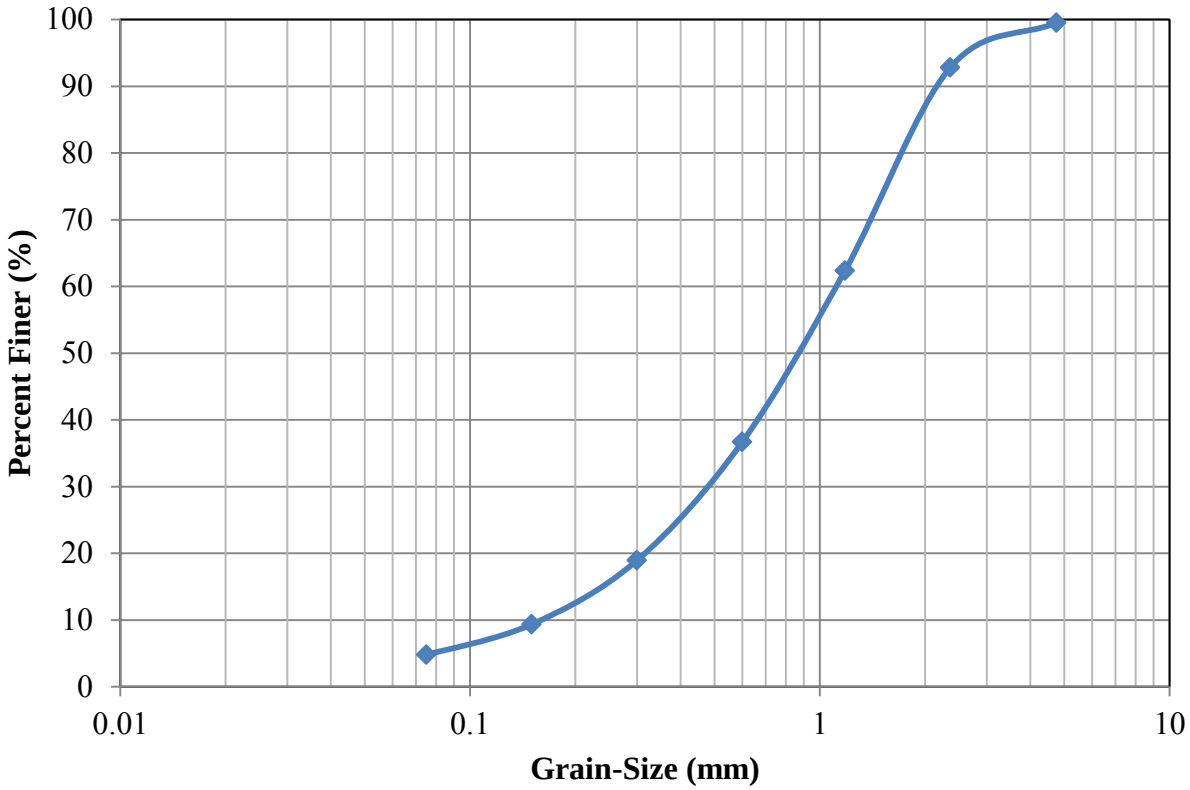

Figure 3.5 Gradation curve of coal dust

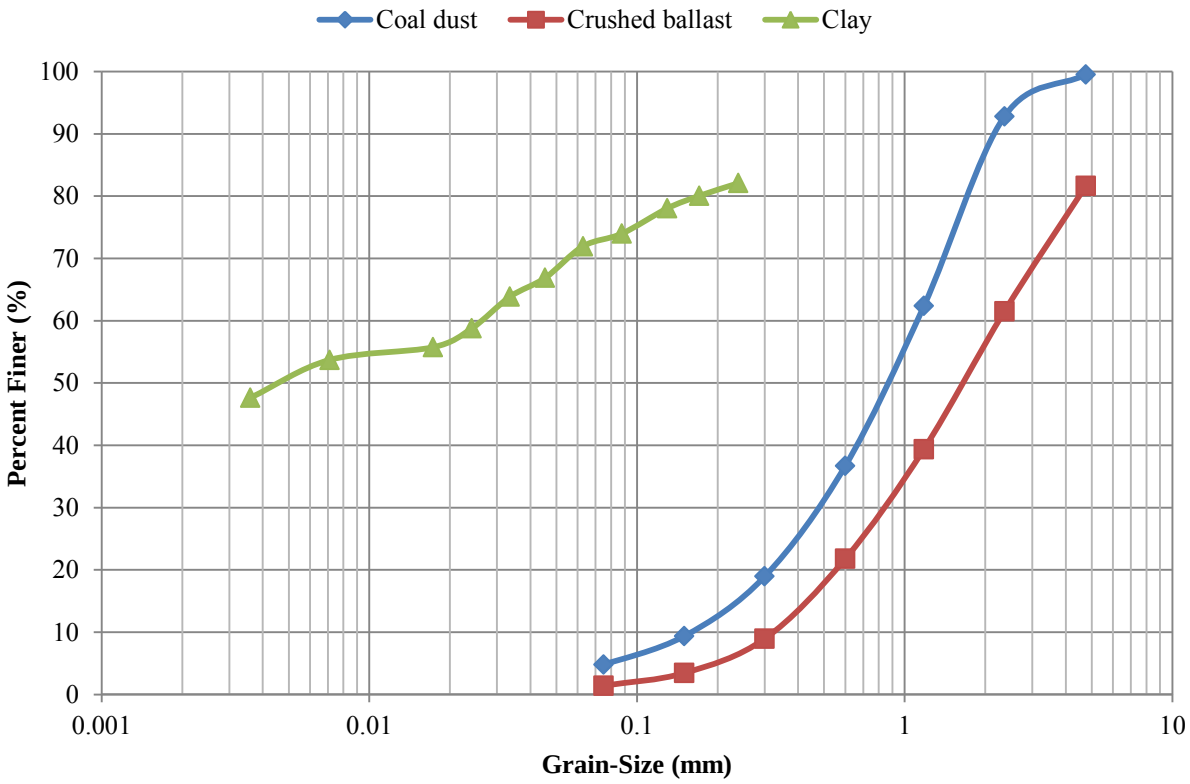

Figure 3.6 Comparison of gradation curves for fouling materials

3.1.5 Specific Gravity and Absorption of Ballast Coarse Aggregates

This test method determines the average density of a quantity of coarse aggregate particles, the specific gravity, and the absorption of coarse aggregates. A sample of aggregates is immersed in water for 24 hours to essentially fill the pores. Then the sample is weighed after it is removed from the water and the surfaces of the particles are towel dried. Next, the sample is submerged in water and weighed. Finally, the sample is oven-dried and weighed for final dry mass. Using the mass values and the formulas provided by the test method will result in obtaining the specific gravity and absorption of the aggregate. This test method was performed in accordance with ASTM C127. Pictures of the test are shown in figures 3.7 through 3.9. Specific gravity was used in calculating void content of aggregates and volume weight conversion. Table 3.4 shows the specific gravity of the ballast coarse aggregates.

Figure 3.7 Ballast aggregates immersed in water

Figure 3.8 Ballast aggregates in SSD condition

Figure 3.9 Wire basket and scale used to measure weight of aggregates when submerged in water

Table 3.4 Specific gravities of ballast coarse aggregates

Bulk Specific Gravity	2.72
SSD Bulk Specific Gravity	2.74
Apparent Specific Gravity	2.76
Absorption	0.54%

3.1.6 Specific Gravity of Crushed Ballast Aggregates

The specific gravity of crushed ballast was determined by the specific gravity of soil solids by water pycnometer test in accordance with ASTM D854-06. The specific gravity was determined to be 2.61.

3.1.7 Specific Gravity of Clay

The specific gravity of the clay was determined using the specific gravity of soil solids by water pycnometer test, in accordance with ASTM D854-06. The specific gravity was determined to be 2.74.

3.2 Summary

The properties of the ballast and fouling materials are shown in tables 3.5 and 3.6.

Table 3.5 Properties of fouling materials

Fouling Material	LL (%)	PL (%)	Specific Gravity	Passing No. 200 Sieve (%)
Crushed Ballast	NA	NA	2.61	1.4
Clay	52	31	2.74	73
Coal Dust	NA	NA	1.54	4.8

Table 3.6 Summary of grain size characteristics of ballast and fouling material

	D_{50} (mm)	D_{max} (mm)	Cc	Cu
Ballast	33	63.5	0.89	2
Crushed Ballast	1.7	9.5	0.959	7.19
Clay	0.075	0.1	NA	NA
Coal Dust	1.2	4.75	1.14	7.35

Chapter 4 Test Setup and Instrumentation

This section includes descriptions of the test setups used for examining the permeability, resistivity and strength of fouled ballast. Three sets of tests were performed; one using crushed ballast as the fouling material, one using clay, and one using coal dust. Different masses of each material added to the ballast during each set of tests.

4.1 Permeability and Resistivity Test Setup and Instrumentation

For each fouling material four tests were conducted to examine the permeability and resistivity at different fouling levels. Constant head permeability tests were conducted in a test box designed for that purpose to determine the hydraulic conductivity of the sample. The same sample was then tested for resistivity with respect to time using a resistivity meter in accordance with the Wenner 4 point method. The box was designed and fabricated at the geotechnical laboratory at the KU Civil, Environmental, and Architectural Engineering (CEAE) Department. The outside dimensions of the box were 42 in. x 29 in. x 28 in. and the inside dimensions were 39 in. x 26 in. x 22 in.. Two layers of plastic support were placed at the bottom of the box and wrapped with fiberglass screen to prevent fines from going through, as shown in figure 4.1.1. The height of a typical sample was approximately 12 in.. The front of the box was cut and replaced with a clear glass wall to permit visual observation, as shown in figures 4.1.2 and 4.1.3. A 2 in. pipe and valve were installed at the bottom of the box, which were used to fill the box with water and drain water out after the test. A 2 in. pipe was also installed at the back side of the box near the top to allow a constant water outflow. A 1 in. diameter plastic standpipe was also clamped and suspended freely beneath the fiberglass screen, used to measure the water level in the box during a test. Two sheets of aluminum were attached to the side walls of the box and two copper rods were held by clamps at equal distances of 13 in. from the side wall of the box, as

shown in figure 4.1.4. The soil resistivity meter measured the resistivity within the sample by connecting all four electrodes to the meter. A schematic diagram of the final setup is shown in figures 4.1.5 and 4.1.6. Figure 4.1.7 shows an actual test sample.

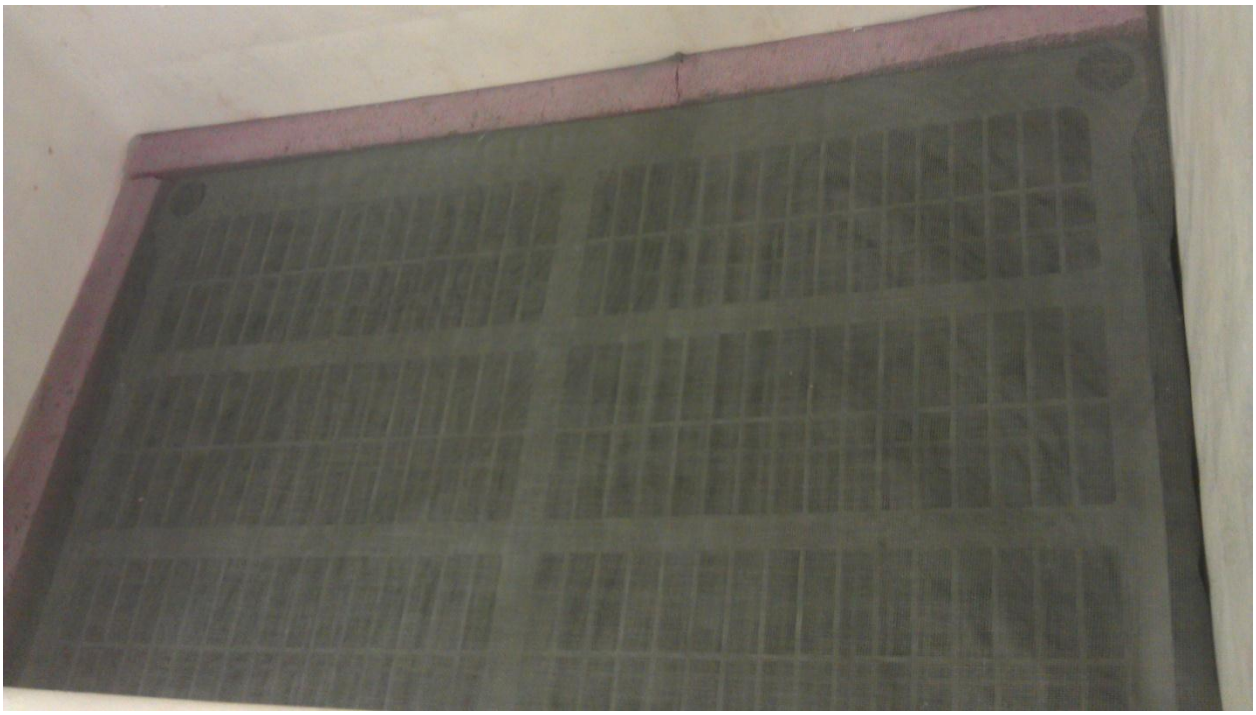

Figure 4.1.1 Plastic support and fiber glass screen

Figure 4.1.2 Cut front wall of the box and place the glass wall

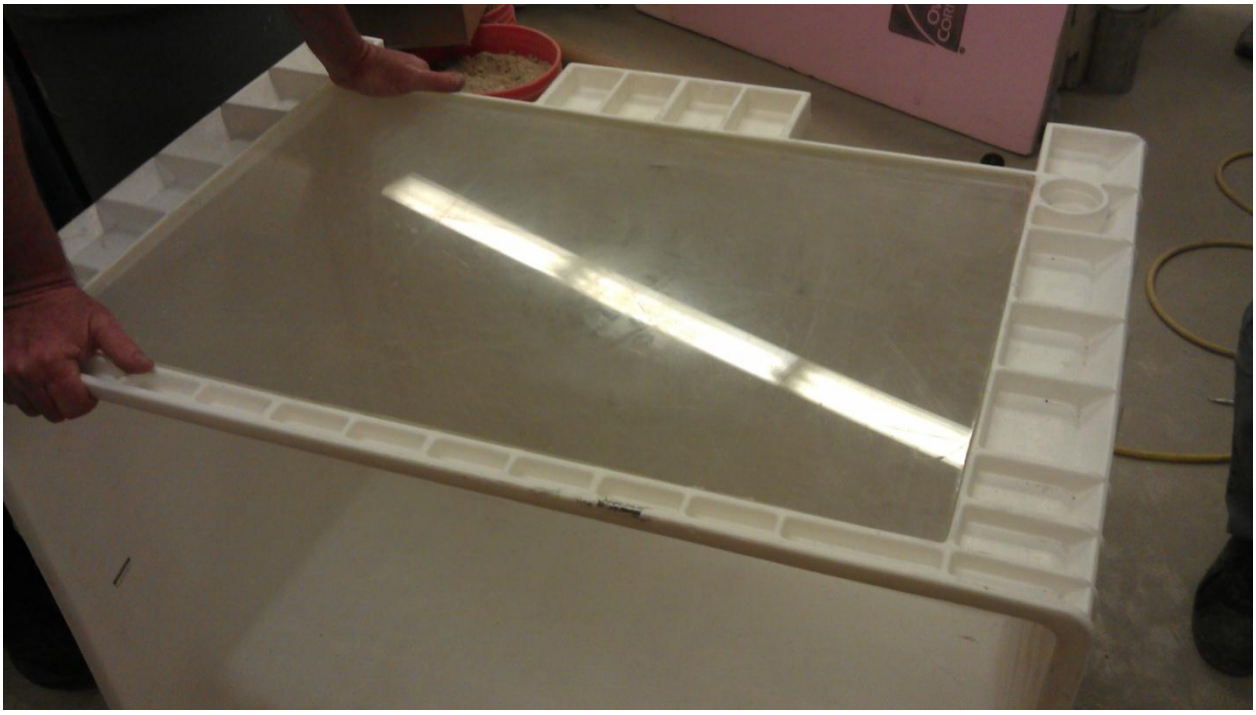

Figure 4.1.3 Secure and seal glass wall

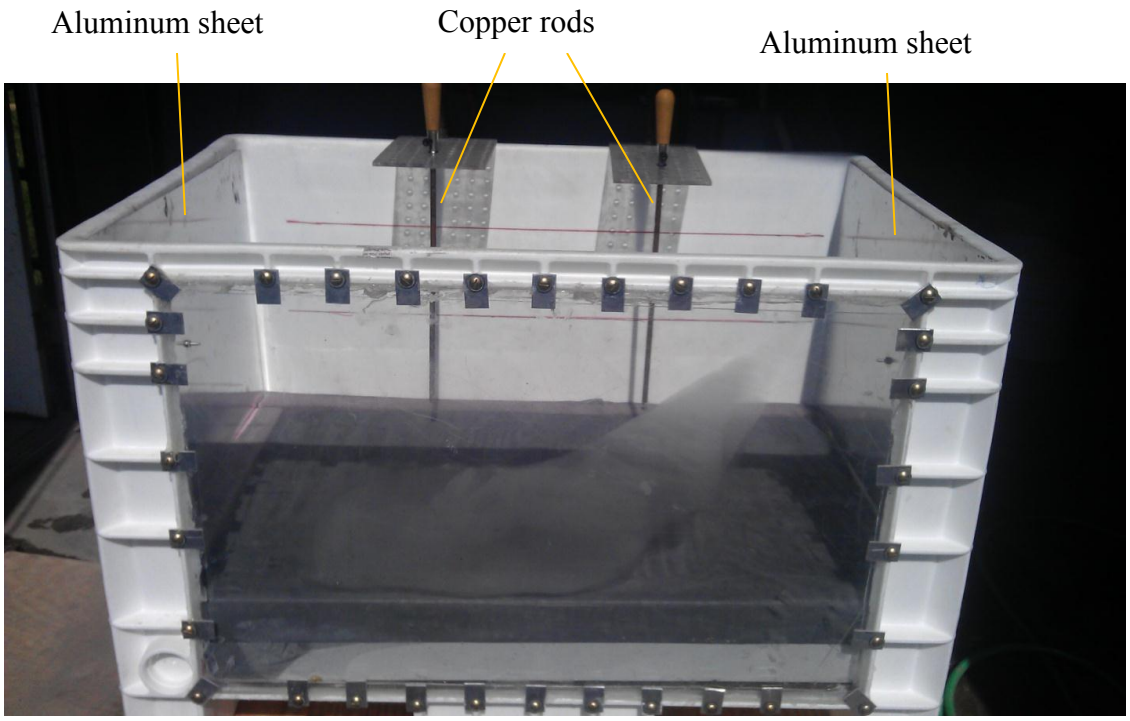

Figure 4.1.4 Aluminum sheets and copper rods spaced equally

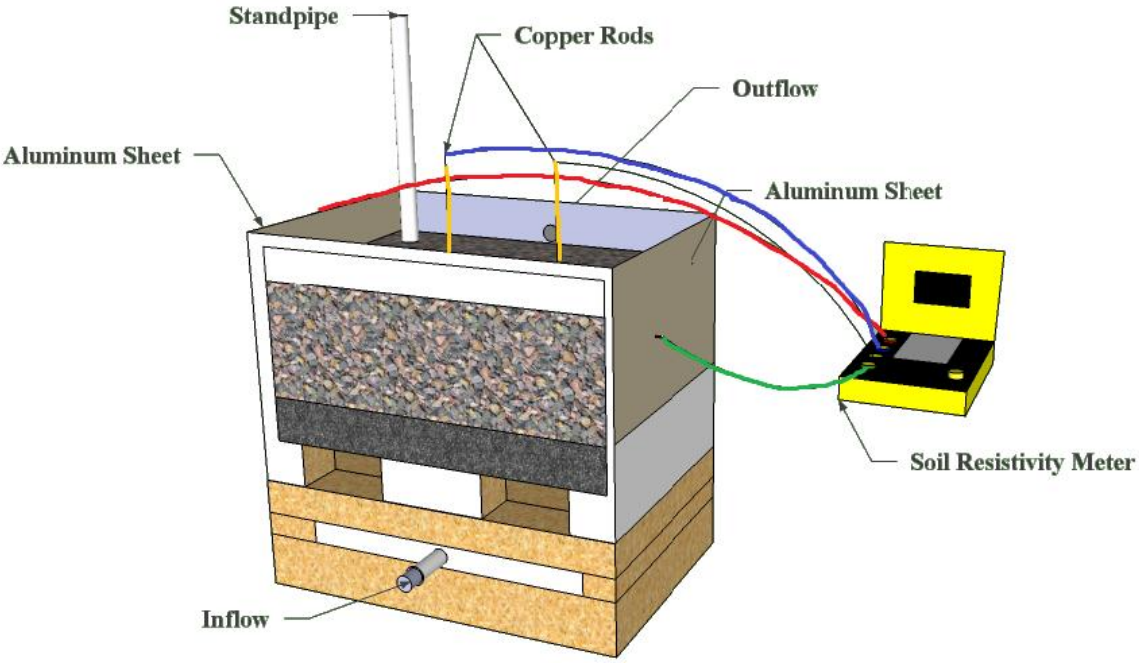

Figure 4.1.5 Schematic diagram for the setup of the test

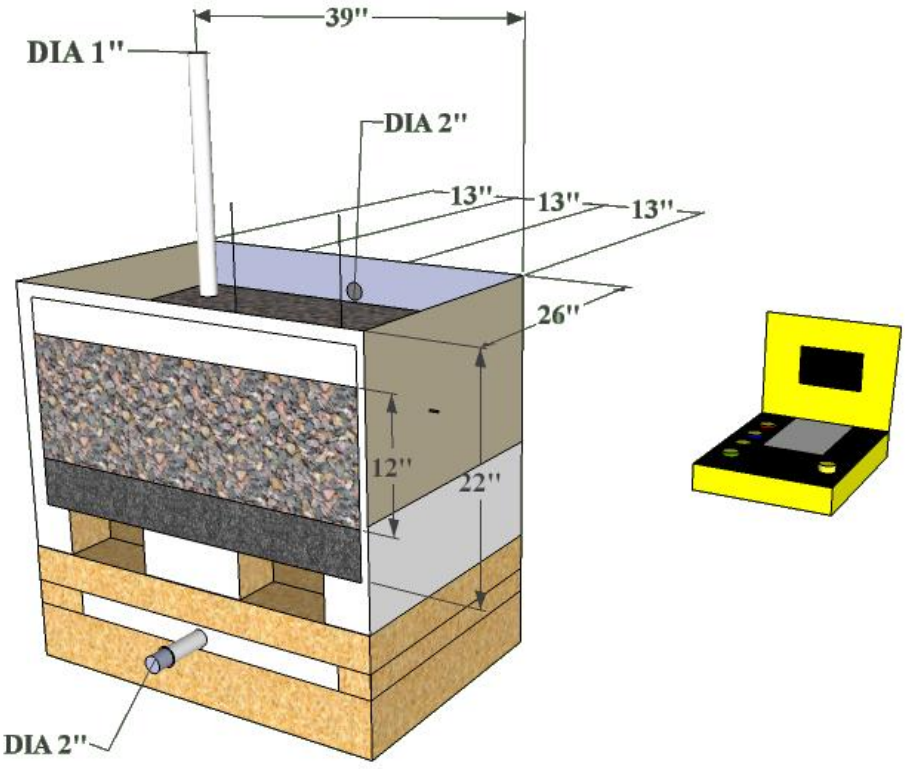

Figure 4.1.6 Schematic diagram for the setup of the test with dimensions

Figure 4.1.7 Picture of actual test setup

4.2 Permeability and Resistivity Test Procedure

This section contains a description of the procedures followed for both the permeability and resistivity tests. First, the box was washed after every test to clean the residue from the previous test. The copper rods, aluminum sheets, standpipe, and screen were also cleaned before setting up for the next test. Then the fiberglass screen was fastened securely on the plastic support and around the corners of the box to prevent fines from migrating around the screen, which was necessary to obtain accurate results for the resistivity test. The box was then checked for level to make sure it was standing on a flat surface. Then, the sample, which consisted of ballast and the fouling material, was added to the box layers and spread out uniformly around the box. The sample was then compacted by tapping the walls of the box with a rubber mallet. The hose was connected to the inflow pipe at the bottom of the box and water was introduced into the sample. A steady state flow condition (constant head) was established as water entered the lower reservoir, passed upward through the sample and into the upper reservoir, and exited through the outflow port. Water was collected from the upper reservoir (outflow) for a measured time period, and the mass and time were recorded. This procedure was repeated twice more before constant head flow was calculated. Constant head flow, Q, was determined by the following equation:

$$Q = \frac{M_w}{t \times \rho_w} \qquad (4.1)$$

where,

M_w = weight of water collected (g)

t = measured time period (s)

ρ_w = density of water, use 1 g/cm.^{3}

For each test the height of the water rise was measured in the standpipe relative to the water level in the sample. Hydraulic conductivity was determined by the following equation:

$$k = \frac{QL}{\Delta h A} \qquad (4.2)$$

where,

L = length of sample (cm)

A= area of sample (cm^2)

Δh = height of water rise in the standpipe.

The electrodes were then connected to the resistivity meter in order to take resistance readings, in accordance with the Wenner 4 point method, as the water drained out from the bottom pipe. The aluminum sheet on the east wall of the box was connected to X in the resistivity meter, the first copper rod was connected to Xv, the second copper rod was connected to Y, and the aluminum sheet on the west wall of the box was connected to Z. The four electrodes were set at equal distances from each other. A current was then passed through the outer electrodes, and the voltage between the two copper rods was measured. The soil resistance was measured by the resistivity meter, and the resistivity of the sample, ρ, was determined using equation 4.3. Time was recorded for each reading taken up to 24 hours.

$$\rho = 2\pi \times R \times A \qquad (4.3)$$

Figures 4.2.1 through 4.2.14 present different steps taken to prepare the test:

Figure 4.2.1 Washing the box prior to testing

Figure 4.2.2 Screen wrapped around support

Figure 4.2.3 Verify box is level

Figure 4.2.4 Tap sides of the wall to compact sample

Figure 4.2.5. First layer of ballast mixed with fouling material

Figure 4.2.6 Box filled with sample and ready for test

Figure 4.2.7 Flooding the sample with water through the bottom pipe

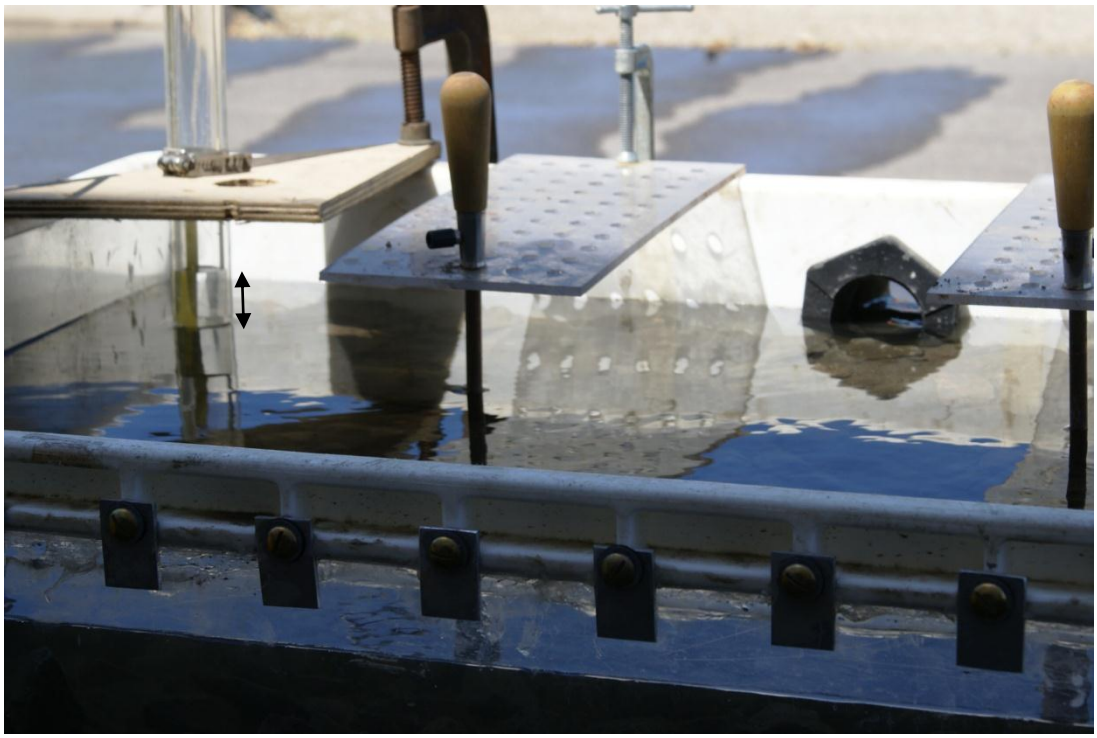

Figure 4.2.8 Water rise in standpipe relative to water level in sample

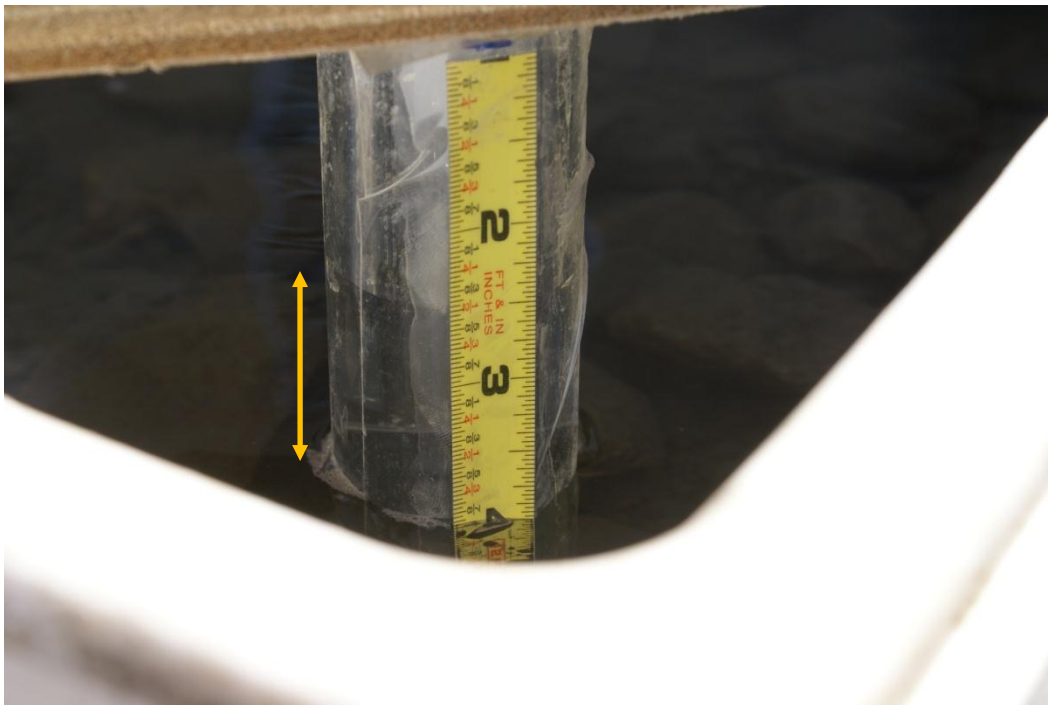

Figure 4.2.9 Close picture of height of water in standpipe

Figure 4.2.10 Constant head flow exiting the outflow pipe

Figure 4.2.11 Collect water for a certain time period

Figure 4.2.12 Verify draining water is clean (no loss of fines)

Figure 4.2.13 Aluminum sheets and copper rods connected to resistivity meter

Figure 4.2.14 Measure resistance in sample

4.3 Large Direct Shear Box Test Setup and Instrumentation

Direct shear strength tests were performed on clean and fouled ballast. The first sets of tests were conducted in a large direct shear box in the geotechnical laboratory at the KU Civil, Environmental, and Architectural Engineering (CEAE) Department. The inside dimensions of the top box were 305mm x 305mm x 102mm (12 in. x 12 in. x 4 in.) and the bottom box dimensions were 406mm x 305mm x 102mm (16 in. x 12 in. x 4 in.). The normal pressure was applied by a cylinder (140 mm inside diameter) on a steel plate (305 mm x 305mm x 25mm). Equivalent normal pressures were calculated based on the area conversion from the cylinder to top plate. The vertical normal load was controlled by a pressure gauge that is connected to an air compressor. Horizontal load cell and displacement gauge were connected to an automatic data acquisition system that was controlled by the user on a personal computer. Figure 4.3.1 through 4.3.4 shows the whole setup of the large direct shear test.

Figure 4.3.1 Large direct shear box

Figure 4.3.2 Pressure gauge and display

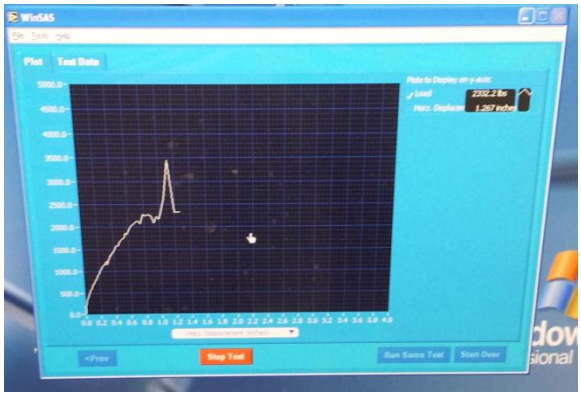

Figure 4.3.3 Test monitor

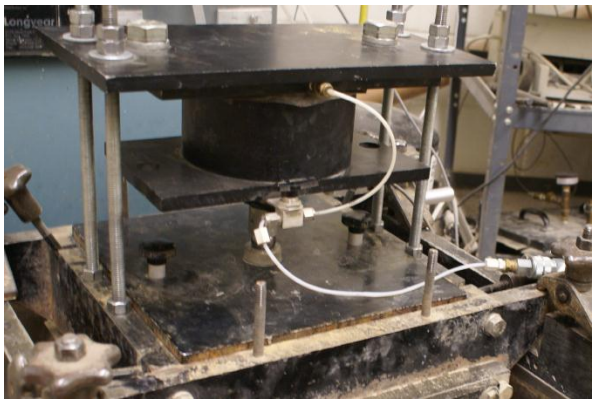

Figure 4.3.4 Cylinder and top plate

4.4 Direct Shear Test Procedure

Samples were prepared in four layers, two in the bottom box and then another two layers after the top box was placed. The weight of ballast was recorded for each layer and then the weight of fouling material to be added was calculated based on the fouling ratio tested. The fouling material was spread on top of the clean aggregates on each layer, this method was adopted from a study performed by (Huang 2009) were coal dust was spread on top of ballast to simulate field conditions. The top box was then fixed in place and the loading plate was placed on top of the sample. The loading frame was then assembled on top of the top box. The air supply was opened and the equivalent normal pressure was set using the pressure gauge. The loading rate was set to 5.1 mm/min (0.2 in./min), and maximum horizontal displacement was set to 15% strain. The load cell and displacement gauges were initiated at the large direct shear box and the data acquisition software. The software was set to record shear force and horizontal displacement. Figures 4.4.1 through 4.4.3 show the test preparation and setup.

Figure 4.4.1 Bottom box (ballast and clay fines)

Figure 4.4.2 Top box fixed

Figure 4.4.3 Loading frame assembled and air supply connected

4.5 Modified Direct Shear Test Setup and Instrumentation

The same set of strength tests were performed using a modified direct shear box. The modification included an extension to the bottom box and a new top box. The inside dimensions of the top box were 305mm x 305mm x 153mm (12 in. x 12 in. x 6 in.) and the bottom box dimensions were 406mm x 305mm x 153mm (16 in. x 12 in. x 6 in.). The same loading setup and instrumentation were used for this test as in the large direct shear box test mentioned in section 4.3. Figures 4.5.1 through 4.5.4 show pictures of the modified box after assembly and sample preparation.

4.6 Modified Direct Shear Test Procedure

The same sample preparation steps mentioned in section 4.3 were performed with the modified direct shear box. However, two more layers were added since the overall volume has increased.

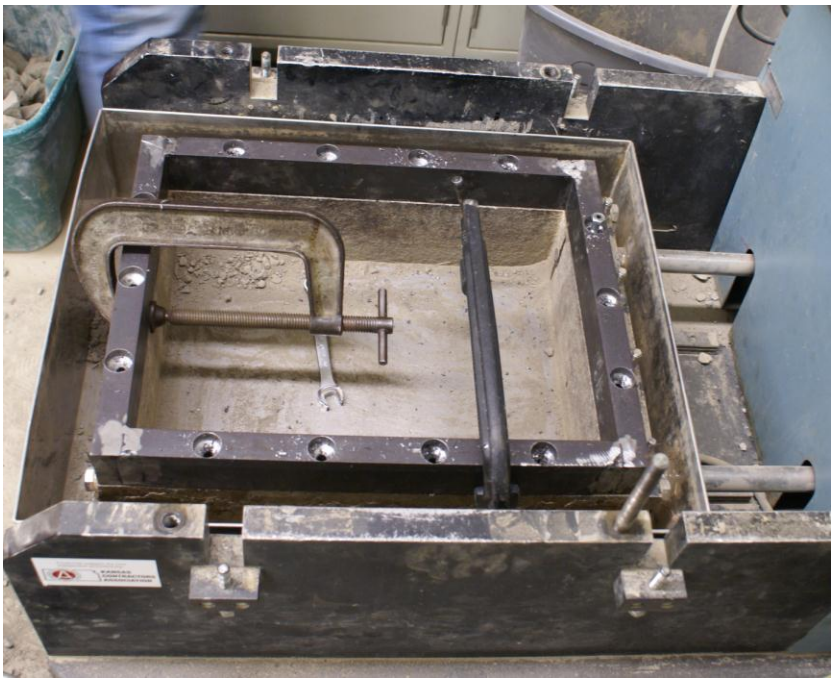

Figure 4.5.1 Installing box extension to bottom box

Figure 4.5.2 Modified direct shear box

Figure 4.5.3 Modified direct shear box with clean ballast

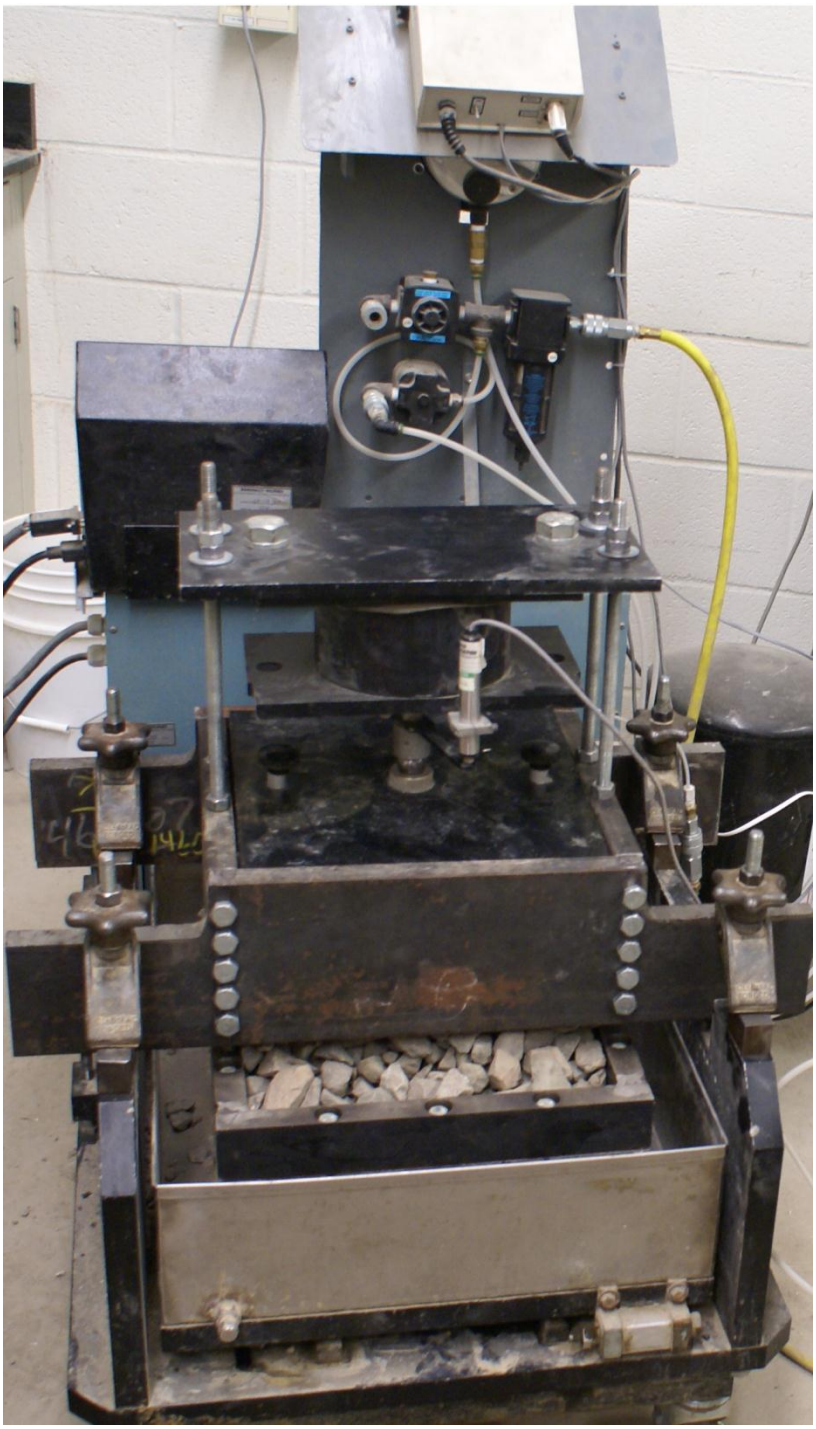

Figure 4.5.4 Modified direct shear box setup

4.7 Large Scale Resistivity Test on Fouled Ballast

Three tests were performed on a large scale pad of fouled ballast at different depths. The pad had a length of ten feet, a width of five feet and height of three feet. The sample was prepared by adding fouled ballast and compacted in six inches layers. The pad contained ballast and crushed ballast fines. Prior to testing water was added to the sample using a garden hose for about five minutes. A wooden board with pre-drilled holes was placed on top of the sample and four copper rods were inserted into the sample at specified spacing. Figure 4.7.1 through 4.7.5 show the sample preparation and setup.

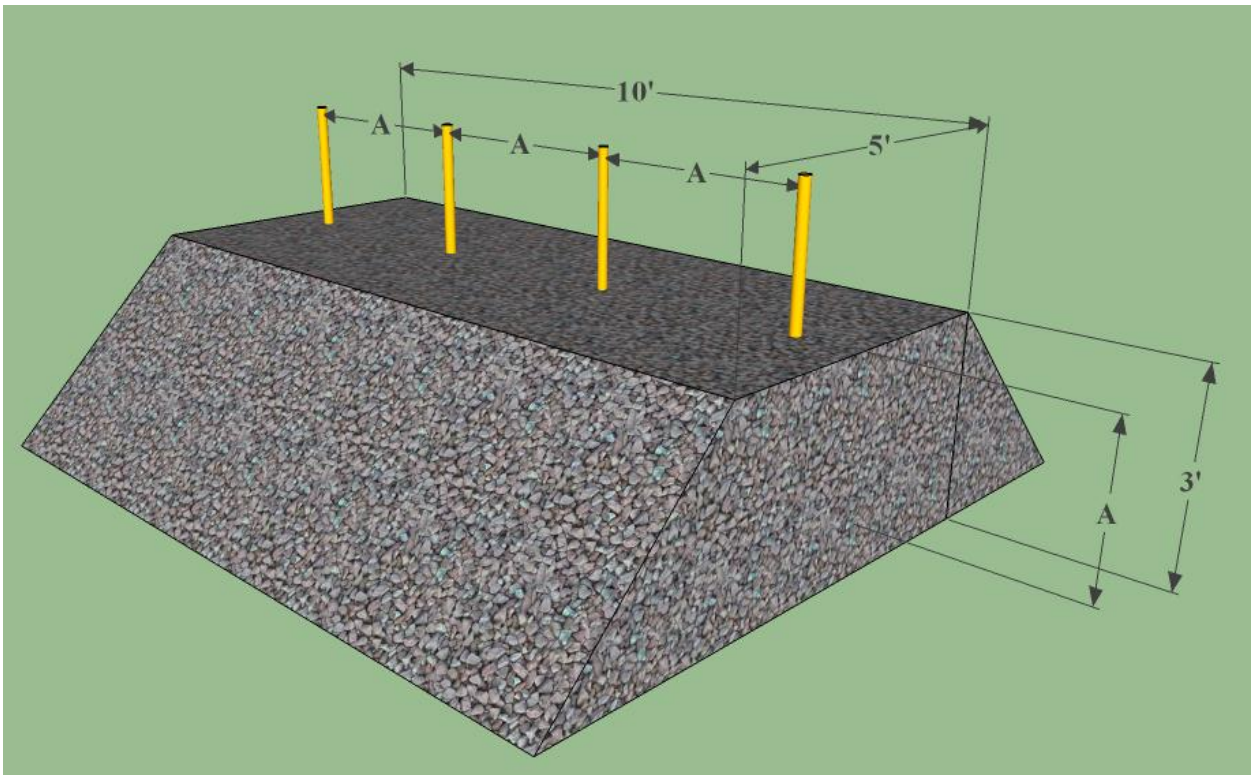

Figure 4.7.1 Schematic diagram of the setup of the test

Figure 4.7.2 Sample of fouled ballast

Figure 4.7.3 Spraying water on top of sample

Figure 4.7.4 Resistivity four point test setup

Figure 4.7.5 Measure resistance in sample

Chapter 5 Results and Discussion

5.1 Permeability Test Data

Four constant head permeability tests were conducted for each fouling material. Samples were prepared at 20, 30, 40, and 50 fouling ratio. According to (Selig and Waters 1994), the Fouling ratio is the ratio of the dry weight of fouled material passing the 9.5mm sieve to the weight of dry ballast. Figures 5.1.1 and 5.1.2 show the relationship of hydraulic conductivity with fouling ratio for crushed ballast fines , coal dust and clay on an arithmetic and logarithmic scale. The hydraulic conductivity was calculated using equation (4.2), and the results are presented in table 5.1.1.

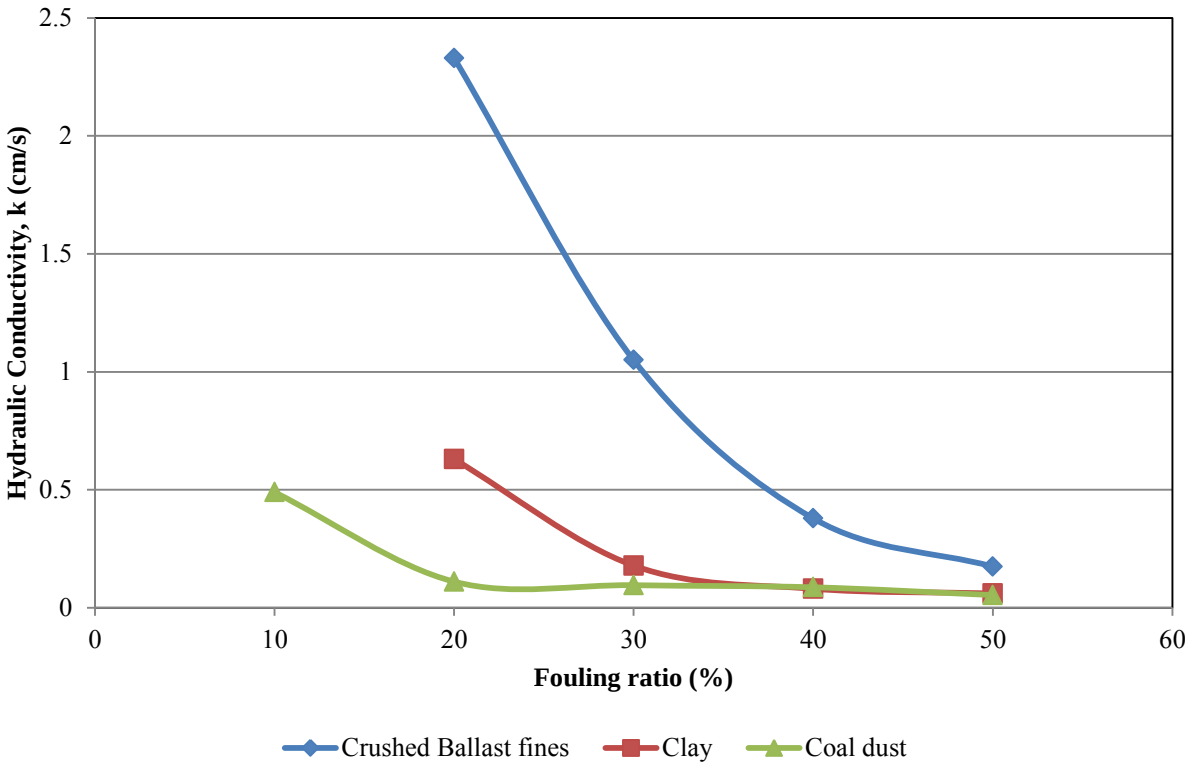

Figure 5.1.1 Measured hydraulic conductivity versus fouling ratio for crushed ballast fines, clay and coal dust

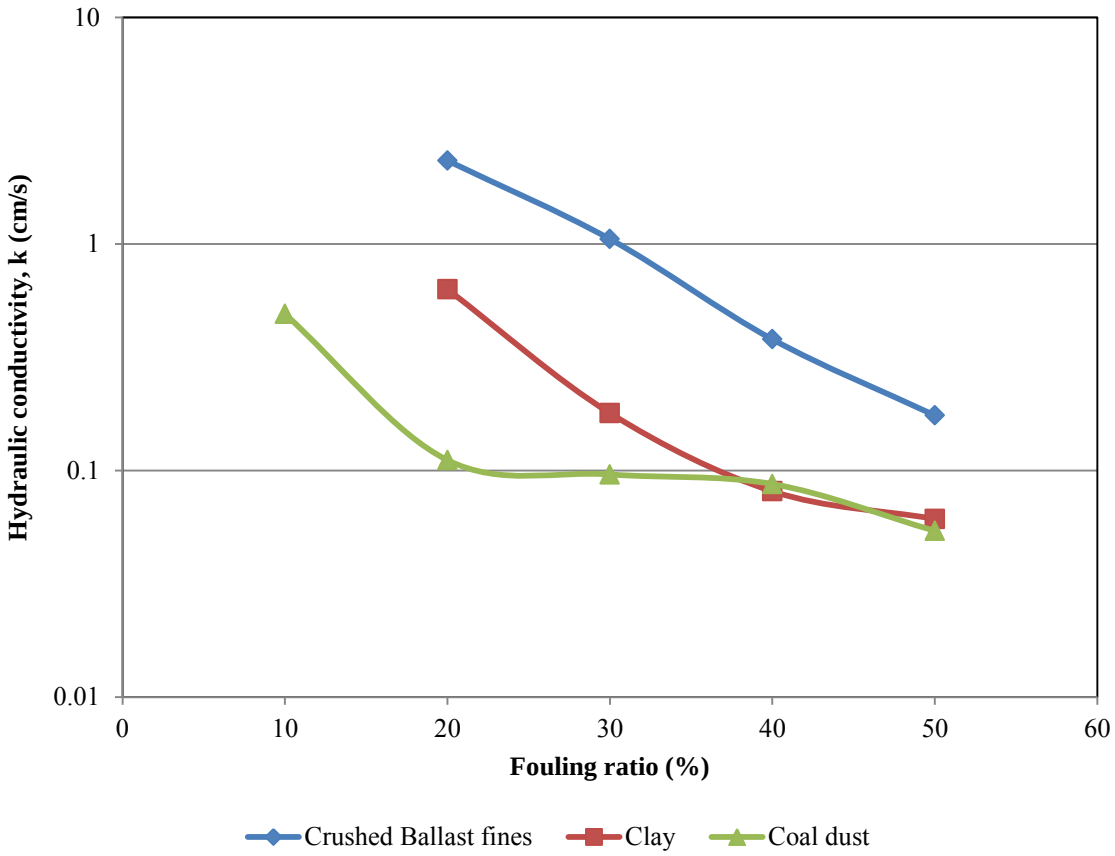

Figure 5.1.2 Measured hydraulic conductivity (log scale) versus fouling ratio for crushed ballast fines, clay and coal dust

Table 5.1.1 Hydraulic conductivity values for different fouling ratios for fouling materials

Permeability Test			
Fouling ratio	**Hydraulic conductivity with crushed ballast, k (cm/s)**	**Hydraulic conductivity with clay, k (cm/s)**	**Hydraulic conductivity with coal dust, k (cm/s)**
10%	NA	NA	0.490
20%	2.33	0.63	0.111
30%	1.05	0.179	0.0964
40%	0.379	0.0809	0.0871
50%	0.175	0.0611	0.0541

The relationships between permeability and fouling ratio are shown in table 5.1.1 and figure 5.1.1. The results confirm that permeability decreases substantially when the fouling ratio increases as fines fill up the voids between ballast coarse aggregate particles and restrict flow. Figures 5.1.1 and 5.1.2 show a sharp decrease in permeability as the fouling ratio increased for all fouling materials, with permeability for the ballast fouled with clay or coal dust consistently below that of ballast fouled with crushed ballast particles. Size distribution played a major role in the comparison between crushed ballast and clay particles. The clay grain size distribution curve shows that more 50% of the clay particles passed the No. 200 sieve compared to 1.4% of crushed ballast particles. Specific gravity is a major factor as coal dust has a low specific gravity compared to crushed ballast fines and clay, therefore, more coal dust particles are present in samples fouled with coal dust as compared with clay and crushed ballast fines.

For the 40% and 50% coal dust fouled ballast, the samples experienced a significant loss of material due to the light weight of coal dust particles. Figure 5.1.3 shows a close up picture of the change of height in the sample after water was let out. A layer of geotextile was placed on top of the sample to minimize material loss and the effect of geotextile on permeability was assumed to be negligible. Figures 5.1.4 shows a picture of the sample with geotextile placed on top after box was filled with water and figure 5.1.5 shows a picture of clean water flowing out.

Figure 5.1.3 Close up picture of material loss after sample is filled with water

Figure 5.1.4 Geotextile placed on top of sample

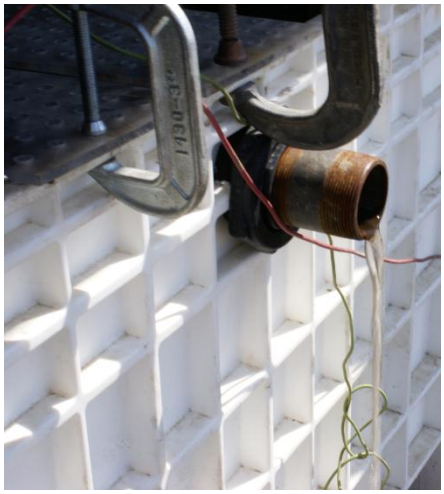

Figure 5.1.5 Clean water flow out of pipe

Figure 5.1.6 presents the hydraulic conductivity versus fouling index of fouled ballast. The fouling index was proposed by (Selig and Waters 1994) and is represented by the sum of the percentages that passed the No. 4 sieve and the No. 200 sieve. The fines that passed the No. 200 sieve are accounted for twice in this index due to the significance of the size of fine particles in decreasing the drainage capacity. Plotting of fouling using the fouling index resulted in similar hydraulic conductivity values for different materials with the same fouling index. The fouling index adjusts for the different grain size distribution, and was therefore less dependent on fouling material type. Also, percentage of fouling can be calculated using the fouling ratio to define the level of fouling of the ballast. Fouling ratio is equal to ratio of percentage fouling to one minus percentage fouling.

According to (Indraratna 2006), and as shown in table 5.1.2, the ballast layers are considered highly fouled when the fouling ratio is greater than 50%, or the fouling index is 40%or greater.

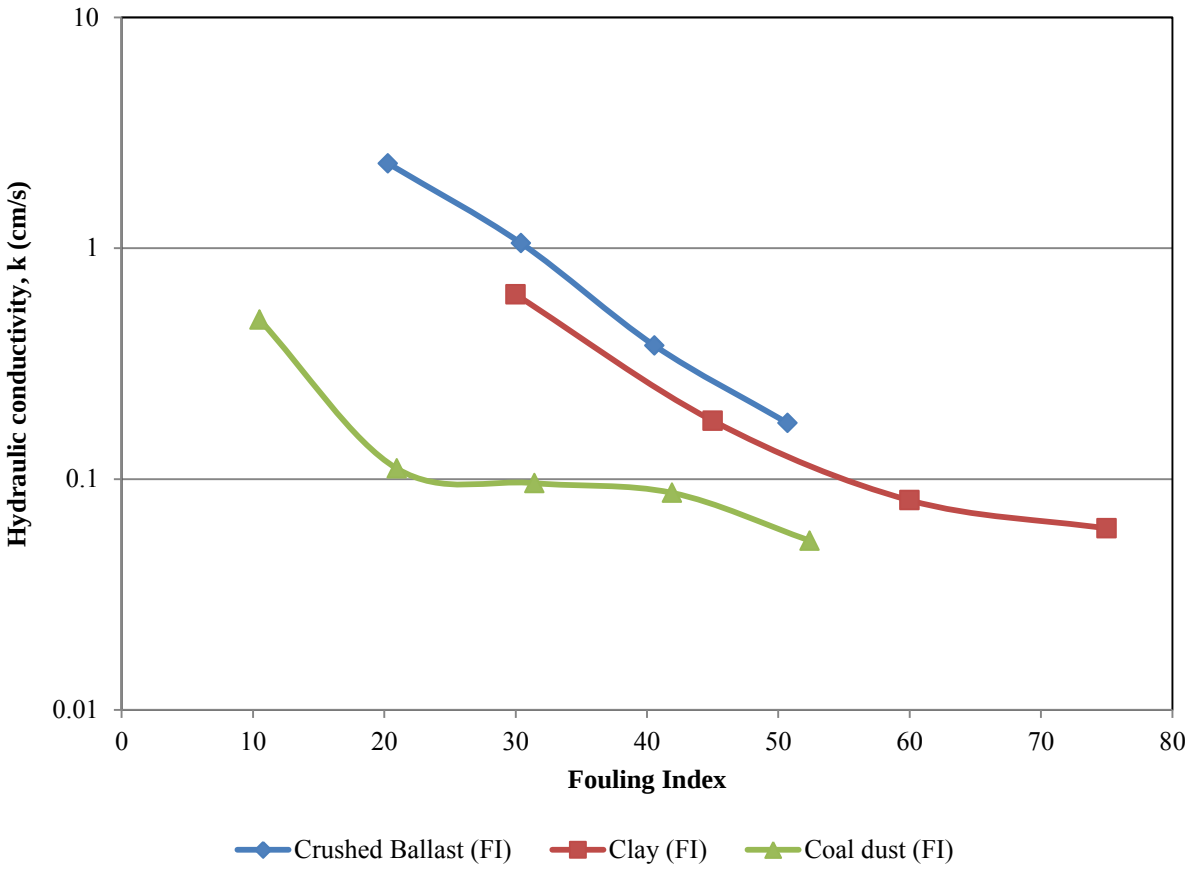

Figure 5.1.6 Hydraulic conductivity (log scale) versus fouling index of fouled ballast

Table 5.1.2 Categories of fouling based on fouling ratio and fouling index (Indraratna, 2006)

Category	Fouling ratio (%)	Percentage of fouling (%)	Fouling Index (Selig and Waters) (%)
Clean	< 2	< 2	< 1
Moderately clean	2 to < 10	2 to < 9.5	1 to < 10
Moderately fouled	10 to < 20	9.5 to < 17.5	10 to < 20
Fouled	20 to < 50	17.5 to < 34	20 to < 40
Highly fouled	≥ 50	≥ 34	≥ 40

5.2 Resistivity Test Data

For each sample, a resistivity test was conducted at different time intervals up to 24 hours. As the water drained out of the sample, resistance readings were taken at recorded time periods to develop a resistivity range for each fouling material and the fouling ratio. Figures 5.2.1, 5.2.2 and 5.2.3 show the relationship of resistivity of fouled ballast (crushed ballast, clay and coal dust) with time at 20, 30, 40 and 50 fouling ratio. An additional test of 10% fouled ballast with coal dust was also conducted. Also, tables 5.2.1, 5.2.2 and 5.2.3 show the resistivity range for each fouling ratio of crushed ballast fines, clay, and coal dust. Figure 5.2.4 shows the resistivity for each test at the 18^{th} hour measurement. Table 5.2.4 shows the actual resistivity measurement comparison for the fouled ballast with crushed ballast fines , clay and coal dust at the 18^{th} hour. Figure 5.2.5 shows the hydraulic conductivity and resistivity plotted versus the fouling ratio.

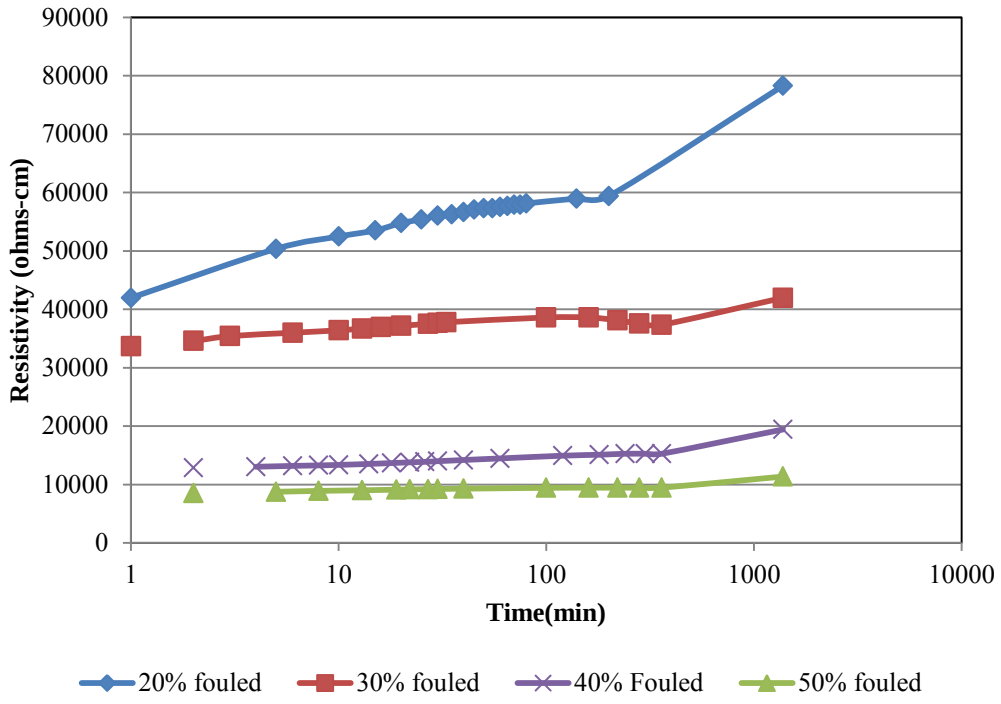

Figure 5.2.1 Measured resistivity of fouled ballast (crushed ballast fines) versus time (log scale) at different fouling ratio

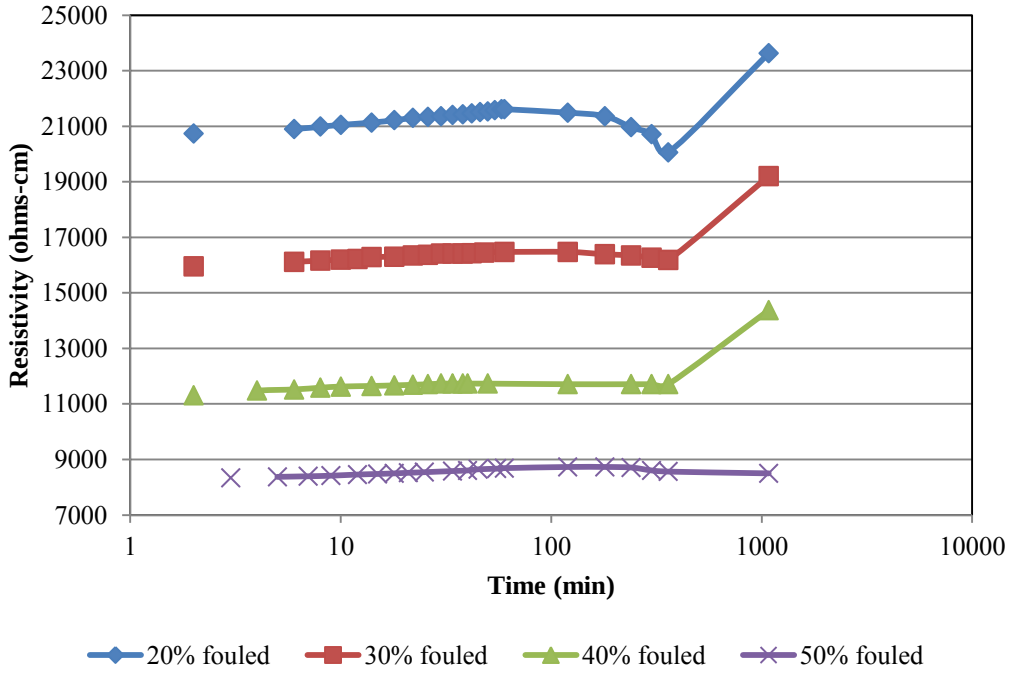

Figure 5.2.2 Measured resistivity of fouled ballast (clay) versus time (log scale) at different fouling ratio

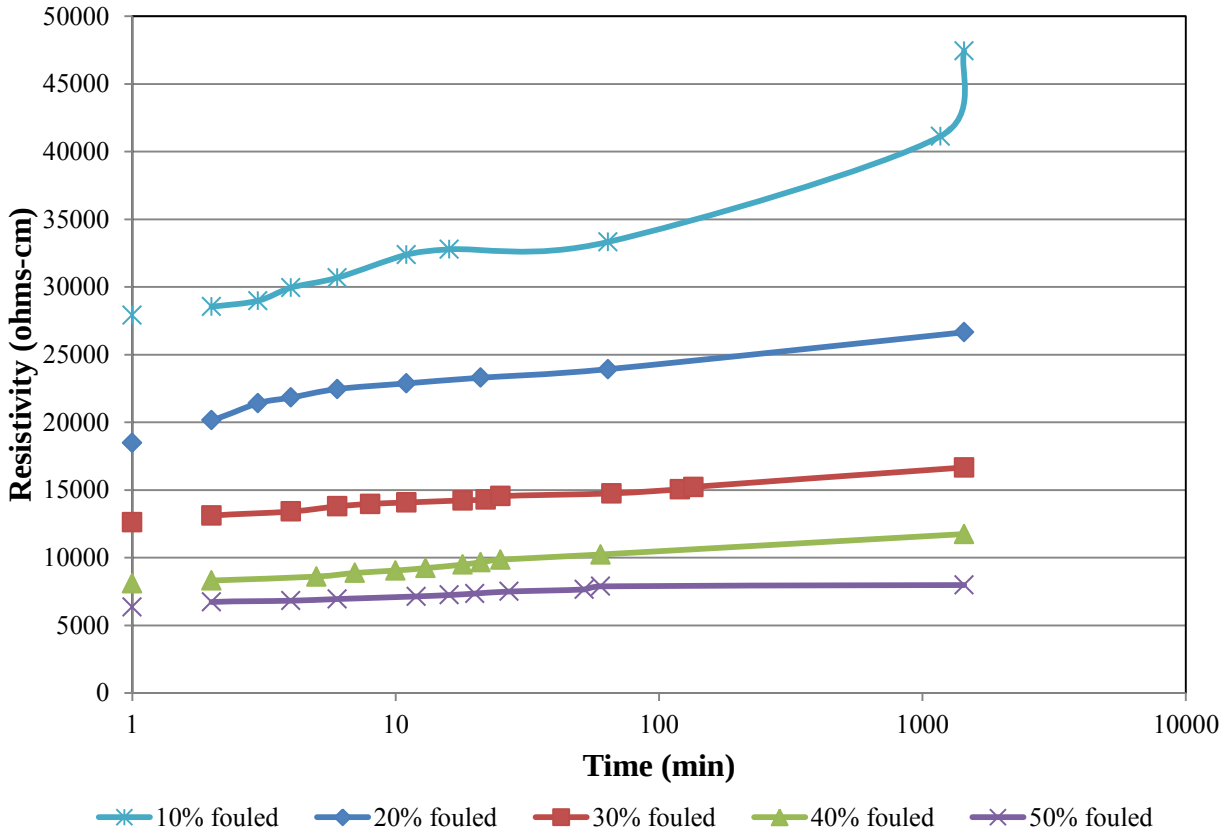

Figure 5.2.3 Measured resistivity of fouled ballast (coal dust) versus time (log scale) at different fouling ratio

Table 5.2.1 Measured resistivity range for each fouling ratio for crushed ballast fines

Crushed Ballast	
Fouling ratio	**Resistivity (ohms-cm) Range**
20%	42,000 - 80,000
30%	32,000 - 42,000
40%	12,000 - 20,000
50%	8,000 - 12,000

Table 5.2.2 Measured resistivity range for each fouling ratio for clay

Clay	
Fouling ratio	**Resistivity (ohms-cm) Range**
20%	20,000 - 24,000
30%	15,000 - 20,000
40%	11,000 - 15,000
50%	8,000 - 9,000

Table 5.2.3 Measured resistivity range for each fouling ratio for coal dust

Coal Dust	
Fouling ratio	**Resistivity (ohms-cm) Range**
10%	27,000 – 46,000
20%	16,000 - 26,000
30%	12,000 - 16,700
40%	7,800 - 12,000
50%	6,000 – 8,000

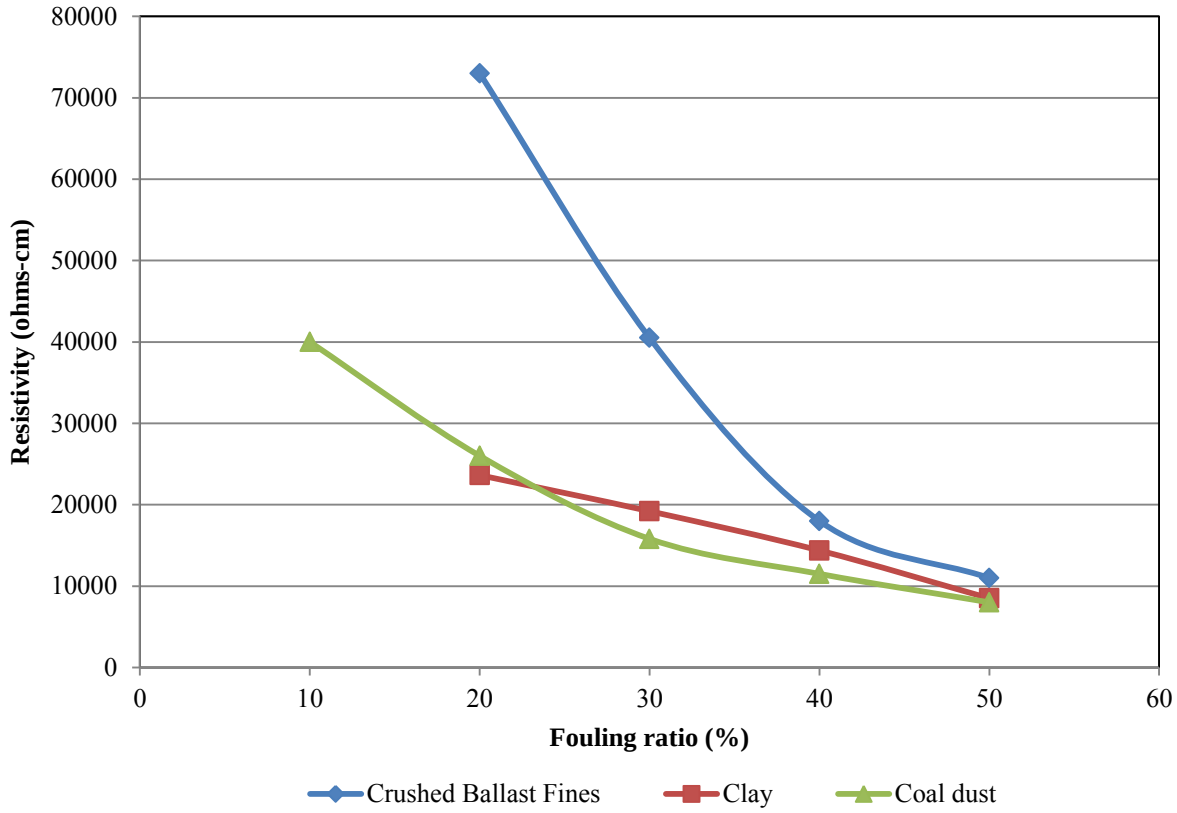

Figure 5.2.4 Measured resistivity of fouled ballast at the 18th hour versus fouling ratio

Table 5.2.4 Comparison of the resistivity of fouled ballast (crushed ballast fines, clay and coal dust) at the 18th hour

	Resistivity (ohms- cm)		
Fouling ratio	**Crushed ballast**	**Clay**	**Coal dust**
10%	NA	NA	40,000
20%	73,000	23,630	26,000
30%	40,500	19,202	15,800
40%	18,000	14,375	11,500
50%	11,000	8,500	8,000

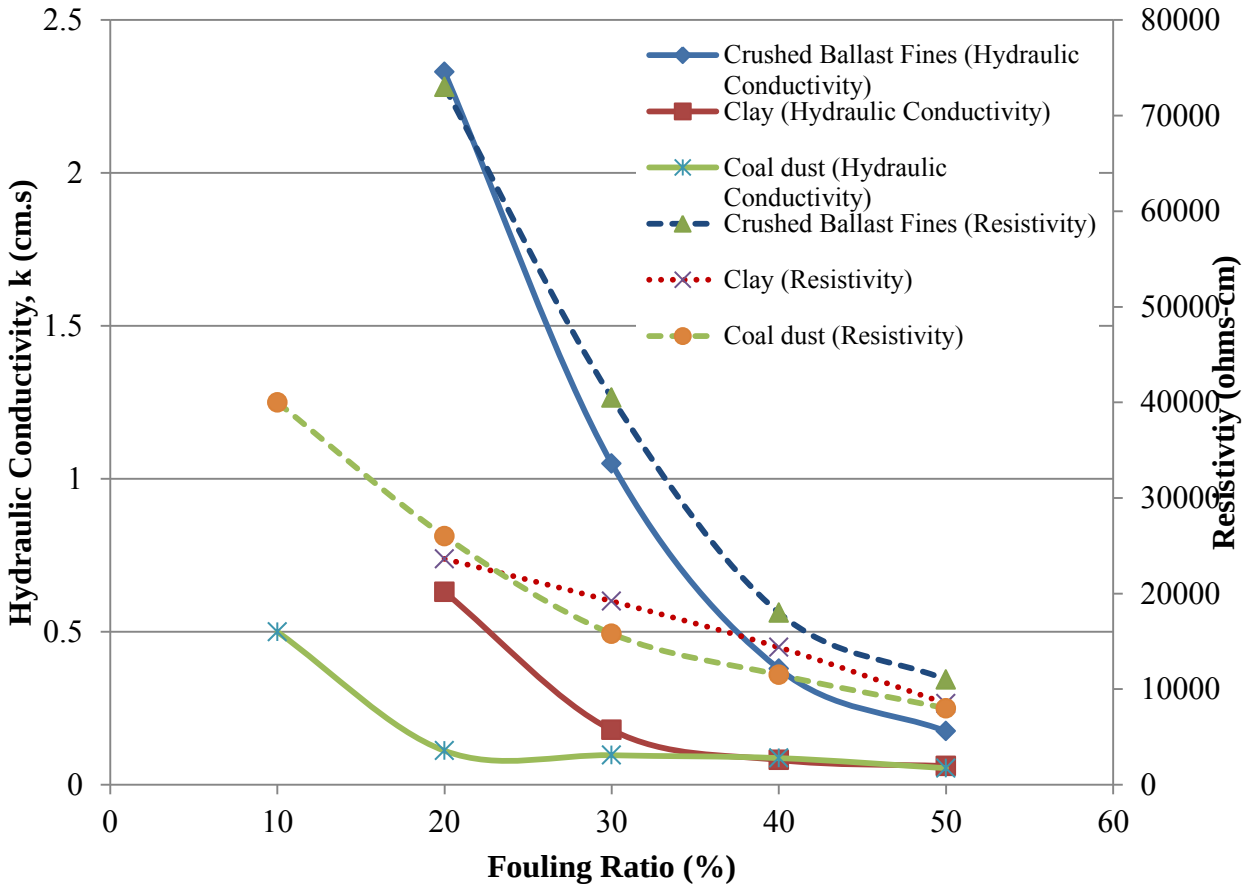

Figure 5.2.5 Comparison between measured hydraulic conductivity and resistivity at 18th hour versus fouling ratio

The values of resistivity of fouled ballast are plotted against time in figures 5.2.1, 5.2.2 and 5.2.3 for different fouling ratios with crushed ballast, clay and coal dust. As expected, the resistivity decreased as the fouling ratio increased. Values of resistivity decreased due to the increase in the amount of water retained as the fouling ratio increased. As evident in figures 5.2.1, 5.2.2 and 5.2.3, resistivity values were measured at short time intervals. The resistivity increased rapidly as the water drained out of the sample before stabilizing after few hours. A final reading was taken 23 hours after the sample had the opportunity to drain, which resulted in the high value shown at the end of each curve in figures 5.2.1, 5.2.2 and 5.2.3. However, as the

fouling ratio increased, the resistivity values also increased to a lesser extent during the early times as the water drained out. This was due to a decrease in the rate of drainage, as shown in figure 5.2.1, for 40% and 50% fouling in the ballast. In addition, the reading taken after 23 hours for the samples with 40% and 50% fouling increased to a lesser extent compared with the samples with 20% and 30% fouling.

Moreover, the results of the resistivity test are consistent with the permeability trends, since the resistivity drops dramatically at 30% and 40% fouling, and the water drains out more slowly due to the low permeability of the sample at higher fouling ratios.

As shown in figure 5.2.1, the curve of the 30% fouled sample showed a slight decrease in the resistivity values after three hours of testing, before increasing for the final reading. The decrease in resistivity observed in some of the curves could have been caused by the increase of temperature during the day. All the tests shown in figure 5.2.1 were conducted in the open air outside of the laboratory, where the weather varied during the day and night for each test; however tests were begun in the morning, so temperatures generally increased during the initial 6-10 hours of testing, before decreasing with nightfall. Similar behavior was observed for the clay samples, as shown in figure 5.2.2 According to (Tagg 1964), the resistivity will decrease as temperature increases. This effect was presented in a study by (Samouelian 2005), which stated that ion agitation increases with temperature, resulting in a decrease in electrical resistivity.

Figure 5.2.2 presents the results of resistivity tests of fouled ballast with clay fines at different percentages. The patterns of resistivity vs. time were similar to ballast fouled with crushed ballast fines, with a decrease in resistivity occurring as fouling ratio increased. Tests of the 20%, 30%, and 40% fouling ballast were conducted in the open air outside of the laboratory, and measurements were taken for up to 18 hours. The sample with 50% fouling was conducted

inside the laboratory due to extreme weather conditions. As evident in figure 5.2.2, the curve for 50% fouling shows a steady line for resistivity measurements, presumably because the sample was not affected by temperature. Overall, as the fouling ratio increased, more water was retained due to the reduction in rate of drainage, which resulted in less permeable and resistive ballast.

Figure 5.2.3 presents the resistivity results with time for coal dust fouled ballast at different percentages. As expected, the resisitivity of ballast decreased as the percentage of coal dust increased. The weight of coal dust particles is relatively small compared to crushed ballast fines and clay, therefore, more particles were added to the sample and as a result more water was retained.

Tables 5.2.1, 5.2.2 and 5.2.3 present the range of resistivity measurements for each fouling ratio sample for crushed ballast fine ,clay and coal dust. The ranges for each sample are relatively small compared to the large differences in resistivity with changes in fouling ratio. The absolute values and the trends present in tables 5.2.1 and 5.2.2 are also consistent with the reference values for clay, sand, and crystalline rocks reported in table 2.1.

Figure 5.2.4 and table 5.2.4 show a comparison between permeability and resistivity of fouled ballast at the 18^{th} hour. The 18^{th} hour reading was chosen for the comparison since the clay samples were tested for 18 hours only due to time limitation. Solid curves represent the permeability test results and the dotted curves represent the resistivity results. As evident in figure 5.2.5, the patterns are similar, and show that as fouling ratio increased, permeability and resistivity decreased at a comparable rate and were clearly correlated with each other and with fouling. This indicates that measurements of either permeability or resistivity could be used to estimate the degree of fouling.

5.3 Direct Shear Test Data

For each sample a direct shear test was performed at three normal pressures, 35 kPa, 70 kPa, and 105 kPa (5 psi, 10 psi and 15 psi). Fouled samples were prepared with 20, 30, 40, and 50 fouling ratio content (by weight) for each type of fouling material. A series of tests with 10% fouled ballast with coal dust were performed. Additionally, a test on clean ballast was performed to compare the strength properties of fouled and clean ballast. The maximum shear stress for each test was evaluated and plotted according to ASTM D3080-04 to determine friction angle and cohesion. For each test, a shear stress and horizontal displacement curve was plotted to show the behavior of sample during the shearing process. Figures 5.3.1 and 5.3.3 through 5.3.19 present the results of direct shear tests of clean and fouled ballast at the three normal pressures. The curves plotted for each test are not smooth due to particle crushing during the shearing process. Also, the variability of particle size can cause this disturbance in the results for those tests. For these figures the solid lines represent the actual data retrieved from software and the dashed lines represent the predicted path of the curve (neglects disturbance caused by particle crushing) where the maximum shear stress values were evaluated. Crushing of the particle was observed visually on the display chart of the software and on the display of the machine, which showed the load increasing and suddenly falling after the particle was crushed. Also, crushing of ballast particles occurred during the end of some tests and the test had to be terminated due to reaching maximum travel in the machine. The data that was recorded during the crushing was neglected and was represented by a dashed circle as shown in several figures presented in section 5.3.

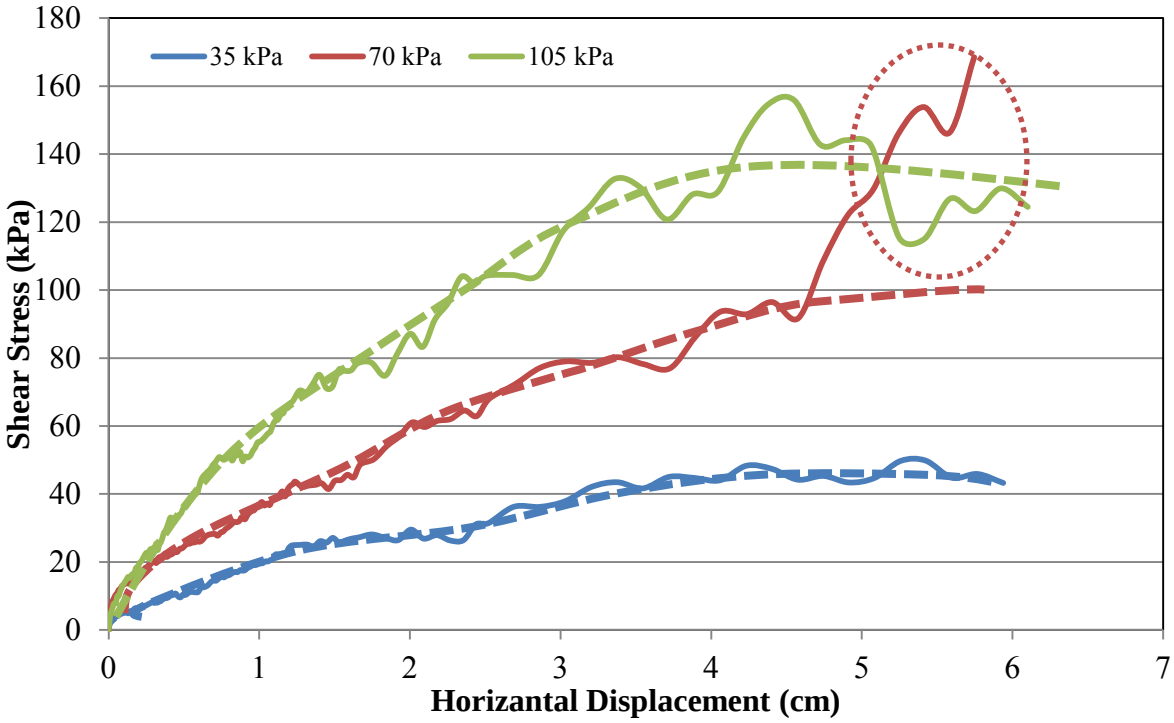

Figure 5.3.1 Shear stress versus horizontal displacement of clean ballast

Figures 5.3.1 shows the shear stress versus horizontal displacement for clean ballast at three different normal stresses. After the test, crushed ballast fines were observed at the bottom of the box as shown in Figure 5.3.3. As expected, the cohesion of the clean ballast was zero.

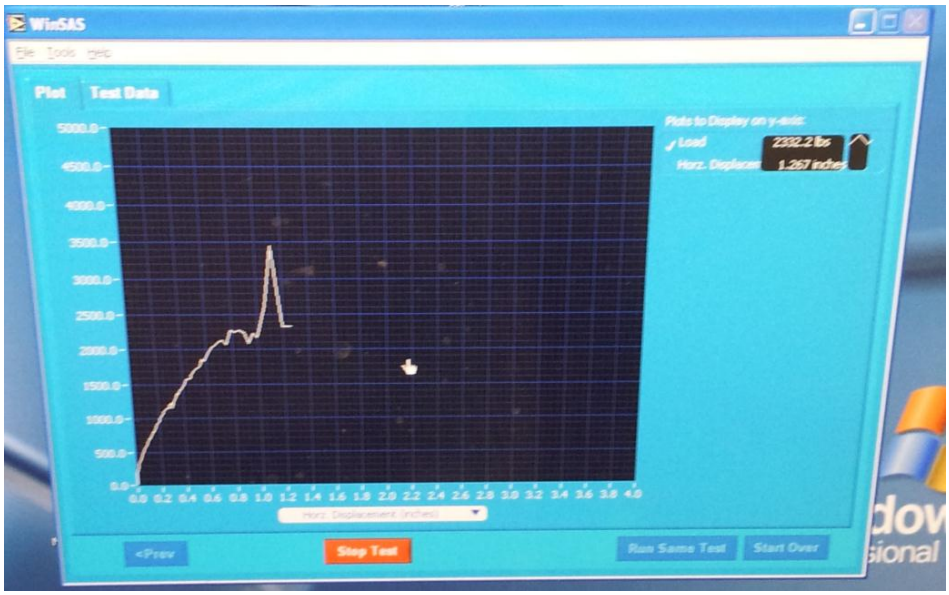

Figure 5.3.2. Display of particle crushing

Figure 5.3.3. Crushed ballast fines after clean ballast direct shear test

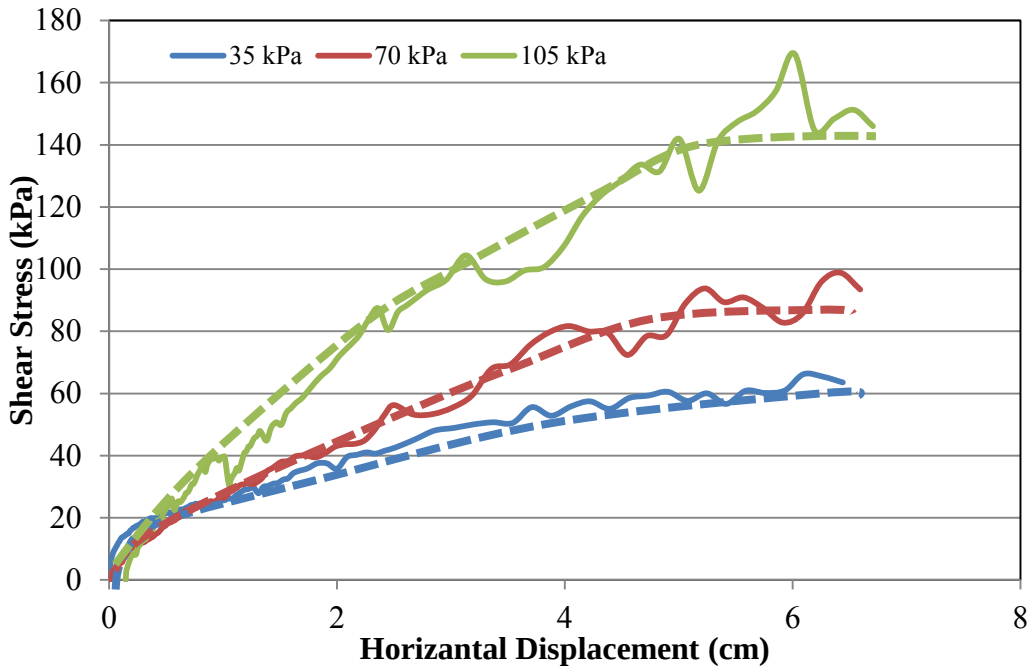

Figure 5.3.4 Shear stress versus horizontal displacement of ballast fouled with 20% crushed ballast fines

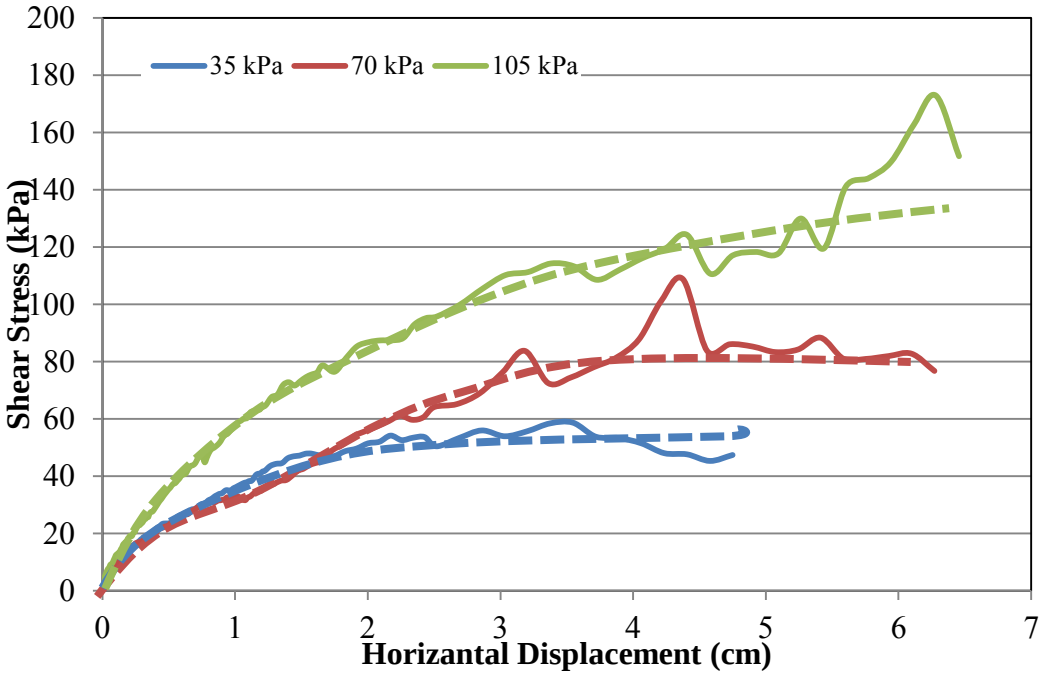

Figure 5.3.5 Shear stress versus horizontal displacement of ballast fouled with 30% crushed ballast fines

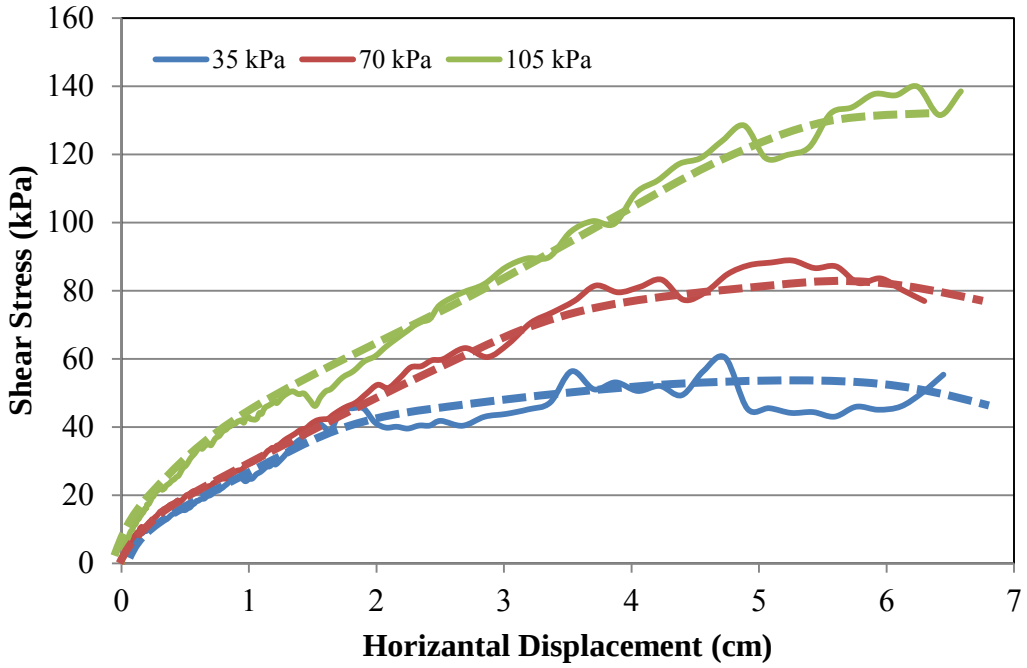

Figure 5.3.6 Shear stress versus horizontal displacement of ballast fouled with 40% crushed ballast fines

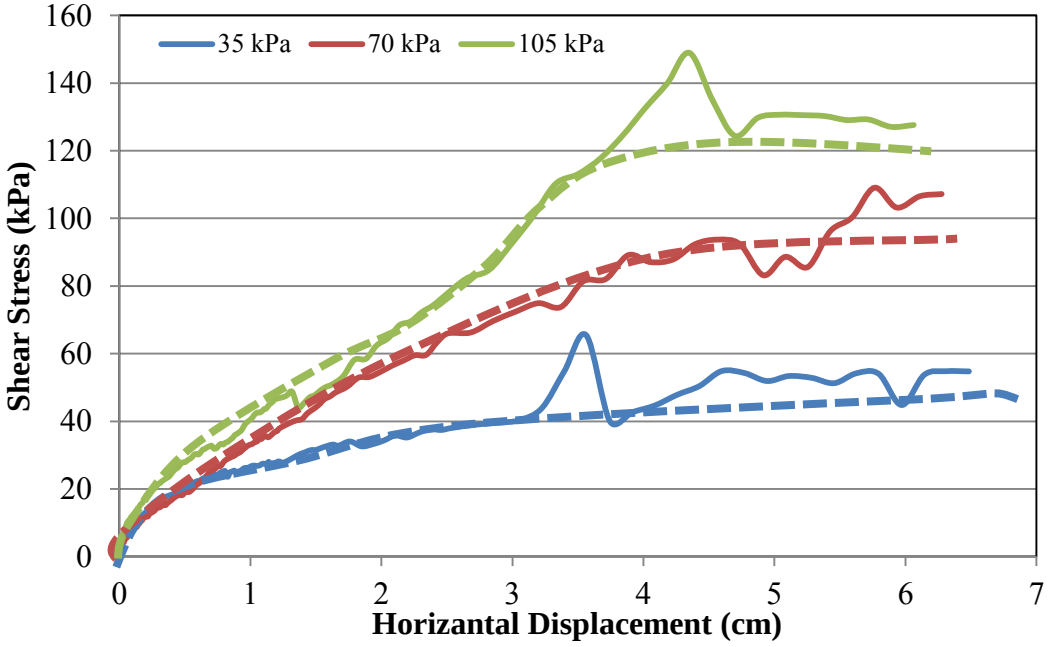

Figure 5.3.7 Shear stress versus horizontal displacement of ballast fouled with 50% crushed ballast fines

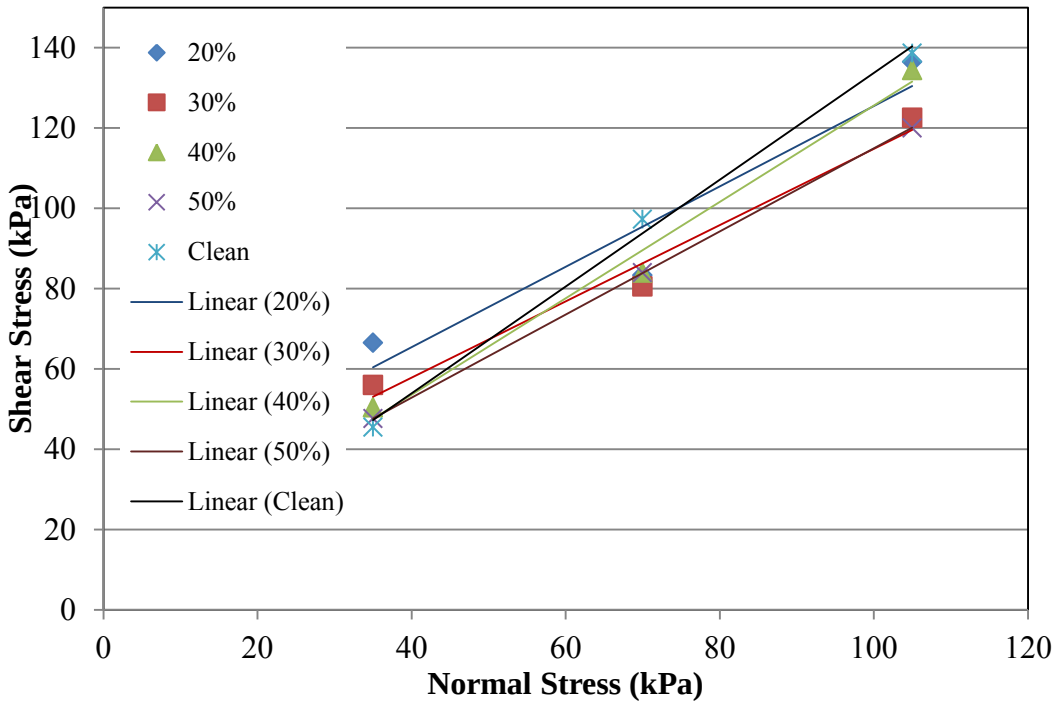

Figure 5.3.8 Failure envelopes of clean ballast and fouled ballast with crushed ballast fines

Figures 5.3.4 through 5.3.7 show the shear stress versus horizontal displacement plots of ballast with crushed ballast fines at different fouling ratios. Figure 5.3.8 presents a comparison of failure envelopes of clean ballast and fouled ballast with crushed ballast fines at different fouling ratios. The results show that clean ballast has a higher friction angle compared with fouled ballast. Typically, as the fouling ratio increased the friction angle decreased. However, the cohesion measured was not expected since all samples were prepared in a dry state. The variability in the results caused by the crushing of the ballast particles may have resulted in the cohesion of the sample

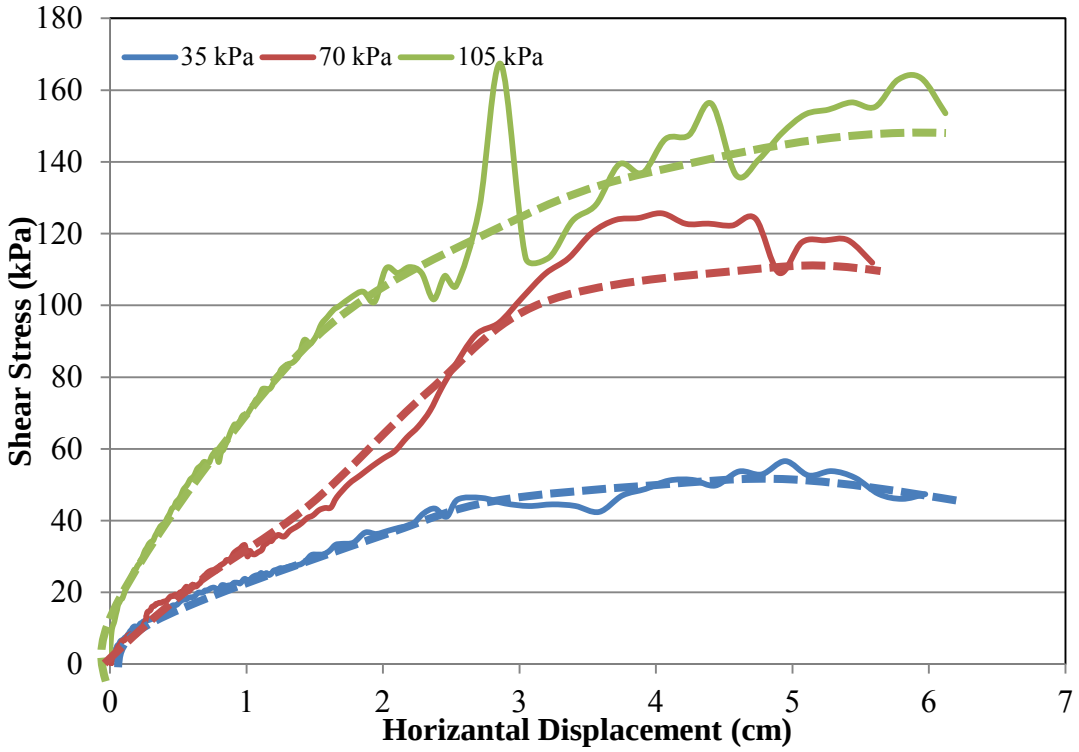

Figure 5.3.9 Shear stress versus horizontal displacement of ballast fouled with 20% clay

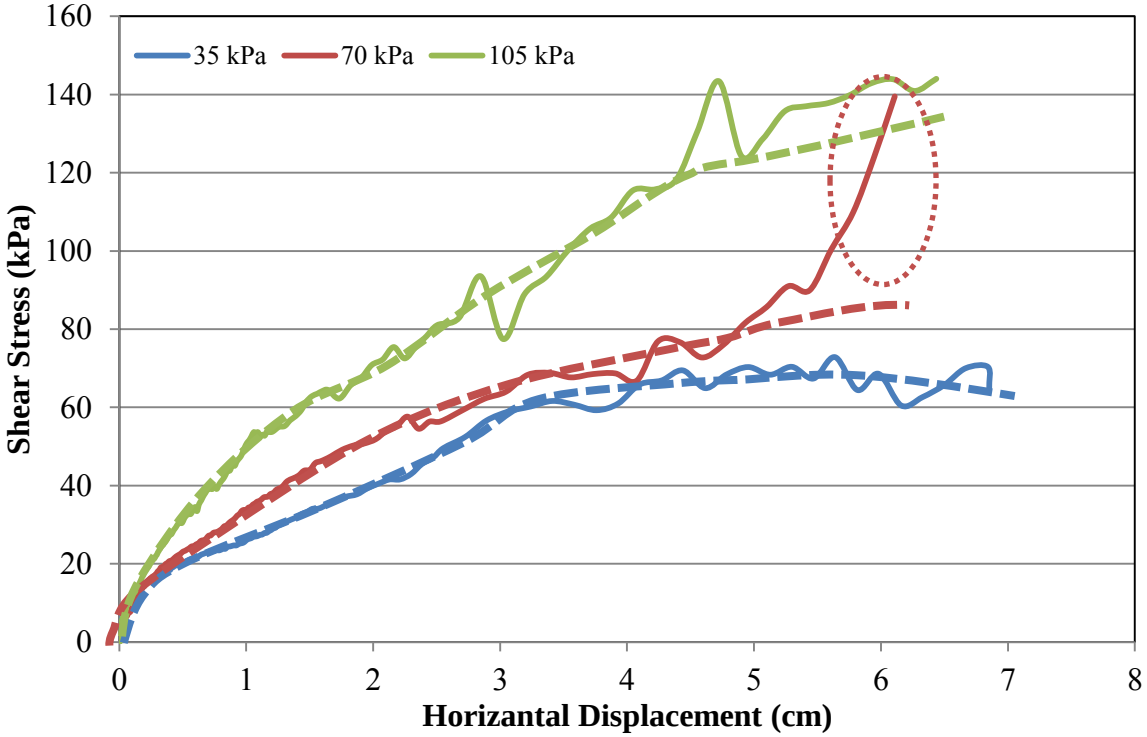

Figure 5.3.10 Shear stress versus horizontal displacement of ballast fouled with 30% clay

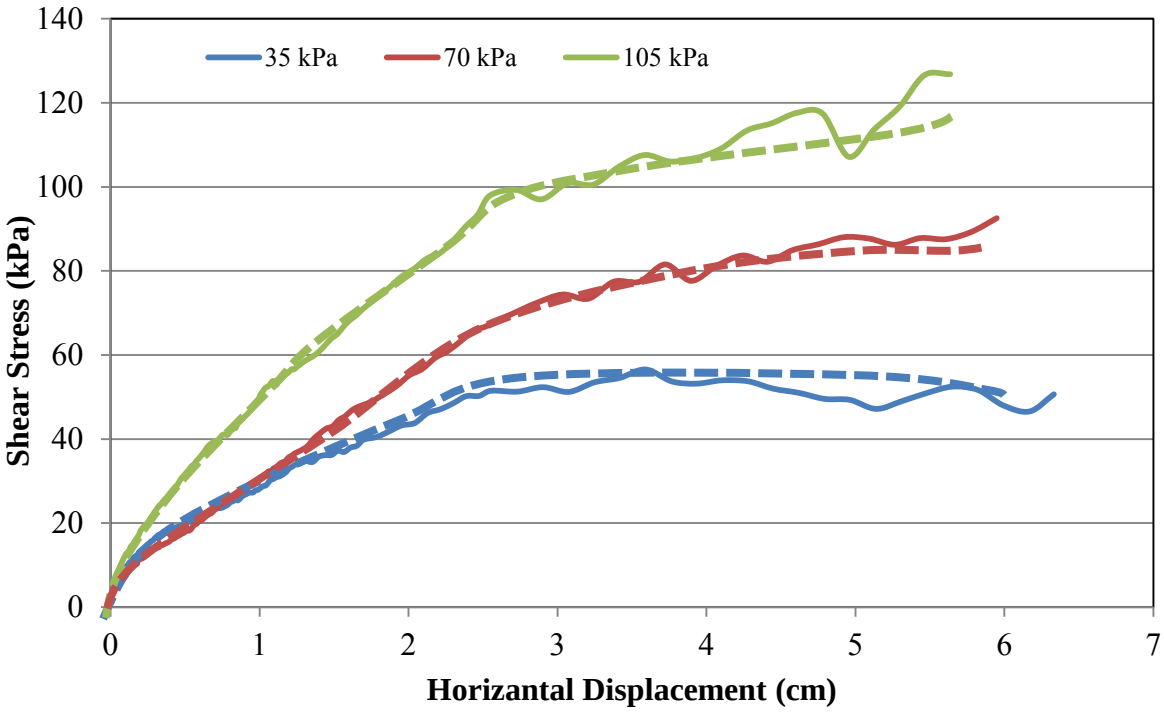

Figure 5.3.11 Shear stress versus horizontal displacement of ballast fouled with 40% clay

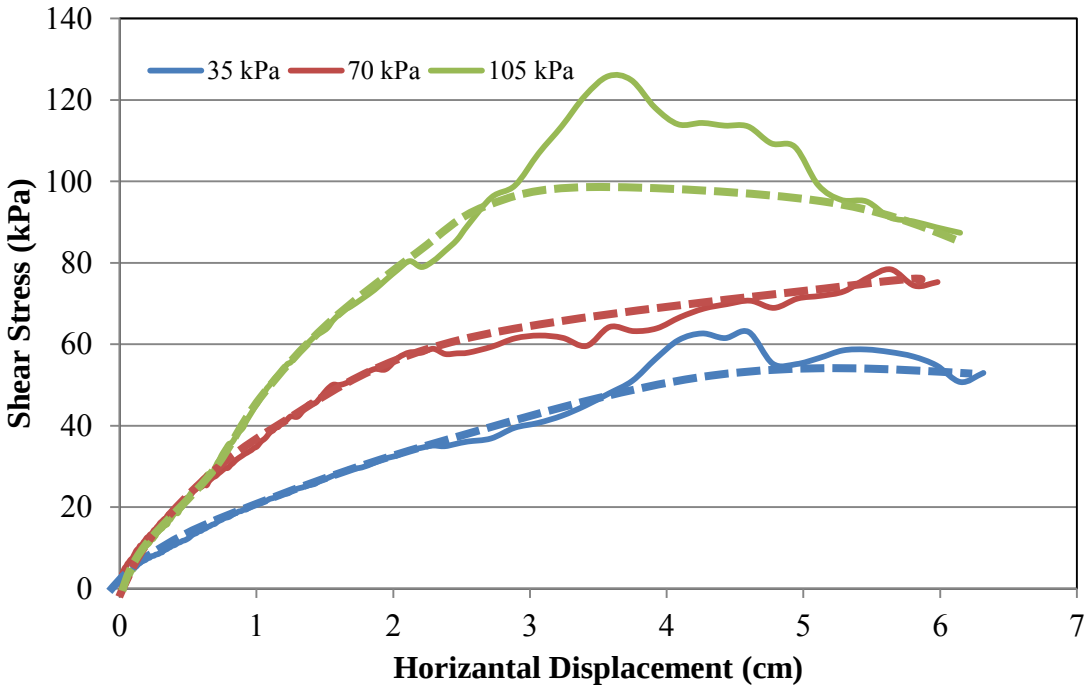

Figure 5.3.12 Shear stress versus horizontal displacement of ballast fouled with 50% clay

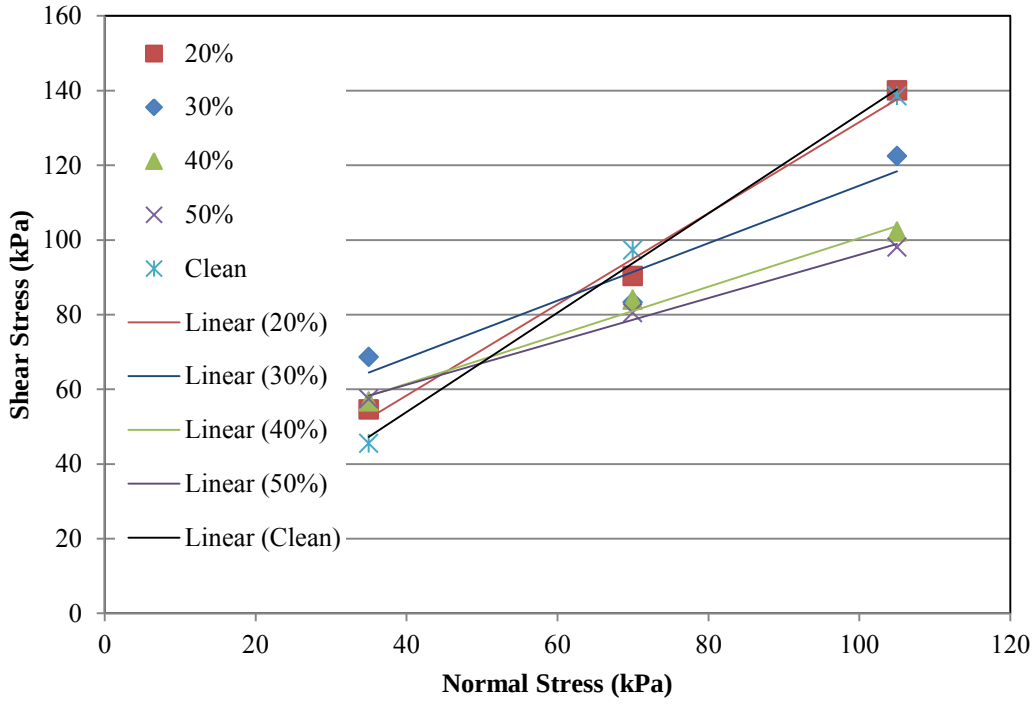

Figure 5.3.13 Failure envelopes of clean ballast and fouled ballast with clay

.

Figures 5.3.9 through 5.3.12 show the shear stress versus horizontal displacement of fouled ballast with clay. Figure 5.3.13 presents the comparison of failure envelopes of clean ballast and fouled ballast with clay at different fouling ratios. The trend of decreasing strength as the fouling ratio increases is similar to that observed for fouled ballast with crushed ballast fines. However, the friction angles are lower compared with crushed ballast fines which was expected due to the differences in the properties of crushed ballast fines and clay.

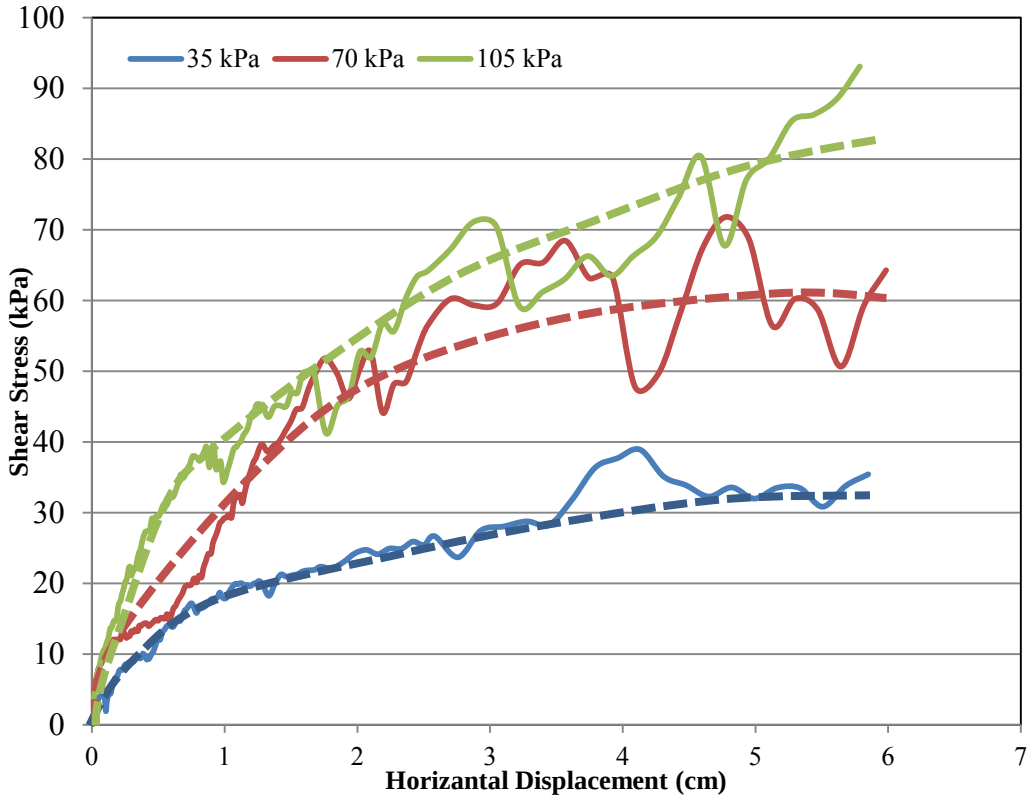

Figure 5.3.14 Shear stress versus horizontal displacement of ballast fouled with 10% coal dust

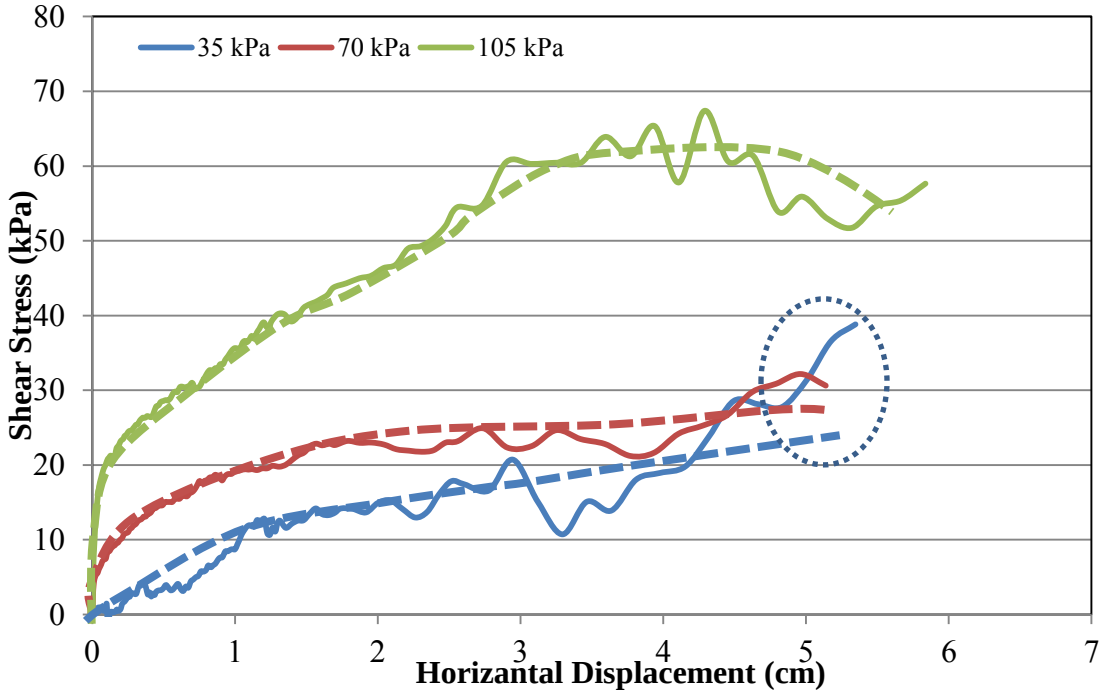

Figure 5.3.15 Shear stress versus horizontal displacement of ballast fouled with 20% coal dust

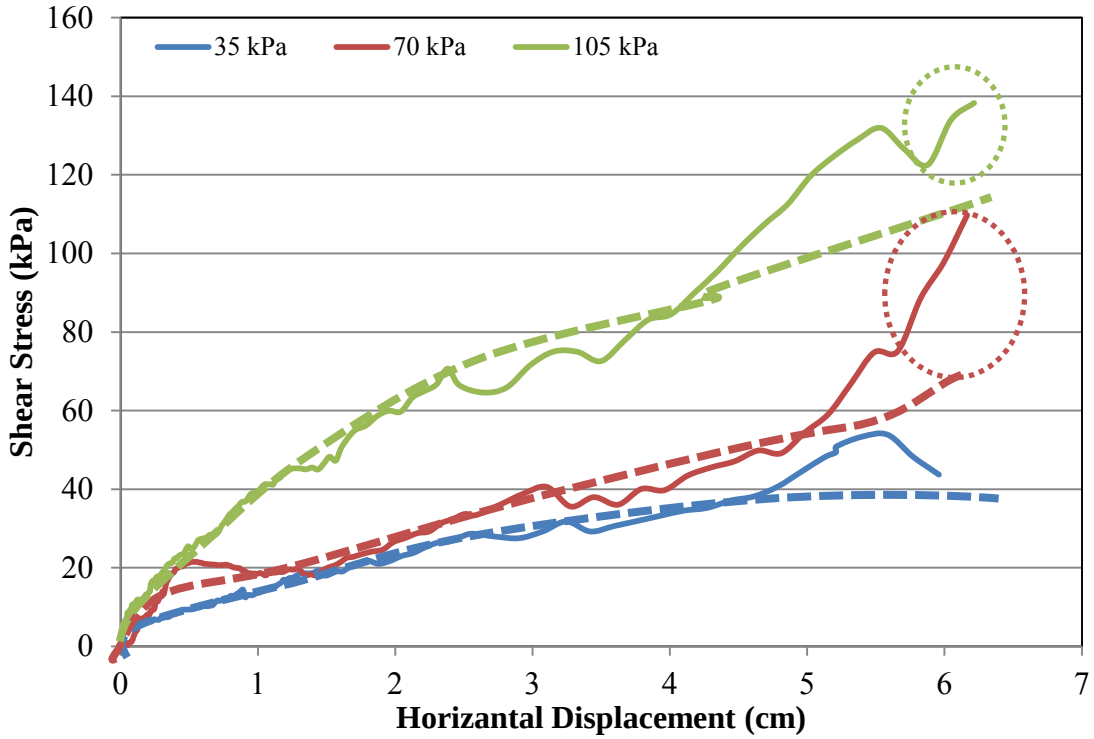

Figure 5.3.16 Shear stress versus horizontal displacement of ballast fouled with 30% coal dust

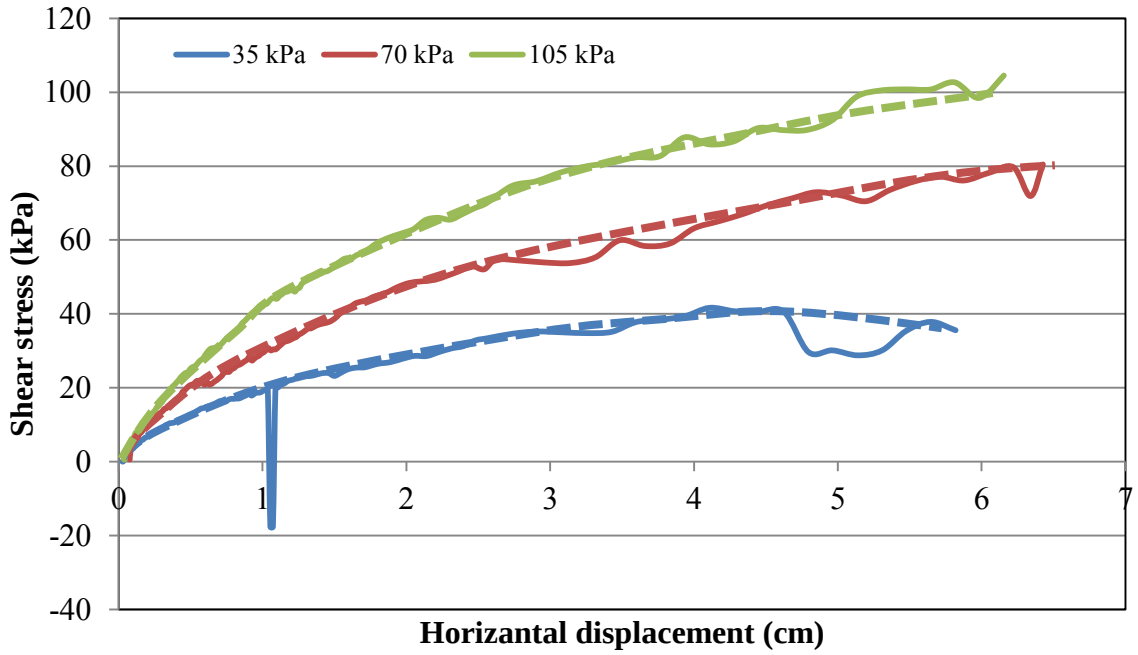

Figure 5.3.17 Shear stress versus horizontal displacement of ballast fouled with 40% coal dust

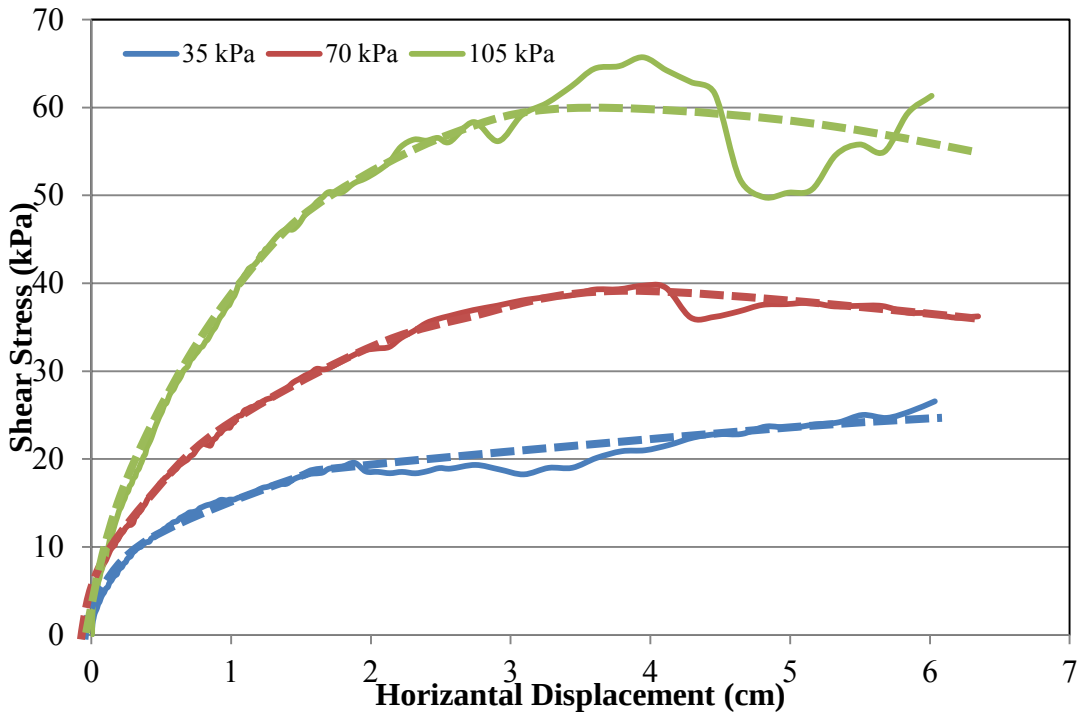

Figure 5.3.18 Shear stress versus horizontal displacement of ballast fouled with 50% coal dust

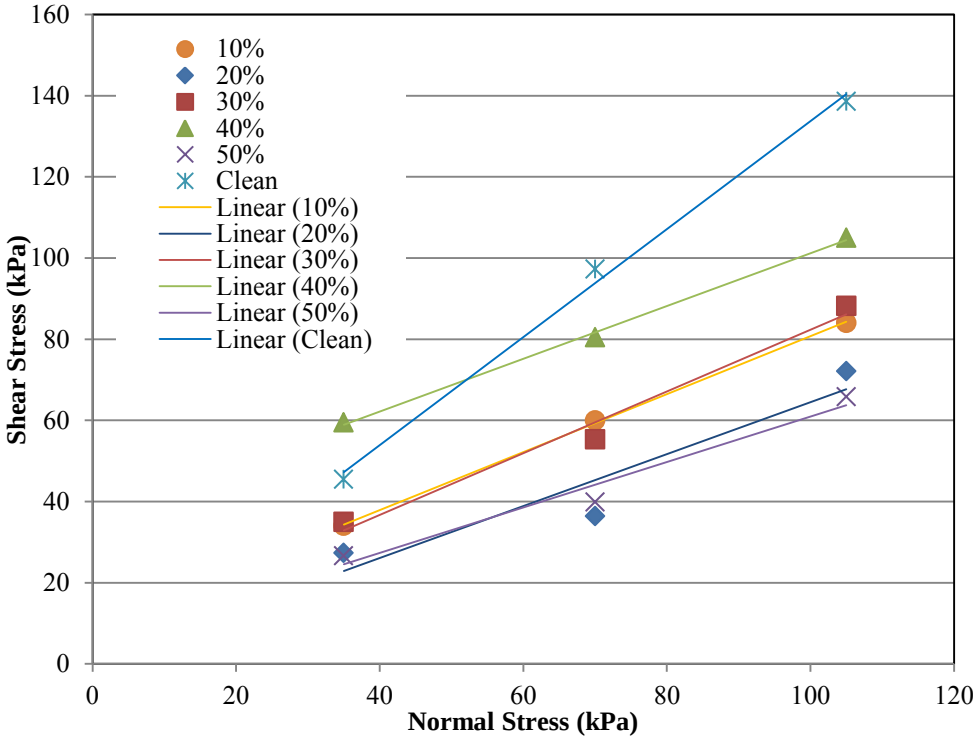

Figure 5.3.19 Failure envelopes of clean ballast and fouled ballast with coal dust

Figures 5.3.14 through 5.3.18 show the shear stress versus horizontal displacement of fouled ballast with coal dust at different fouling ratios. An a additional set of tests of 10% fouled ballast with coal dust were performed and evaluated as shown in section 5.3. According to Huang, ballast fouled with 15% coal dust or more decreases strength significantly (Huang 2009). Therefore, it was beneficial to examine the behavior of fouled ballast with coal dust at 10% and compare the results with different fouling ratios. Moreover, the results for the 20% through 40% fouled ballast with coal dust were inconsistent compared to clay and crushed ballast fines. Figure 5.3.19 presents the comparison of failure envelopes of clean and fouled ballast with coal dust. More evident from the figure, the 40% fouled ballast has higher strength than 20 and 30% fouled ballast, which is not consistent with the expected trend. However, fouled material can gain strength as voids are filled and the sample becomes more dense. Yet, as the fouling ratio increases the ballast particles will be separated and therefore the strength will decrease eventually (Anbazhagan 2010).

Figure 5.3.20 shows a comparison of failure envelopes for clean ballast and fouled ballast at 30% fouling with crushed ballast fines, clay and coal dust. As evident from the figure, coal dust fouled ballast show a significant decrease in strength at 30% fouling compared to clean ballast and other fouling materials.

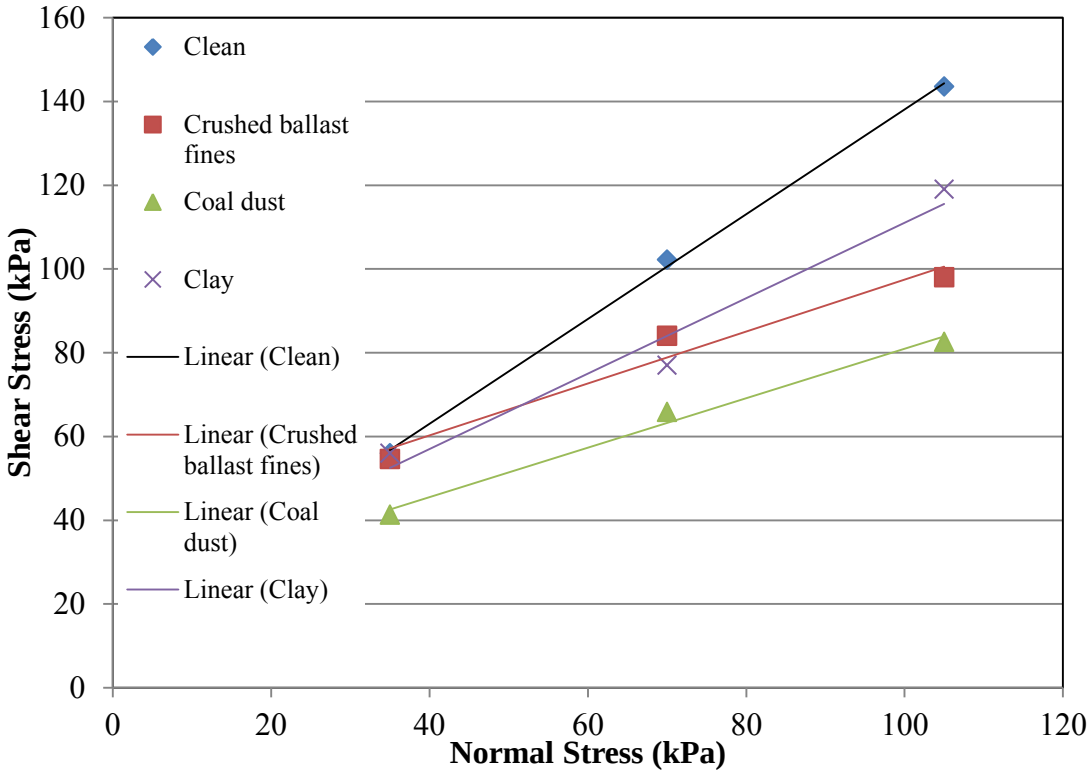

Figure 5.3.20 Comparison of failure envelopes of clean and fouled ballast at 30% fouling

Overall, the trend shows as the fouling ratio increased the friction angle decreased, especially for coal dust and clay. The properties of coal dust and clay resulted in decreases in the strength of ballast and therefore the results shows a similar pattern compared with the hydraulic conductivity of fouled ballast.

However, the crushing of the ballast particles and the tilting of the top plate which caused inaccurate results and high cohesion values. Figure 5.3.21 show the tilting of the top plate during a direct shear test.

Figure 5.3.21. Top plate tilt during direct shear test

5.4 Modified Direct Shear Test Data

The direct shear box was modified by increasing the height of both halves to reduce the crushing of particles and allow more particle movement. The same set of tests and sample preparations were implemented in the modified direct shear box as in the direct shear box and the results were compared. Section 5.4 shows the results of direct shear tests and presents the shear stress and horizontal displacement relationships and comparisons of the failure envelopes of each fouling material at different fouling ratios. A dashed curve was plotted on each stress-displacement curve to show the stress-displacement trend and neglecting the individual variations in the trend caused by particle crushing. Figures 5.4.1 through 5.4.17 present the results of direct shear tests of clean and fouled ballast at the three normal pressures.

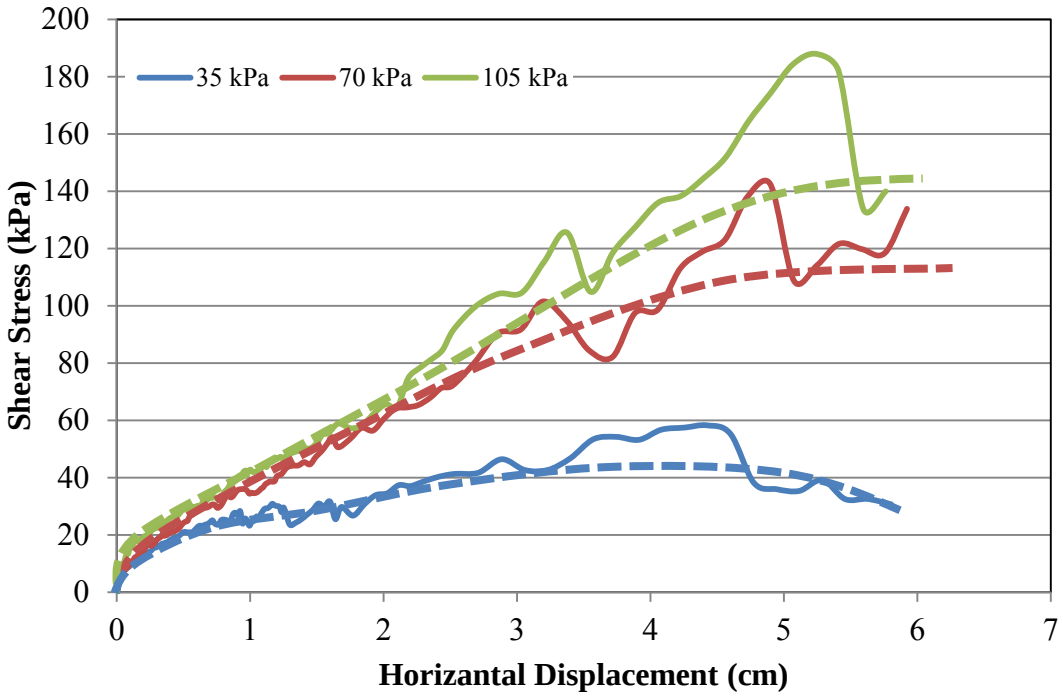

Figure 5.4.1 Shear stress versus horizontal displacement of clean ballast

Figure 5.4.1 shows the shear stress versus horizontal displacement for clean ballast at three different normal stresses. Crushing of the particles was observed during the test but only under high normal pressure. The cohesion value was above zero and that could be due to sample variation or the friction of the ballast particles and the wall of the box.

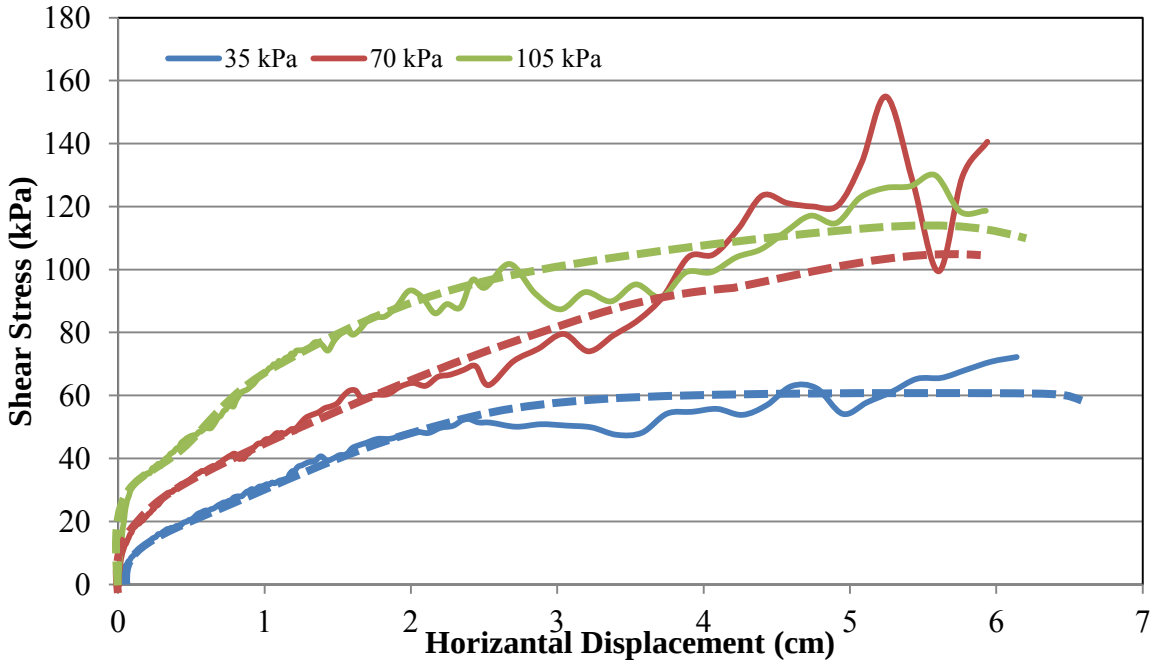

Figure 5.4.2 Shear stress versus horizontal displacement of ballast fouled with 20% crushed ballast fines

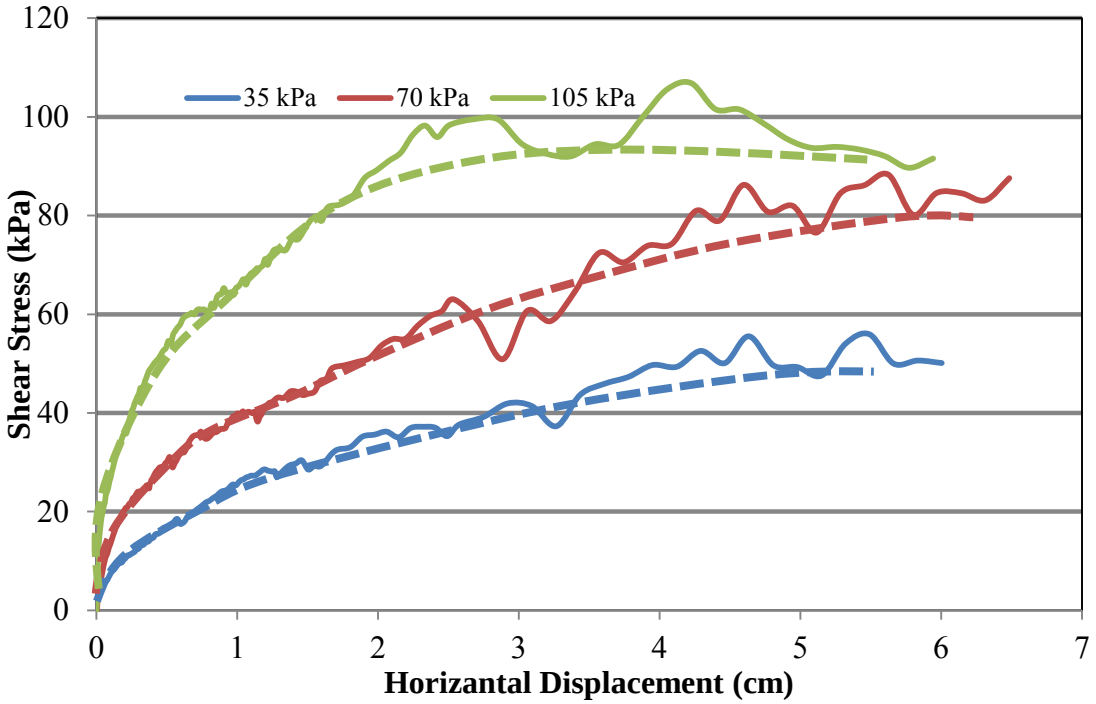

Figure 5.4.3 Shear stress versus horizontal displacement of ballast fouled with 30% crushed ballast fines

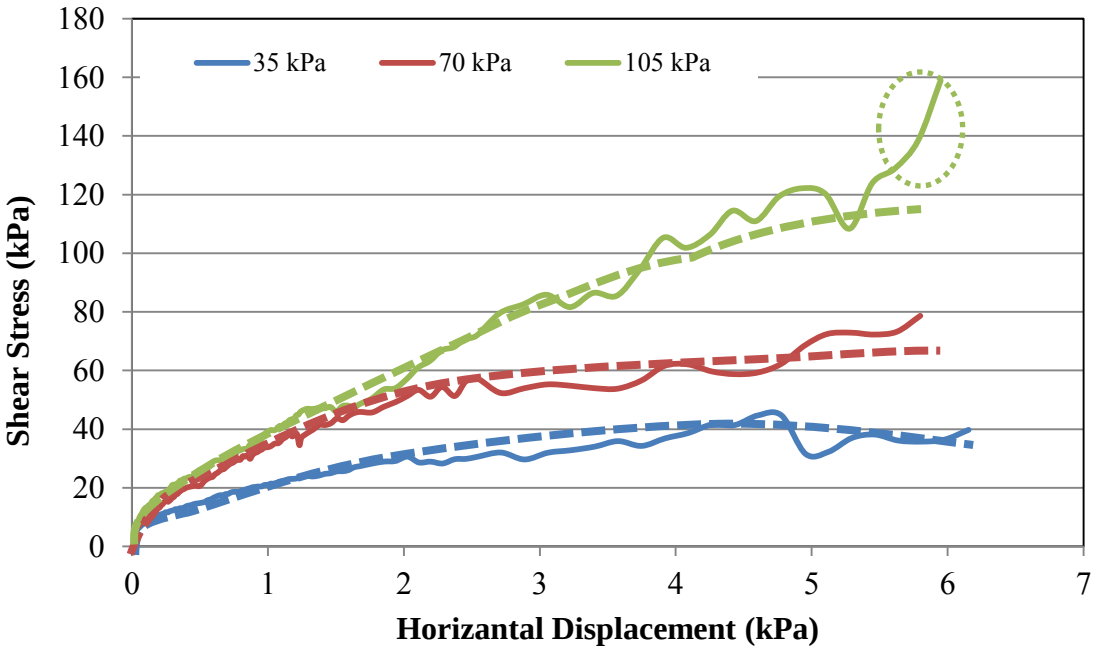

Figure 5.4.4 Shear stress versus horizontal displacement of ballast fouled with 40% crushed ballast fines

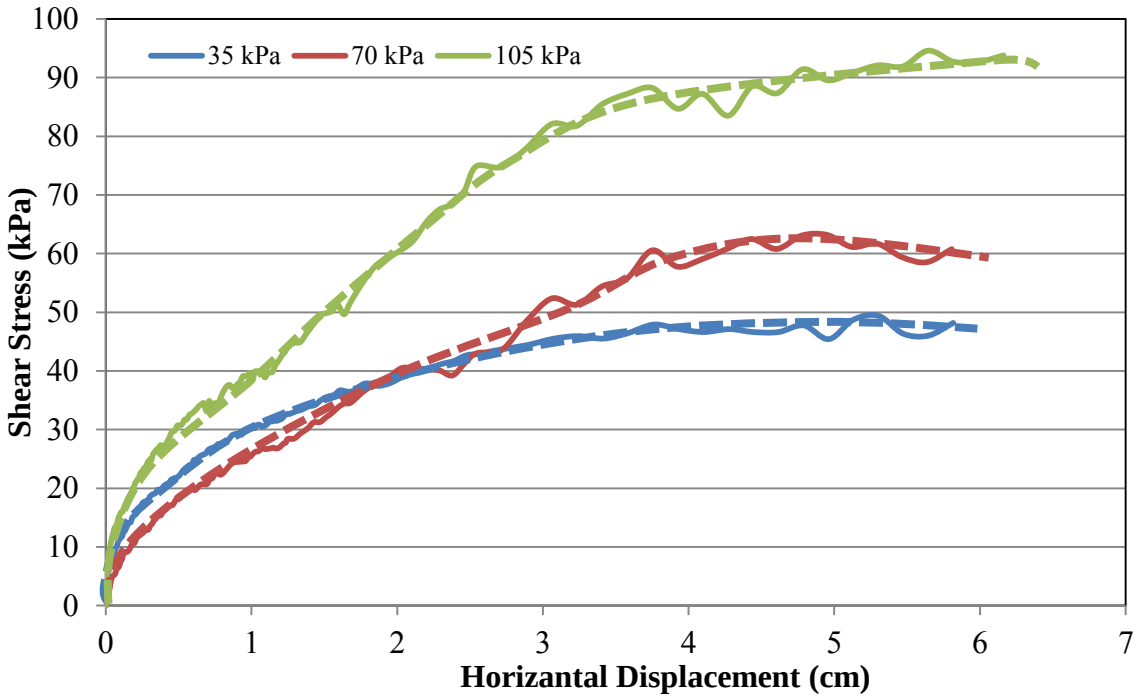

Figure 5.4.5 Shear stress versus horizontal displacement of ballast fouled with 50% crushed ballast fines

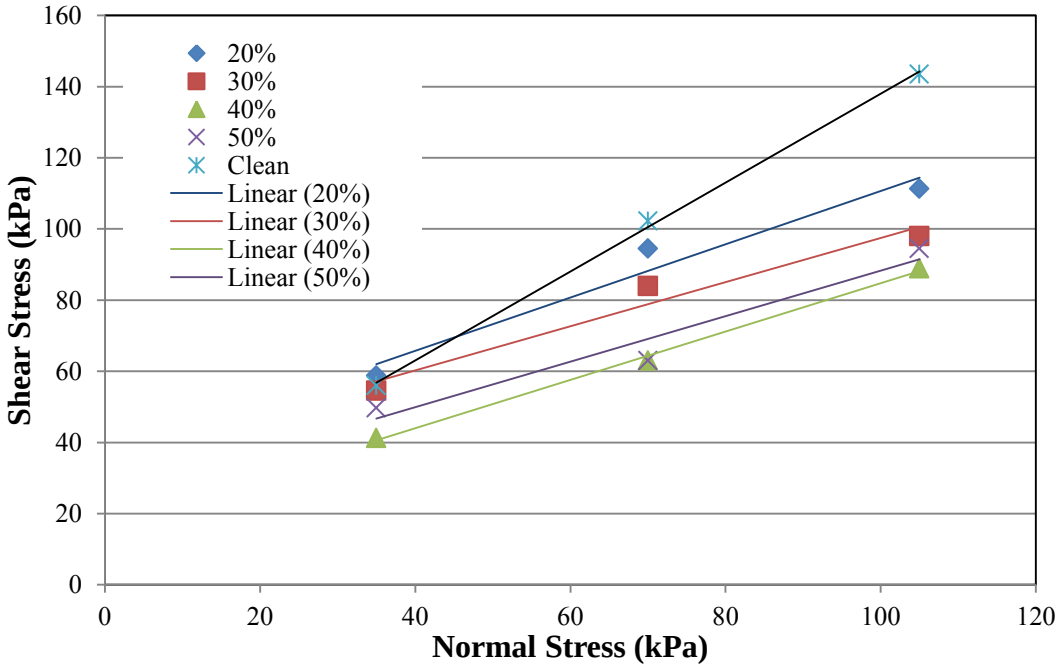

Figure 5.4.6 Failure envelopes of clean ballast and fouled ballast with crushed ballast fines

Figures 5.4.2 through 5.4.5 show the shear stress and horizontal displacement relationship for different fouling ratios with crushed ballast fines. The trend shows as the fouling ratio increased, shear strength generally decreased. Crushing of particles evidently occurred during some the tests as shown in figures 5.4.2 (at normal pressure of 70 kPa) and 5.4.4 (at normal pressure of 105 kPa). The results in figure 5.4.6 show a pattern of decrease in the friction angle as the fouling ratio of crushed ballast fines increased.

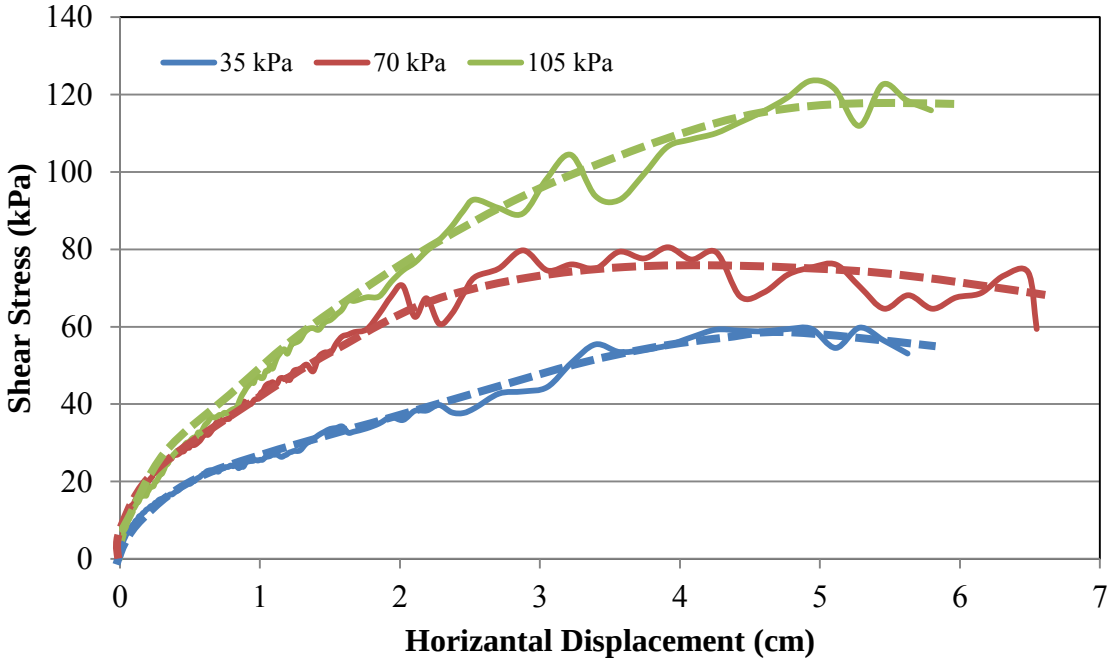

Figure 5.4.7 Shear stress versus horizontal displacement of ballast fouled with 20% clay

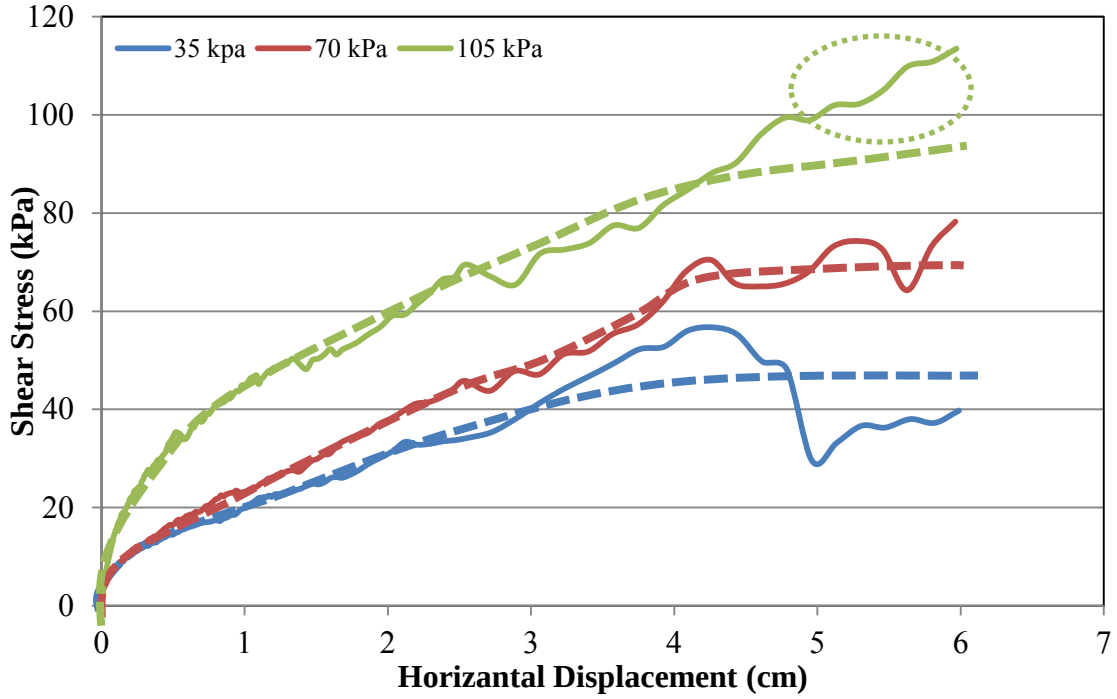

Figure 5.4.8 Shear stress versus horizontal displacement of ballast fouled with 30% clay

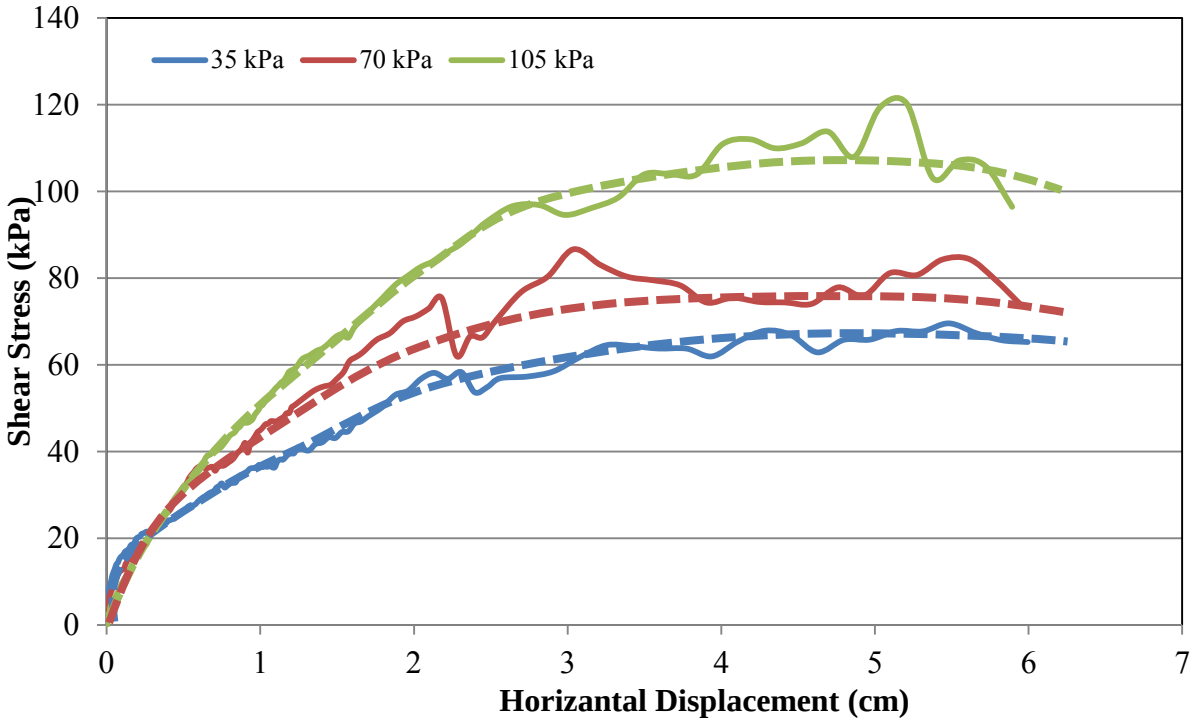

Figure 5.4.9 Shear stress versus horizontal displacement of ballast fouled with 40% clay

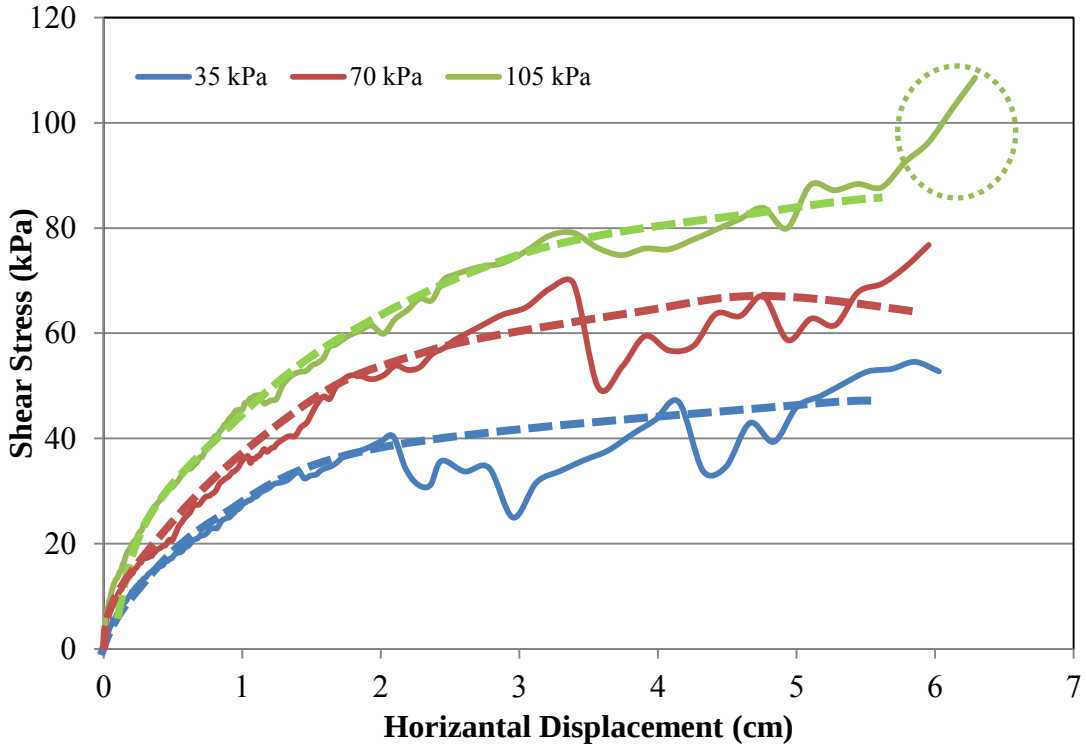

Figure 5.4.10 Shear stress versus horizontal displacement of ballast fouled with 50% clay

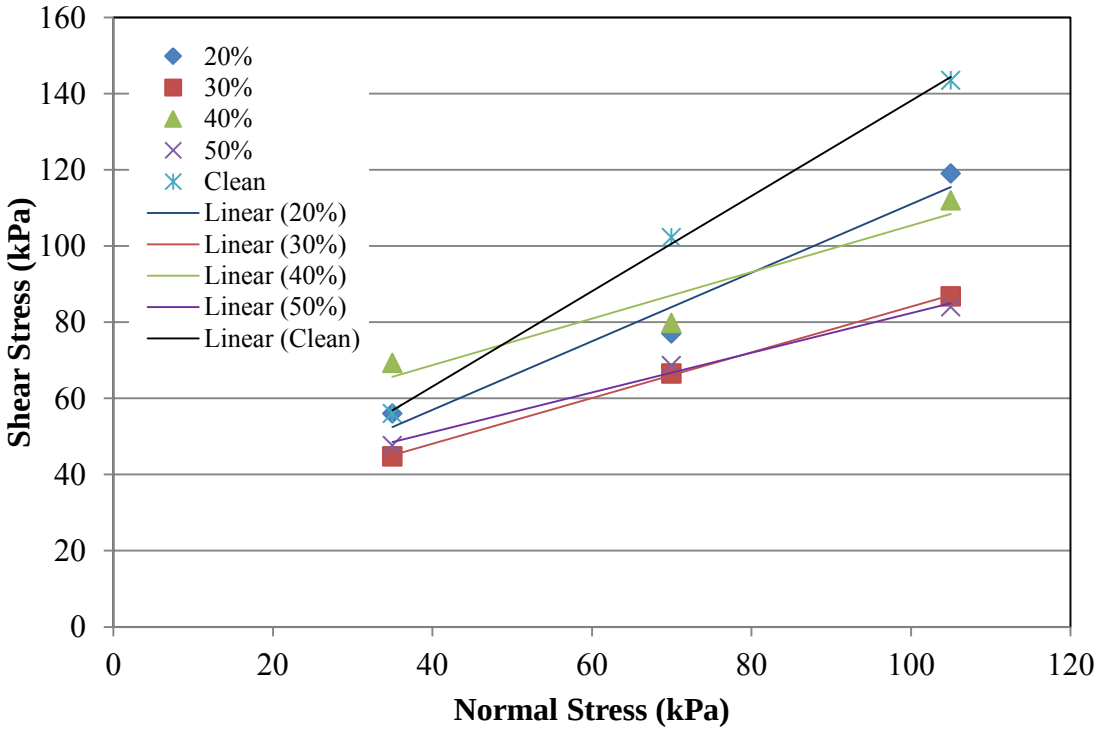

Figure 5.4.11 Failure envelopes of clean ballast and fouled ballast with clay

Figures 5.4.7 through 5.4.10 show the shear stress and horizontal displacement relationship as the percentage of clay increased. A similar trend for the crushed ballast fines could be interpreted from the results shown in these figures. However, the 40% fouled sample with clay was determined to have higher shear strength than 30% fouled sample which does not follow the expected pattern. As voids are partially filled with clay particles, the free movements of ballast particles are limited and the strength of the sample may increase temporarily and that could be the reason the sample gained strength at 40% fouling.

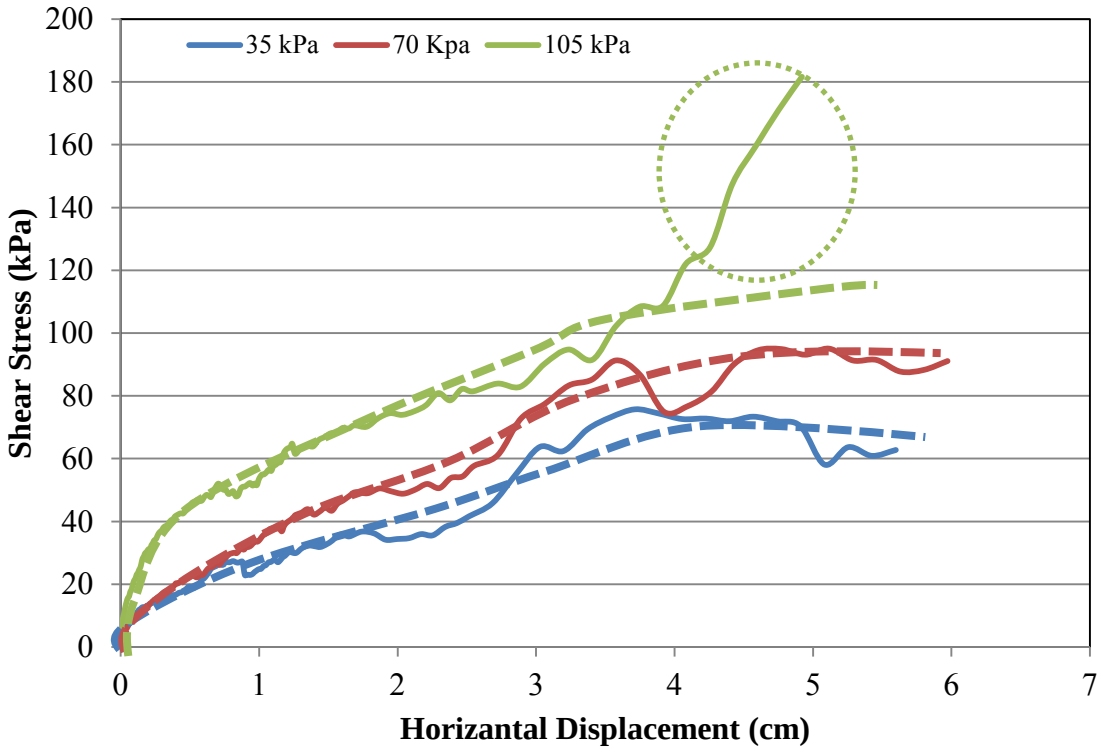

Figure 5.4.12 Shear stress versus horizontal displacement of ballast fouled with 10% coal dust

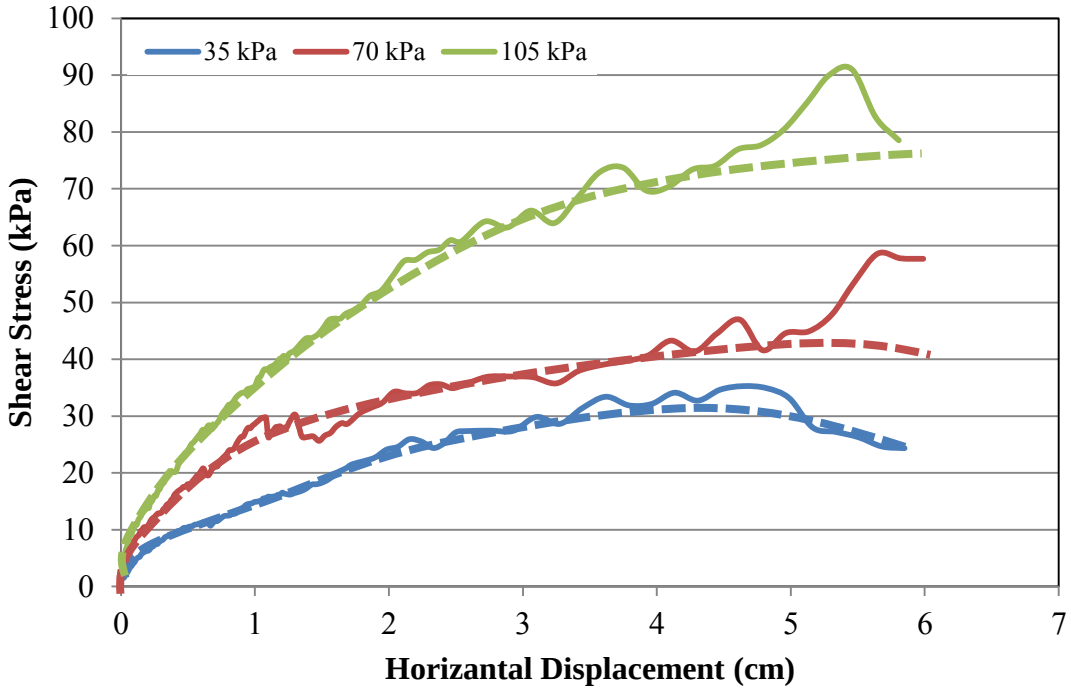

Figure 5.4.13 Shear stress versus horizontal displacement of ballast fouled with 20% coal dust

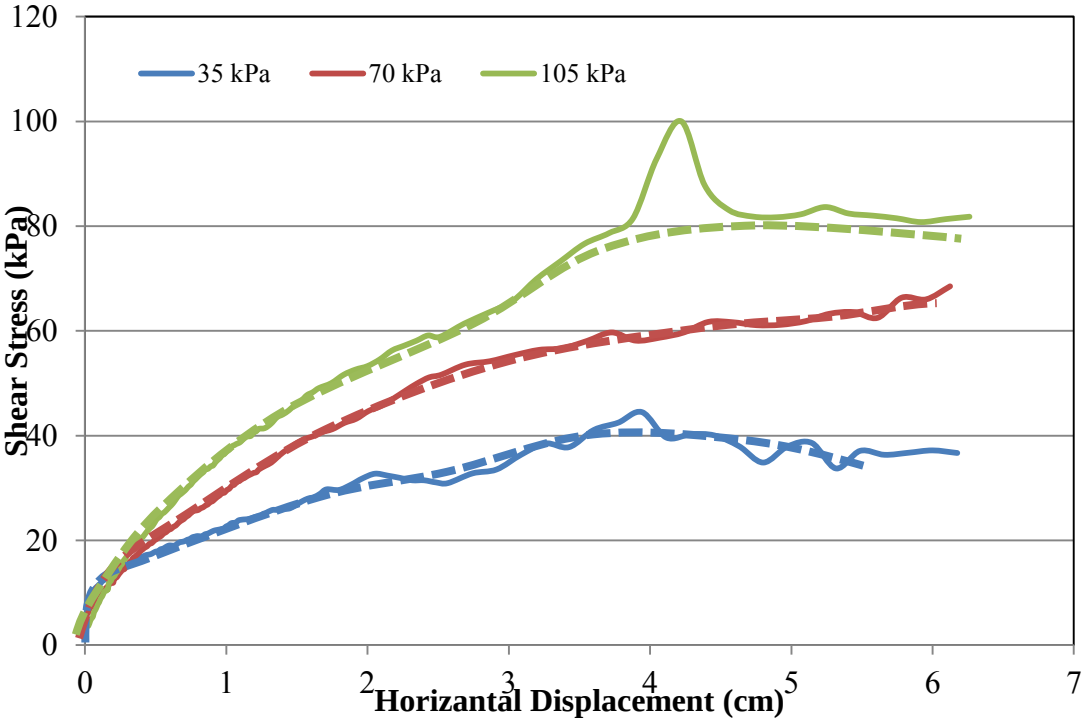

Figure 5.4.14 Shear stress versus horizontal displacement of ballast fouled with 30% coal dust

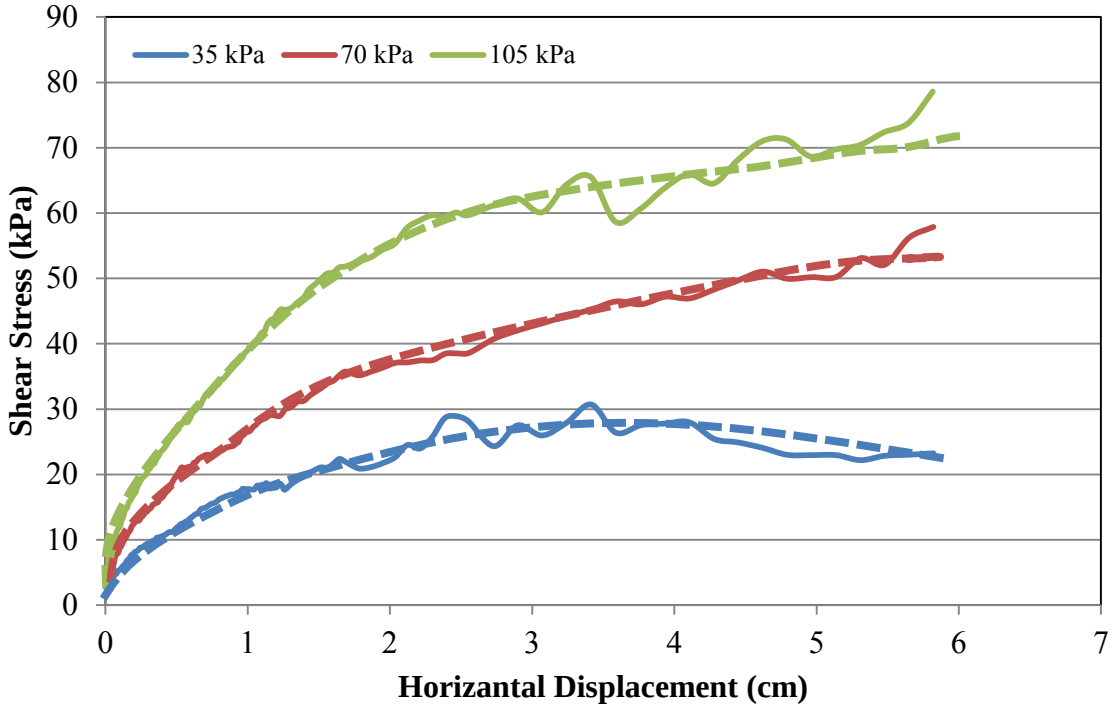

Figure 5.4.15 Shear stress versus horizontal displacement of ballast fouled with 40% coal dust

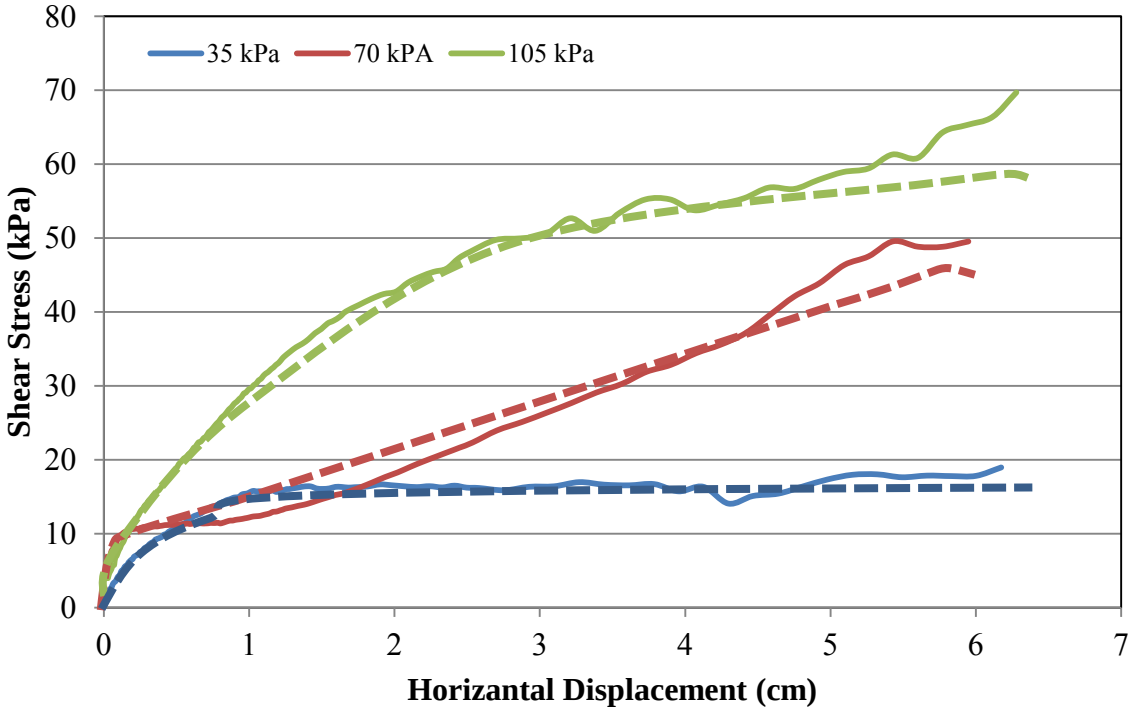

Figure 5.4.16 Shear stress versus horizontal displacement of ballast fouled with 50% coal dust

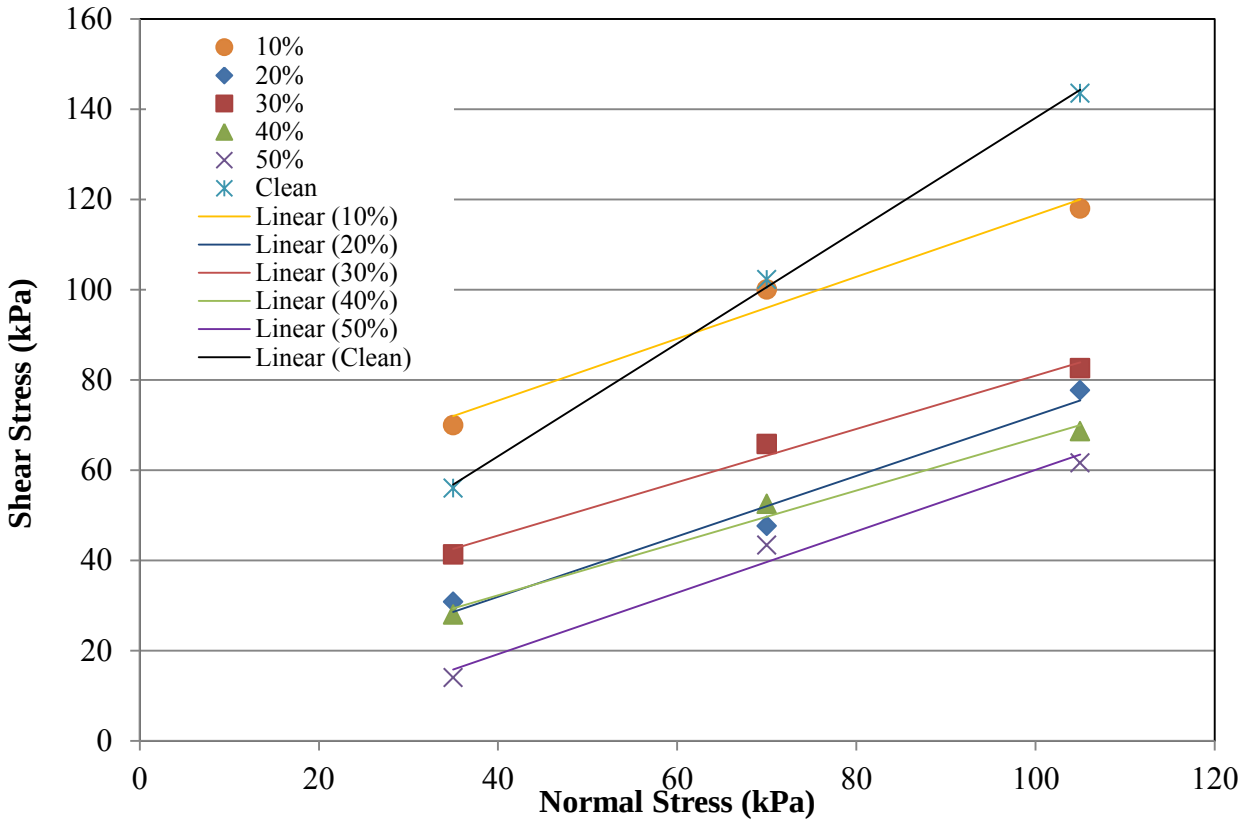

Figure 5.4.17 Failure envelopes of clean ballast and fouled ballast with coal dust

Figures 5.4.12 through 5.4.17 show the results of strength tests on ballast fouled with coal dust for different fouling ratios. The results show a similar trend with the strength of sample decreasing as the fouling ratio increased,. Also, figure 5.4.17 show a significant decrease in shear strength for sampleswith more than 10% coal dust.

Overall, the results show a similar trend for all fouling material which indicates that as fouling ratio increased, strength of fouled ballast decreased. For the modified direct shear box, the results are more well-defined compared with results from the direct shear box as shown in the failure of envelopes graphs. The strength of ballast decreased significantly with coal dust fouled ballast and clay fouled ballast as the fouling ratio increased. Figure 5.4.18 shows a comparison of

failure envelopes for clean ballast and fouled ballast at 30% fouling with crushed ballast fines, clay and coal dust. As evident from the figure, coal dust fouled ballast show a significant decrease in strength at 30% fouling compared to clean ballast and other fouling materials. The results are consistent with the permeability test results as the hydraulic conductivity of fouled ballast with coal dust decreased significantly compared with other fouling materials.

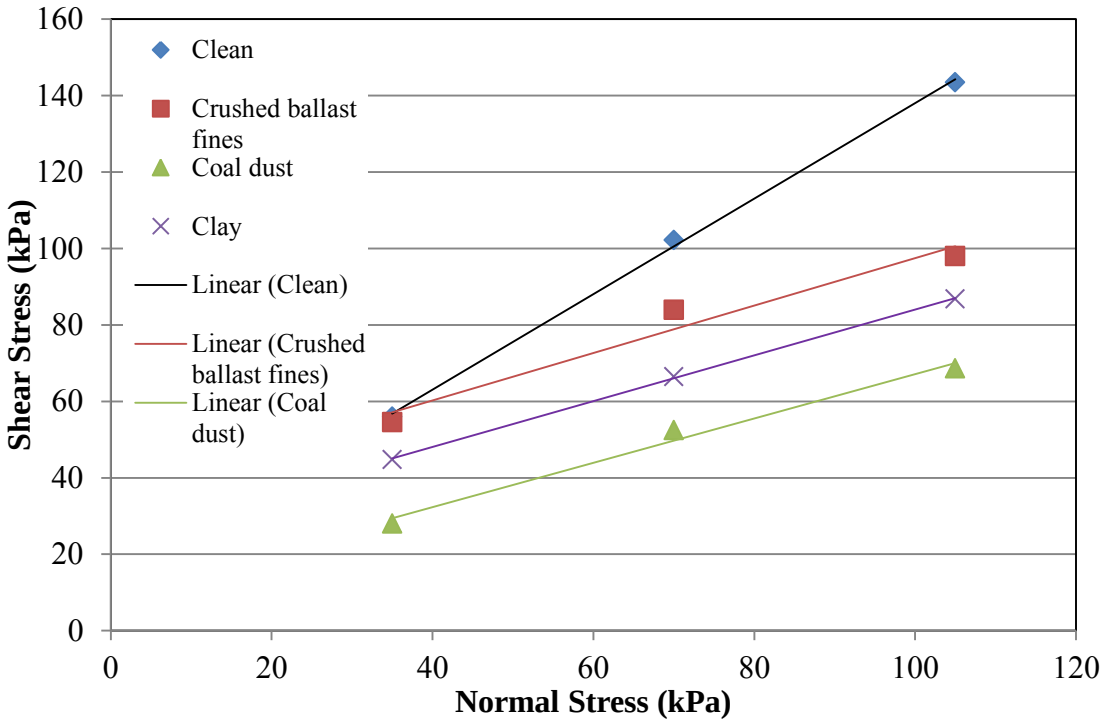

Figure 5.4.18 Comparison of failure envelopes of clean and fouled ballast at 30% fouling

5.5 Summary of Large Direct Shear Box and Modified Direct Shear Box Tests Results

This section presents a summary of direct shear results for the large direct shear box tests and modified direct shear tests. Table 5.5.1 present strength properties (friction angle and cohesion) of clean and fouled ballast for both the direct shear and modified direct shear tests. Figure 5.5.1 shows the comparison of friction angles of clean and fouled ballast for each fouling material tested in the direct shear box. Figure 5.5.2 presents the friction angles of clean and fouled ballast for each fouling material tested in the modified direct shear box.

Table 5.5.1 Summary of strength properties for direct shear and modified direct shear box tests

	Large Direct Shear Box Data			**Modified Direct Shear Box Data**		
Fouling Material	Condition	Cohesion (kPa)	ϕ◦	Condition	Cohesion (kPa)	ϕ◦
NA	Clean	0	53	Clean	13.3	51.3
Coal dust	10%	9.3	35.5	10%	36.3	34.3
	20%	6.3	35.4	20%	4.9	33.8
	30%	6.3	37	30%	21.7	31
	40%	36.1	33	40%	9.1	30.3
	50%	16.8	22.1	50%	0	31.4
Crushed ballast fines	20%	22.4	47	20%	35.7	37
	30%	16.1	45.8	30%	35.7	31.8
	40%	5.6	48.2	40%	16.8	34.2
	50%	21	39.7	50%	23.8	32.9
Clay	20%	17.8	49	20%	21	42
	30%	37.8	37.6	30%	23.8	31
	40%	35.7	33	40%	44.8	31.2
	50%	37.8	30.1	50%	30.1	27.5

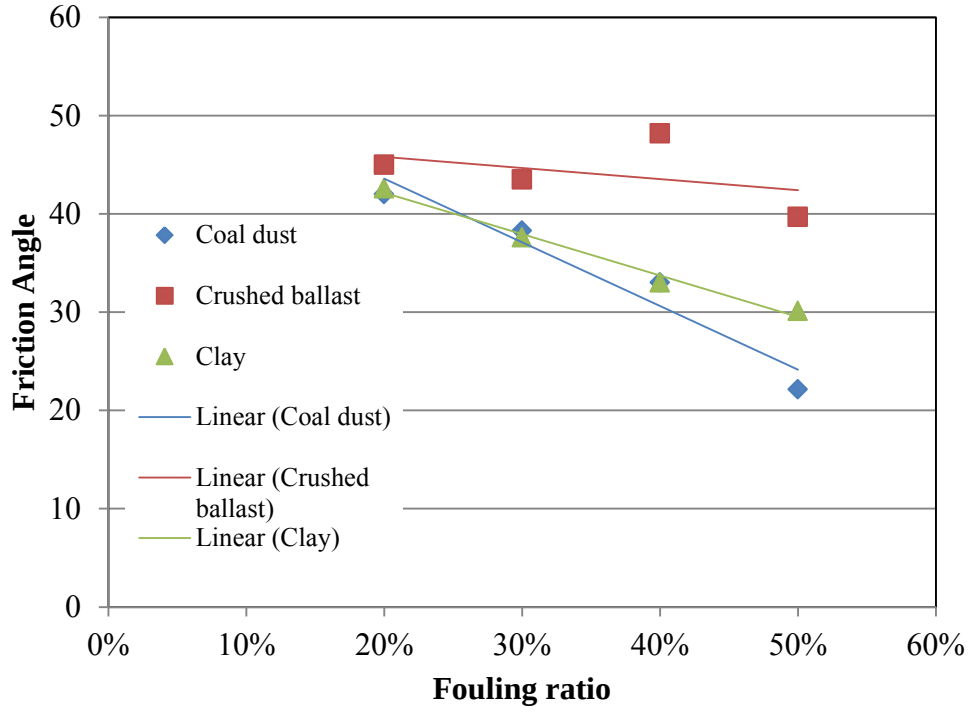

Figure 5.5.1 Friction angle versus fouling ratio for each fouling material (large direct shear box)

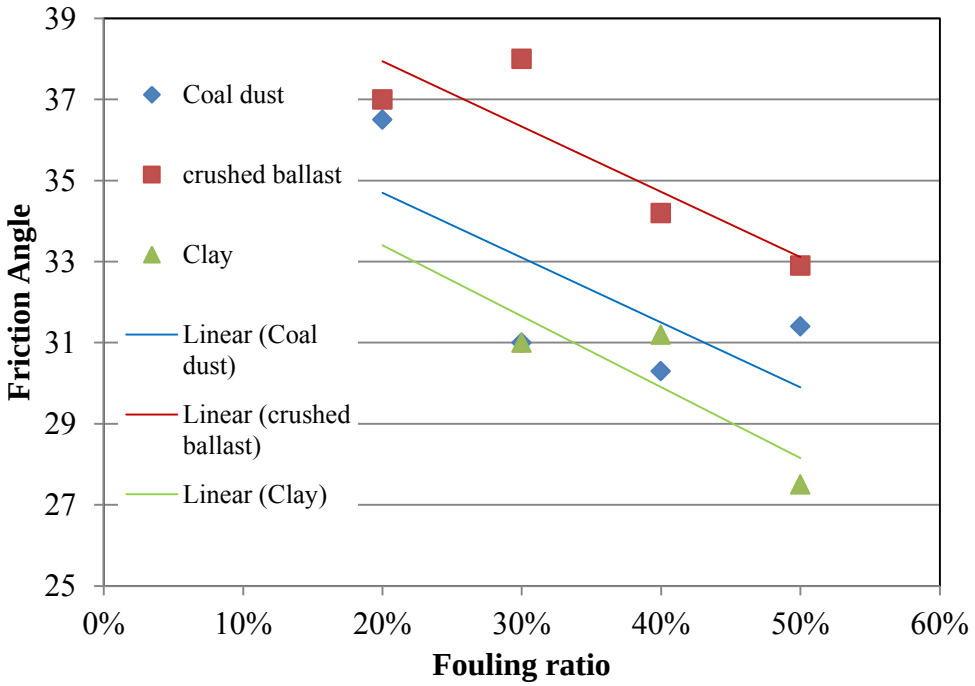

Figure 5.5.2 Friction angle versus fouling ratio for each fouling material (modified box)

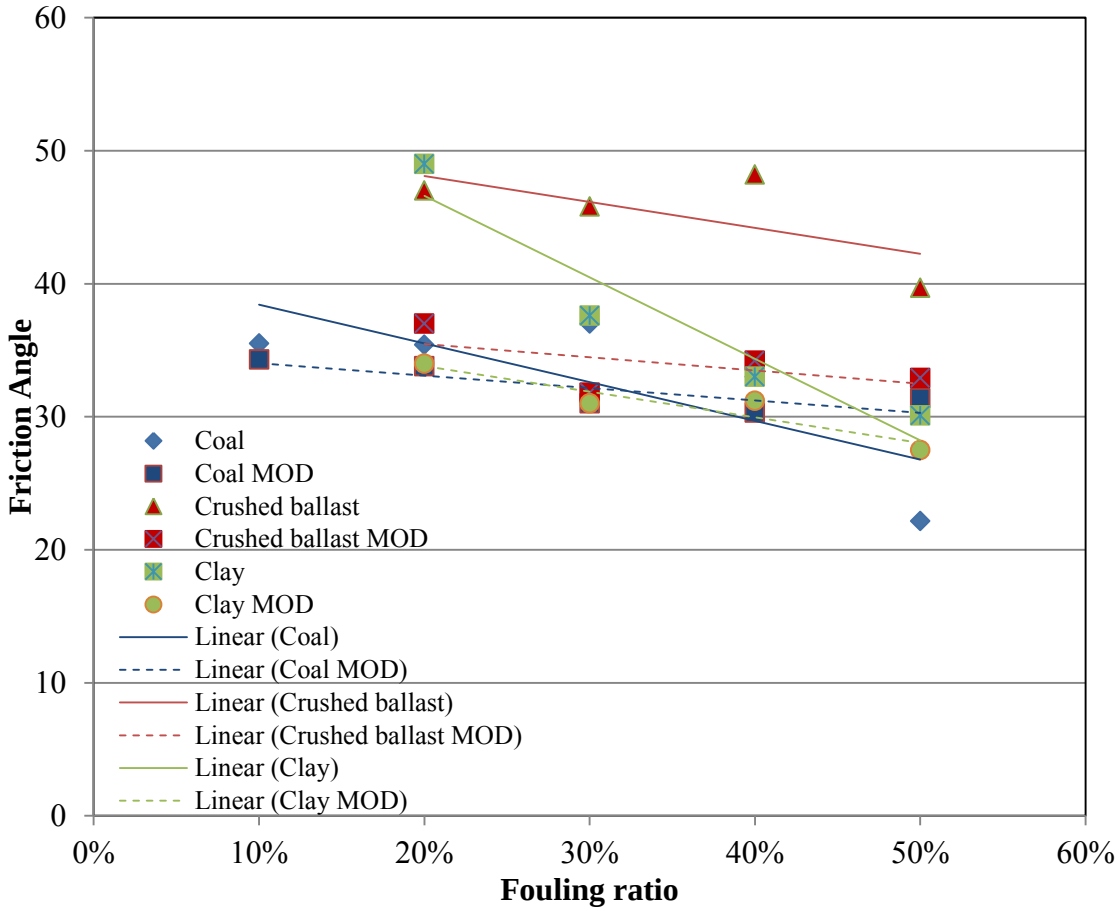

Figure 5.5.3 Comparison of large direct shear and modified direct shear friction angle versus fouling ratio for each fouling material

Table 5.5.1 shows the summary of strength test results of the large direct shear box and modified direct shear box. Both sets of results show the same pattern of decrease in strength of ballast as fouling ratio increased. For the large direct shear box, the strength of ballast fouled with clay and coal dust fines decreased significantly. The properties of clay and coal dust reduced the strength of ballast as the percentage of fines increased. Figure 5.5.1 presents a comparison between the friction angle of fouled ballast with different fouling materials for

various fouling ratios. Coal dust fouled ballast show a significant decrease in friction angle at 50% fouling compared with clay and crushed ballast.

Moreover, the results for the modified direct shear box show a similar pattern as the large direct shear box; however, the results show that clay fines had a more significant effect on strength than coal dust at 50% fouling as shown in figure 5.5.2. Overall, coal dust and clay fines reduced the strength of ballast significantly as the fouling ratio increased. Figure 5.5.3 compares the results from large direct shear and modified direct shear of friction angle vs fouling ratio. The solid lines represent the results from large direct shear box and dashed lines represent the results from modified direct shear box.

5.6 Large Scale Resistivity Test

A large scale sample of heavily fouled ballast was constructed and tested under wet conditions. The four point Wenner method was used to measure resistivity at depths of eighteen inches, twelve inches and six inches. A wooden board with pre-drilled holes at a measured spacing was used to hold the rods during the test. The resistivity readings were taken after water was sprayed on top of the sample. According to Wenner's four point method, the depth of measurement is equal to the spacing of the rods, therefore, the resisitivity of the sample was measured at three depths. Figure 5.6.1 through 5.6.6 show a cross section of each test and a data sheet that show test conditions and results.

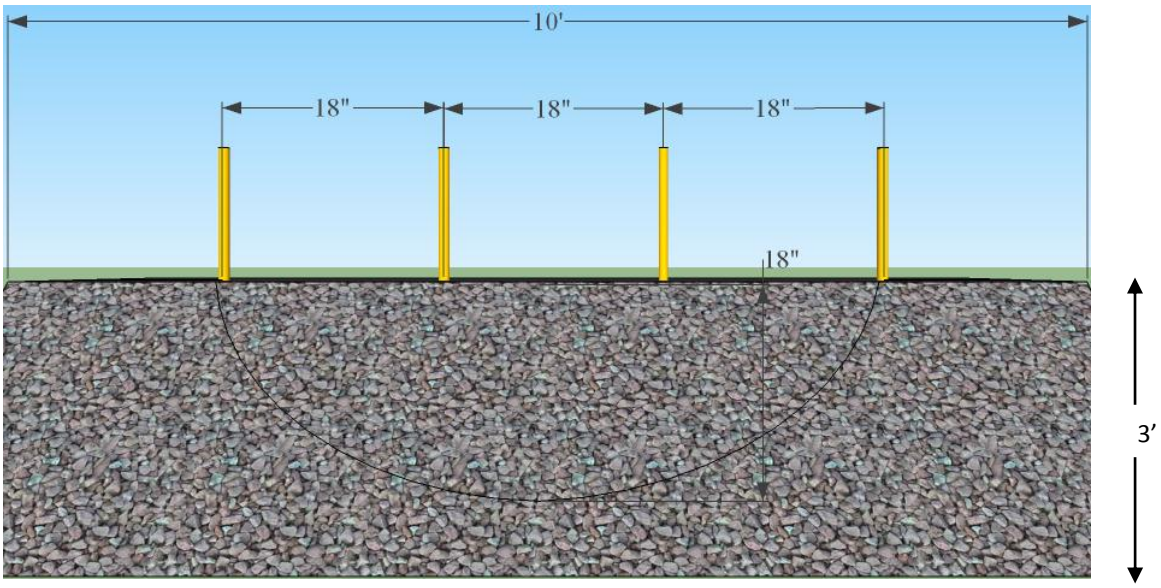

Figure 5.6.1 Schematic diagram of resistivity large scale test at depth of 18 inches

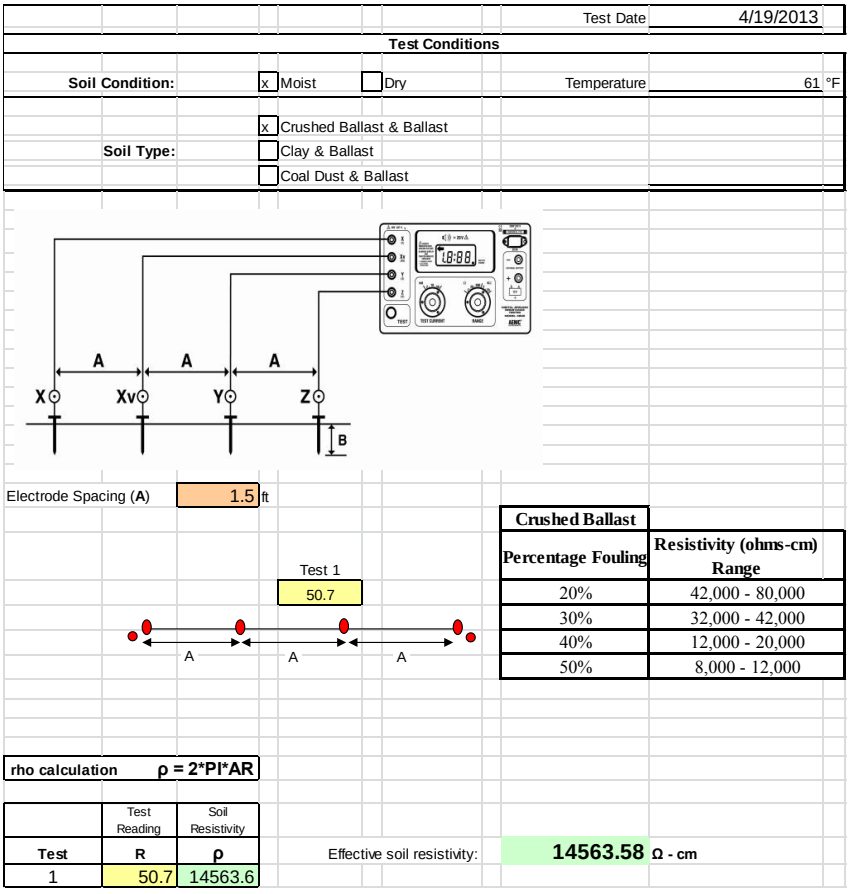

Test Date 4/19/2013

Test Conditions

Soil Condition: [x] Moist [ ] Dry Temperature 61 °F

Soil Type: [x] Crushed Ballast & Ballast [ ] Clay & Ballast [ ] Coal Dust & Ballast

Electrode Spacing (**A**) 1.5 ft

Test 1

50.7

Crushed Ballast	
Percentage Fouling	**Resistivity (ohms-cm) Range**
20%	42,000 - 80,000
30%	32,000 - 42,000
40%	12,000 - 20,000
50%	8,000 - 12,000

rho calculation ρ = 2*PI*AR

	Test Reading	Soil Resistivity
Test	**R**	**ρ**
1	50.7	14563.6

Effective soil resistivity: **14563.58** Ω - cm

Figure 5.6.2 Detailed data sheet for resistivity large scale test at depth of 18 inches (AEMC 2012)

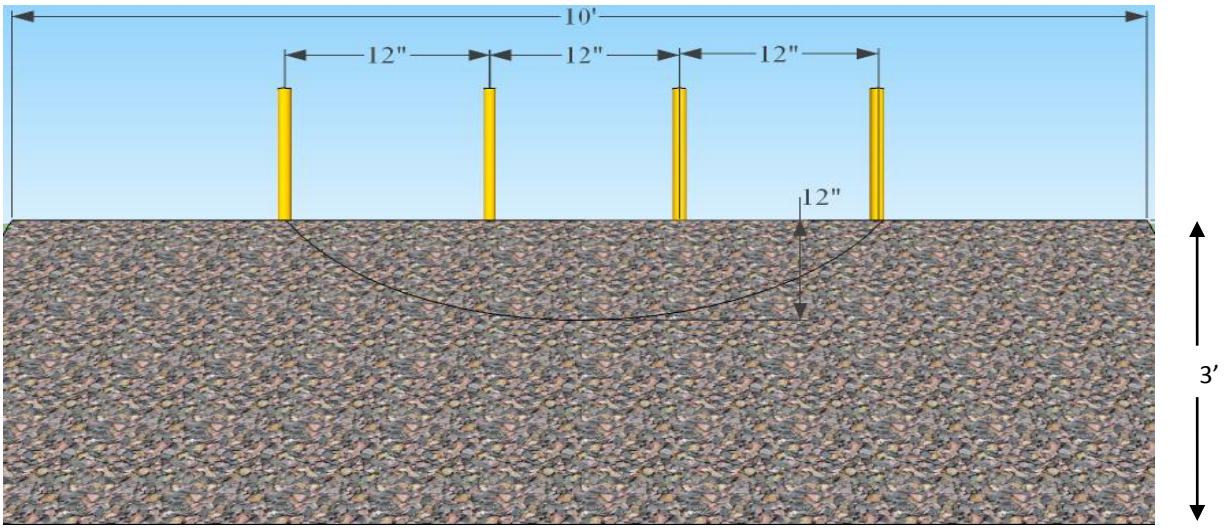

Figure 5.6.3 Schematic diagram of resistivity large scale test at depth of 12 inches

Test Date 4/19/2013

Test Conditions

Soil Condition: [x] Moist [ ] Dry Temperature 61 °F

Soil Type:
[x] Crushed Ballast & Ballast
[ ] Clay & Ballast
[ ] Coal Dust & Ballast

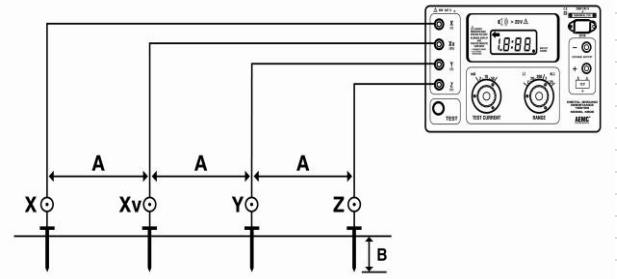

Electrode Spacing (**A**) 1 ft

Test 1
69.1

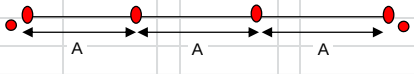

Crushed Ballast	
Percentage Fouling	**Resistivity (ohms-cm) Range**
20%	42,000 - 80,000
30%	32,000 - 42,000
40%	12,000 - 20,000
50%	8,000 - 12,000

rho calculation ρ = 2*PI*AR

	Test Reading	Soil Resistivity
Test	**R**	**ρ**
1	69.1	13232.7

Effective soil resistivity: **13232.65** Ω - cm

Figure 5.6.4 Detailed data sheet for large scale test at depth of 12 inches (AEMC 2012)

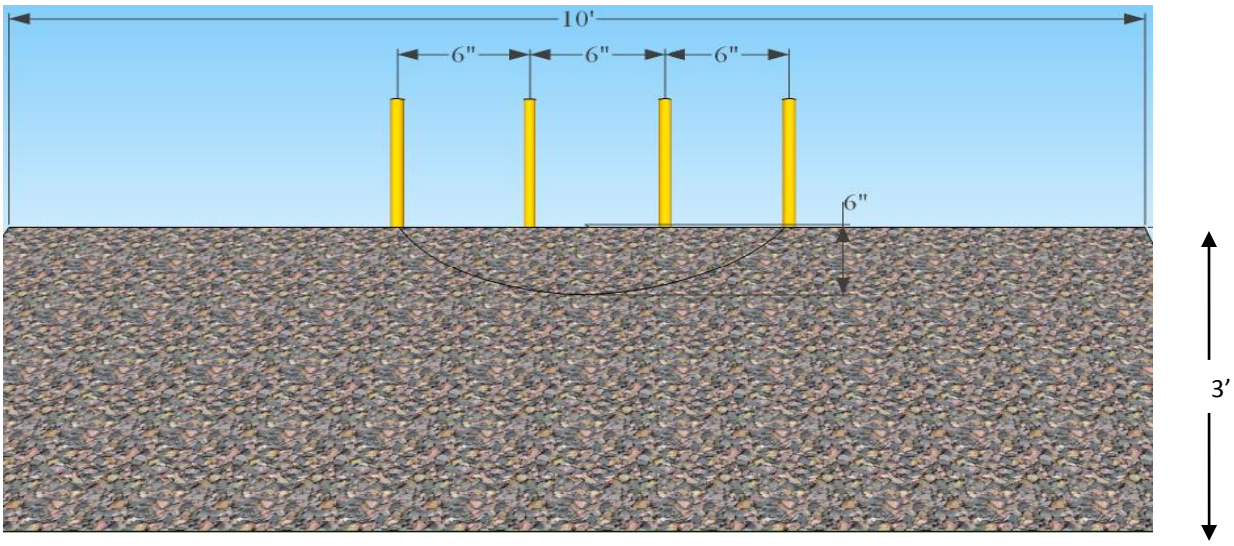

Figure 5.6.5 Schematic diagram of resistivity large scale test at depth of 6 inches

Test Date 4/19/2013

Test Conditions

Soil Condition: [x] Moist [ ] Dry Temperature 61 °F

Soil Type: [x] Crushed Ballast & Ballast [ ] Clay & Ballast [ ] Coal Dust & Ballast

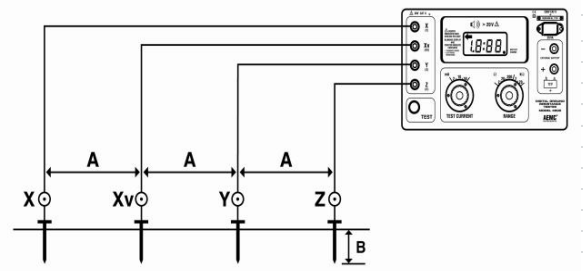

Electrode Spacing (**A**) 0.5 ft

Test 1
83.3

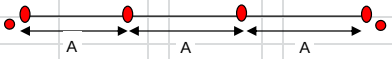

Crushed Ballast	
Percentage Fouling	**Resistivity (ohms-cm) Range**
20%	42,000 - 80,000
30%	32,000 - 42,000
40%	12,000 - 20,000
50%	8,000 - 12,000

rho calculation **ρ = 2*PI*AR**

	Test Reading	Soil Resistivity
Test	**R**	**ρ**
1	83.3	7975.98

Effective soil resistivity: **7975.98** **Ω - cm**

Figure 5.6.6 Detailed data sheet for resistivity large scale test at depth of 6 inches (AEMC 2012)

Table 5.6.1 Summary of fouled resisitivity with depth

		Test Reading	Soil Resistivity
Depth (in)	**Test**	**R (Ω)**	**ρ (Ω-cm)**
18	1	50.7	14564.4
12	2	69.1	13233.4
6	3	83.3	7976.5

. Figures 5.6.1, 5.6.3 and 5.6.5 show schematic diagrams of the setup at different depths with dimensions. Figures 5.6.2, 5.6.4 and 5.6.6 show a detailed data sheet of test setup and conditions which was obtained from AEMC (manufacturer of the soil resistivity meter). The data sheet was adjusted to be compatible with railroad ballast resistivity testing, and a table of resistivity ranges was added to be able to determine the fouling ratio from the resistivity of the sample tested. The results show that as the depth increased, resistivity increased. The higher resistivites at greater depths were interpreted to be representative of drier material, while the near suface material had a lower resistivity due to the addition of water to the surface.

Chapter 6 Conclusions

This study represents the first step in attempting to evaluate the fouling ratio in a ballast layer using resistivity and permeability methods. Relationships between permeability, resistivity, and fouling were identified during this study, which suggests the goal of using measurements of either resistivity or permeability as a proxy for fouling may be successful.

A series of laboratory tests were conducted at the University of Kansas on fouled ballast obtained from Gardner, Kansas, and coal dust from Wyoming, BNSF line milepost 61. The tests measured the permeability and resistivity of ballast fouled with three different fouling materials. Each fouling material was mixed with clean aggregates to obtain 20%, 30%, 40% and 50% fouling by dry weight. Results from using crushed ballast fines, clay and coal dust as fouling material showed similar patterns in permeability and resistivity. Hydraulic conductivity of ballast decreased as the fouling ratio increased. Resistivity decreased in a similar manner as the fouling ratio increased. Fouling index was observed to be a better proxy for hydraulic conductivity than fouling ratio, because fouling index better accounted for the type of fouling material.

Moreover, strength properties were also examined for the same samples prepared for permeability and resistivity tests. Strength properties were determined by running large direct shear box and modified direct shear box tests. Results of direct shear and modified direct shear tests show that as fouling ratio increased, strength of ballast decreased. However, the modified direct shear box presented a clear pattern of decreasing strength as the fouling ratio increased. Also, the modified direct shear box experienced less top plate tilting which indicates more accurate results were obtained from the modified setup. Moreover, the modified direct shear results show that friction angles were lower for the same samples tested in the large direct shear

box, however, higher cohesion values were observed in modified direct shear tests which could be due to more friction between ballast particles and the walls of the box. Both the large direct shear and modified direct shear tests experienced ballast crushing during the test, however, the modified direct shear box allowed more particle movement than the large direct shear box and the results were less variable. Overall, ballast fouled with clay and coal showed a significant decrease in strength in both the large direct shear box and modified direct shear tests. The results compare well with the measured hydraulic conductivities of fouled ballast with clay and coal dust.

A large scale resistivity test on heavily fouled ballast was performed on a sample prepared outdoors with a near-surface wet condition. The resistivity of the sample was measured using the Wenner's four point method at three different depths. The results showed that resistivity changed with depth since more water is retained towards the surface, therefore, higher resistivity values were measured as depth increased.

Recommendations

The resistivity and permeability values from the fabricated box showed a good pattern on how the percentage of fouling affects drainage and resistivity values and how each fouling agent behaved differently due to its properties. However, I believe further studies must be done on this method to be able to investigate other factors such as moisture contents at different depths since it could change resistivity values. Also, it would be more accurate to test the resistivity of each sample at different depths and take an average value. Some tests were terminated after 18 hours, giving results that could be improved if the test is terminated when it reaches certain moisture content and that could show a better comparison between permeability and resistivity curves.

For the strength tests, I suggest constructing a new box with larger dimensions to be able to test the strength of clean and fouled ballast and eliminating the limitations that were experienced in the large direct shear box and modified direct shear box. Also, the inside walls of the box should be coated with a smooth surface to minimize the friction between ballast particles and walls of box. The box should be water tight to be able to test samples under submerged conditions.

Moreover, field testing will be beneficial to be able to apply methods presented in this study from this study and verify results obtained from this paper. I suggest Wenner's 4 point method to measure resistivity in the field and excavate several sections from the field and bring samples to the lab to evaluate the level of fouling. This will improve the test procedure and increase confidence in using the suggested method to be able to evaluate the level of fouling by using an effective non-destructive testing method.

References

AEMC Instruments (2012). 15 Faraday Drive. Dover, NH. http://www.aemc.com/products/html/minfindex.asp?id=50306&dbname=products

Anbazhaga, P., B. Inraratna, C. Rujikiatkamjorn, and L. Su. 2010. "Using a seismic survey to measure the shear modulus of clean and fouled ballast." *Geomechanics and Geoengineering: An International Journal*, 5, no. 2: 117-126.

Chiang, C. C. 1989. "Effects of water and fines on ballast performance in box tests*." Master of Science Degree Project Report No. AAR89-366P*. University of Massachusetts, Amherst, MA.

Ebrahimi, A., D. Fratta, and J. Tinjum. 2008. "Detection of fouling in ballast by electromagnetic survey." *Research in Nondestructive Evaluation*,19, no. 4: 219-237.

Feldman, F. and D. Nissen. 2002. "Alternative testing method for the measurement of ballast fouling: Percentage voids contamination." *Proceedings of the Conference on Railway Engineering, Wollongong, Australia*. Railway Technical Society of Australia, Canberra, Australia, 101-109.

Han, X., and E. T. Selig. 1997. "Effects of fouling on ballast settlement." *Proceedings of the 6th International Heavy Haul Railway Conference*, Cape Town, South Africa.

Huang, H., E. Tutumluer, and W. Dombrow. 2009. "Laboratory characterization of fouled railroad ballast behavior." *Transportation Research Record*, 2117: 93-101.

Indraratna, B., H. Khabbaz, W. Salim, and D. Christie. 2006. "Geotechnical properties of ballast and the role of geosynthetics in rail track stabilisation. *Ground Improvement*, 10, no. 3: 91-101.

Indrartna, B., W. Salim, and C. Rujikiatkamjorn. 2011. *Advanced rail geotechnology –Ballasted track*. University of Wollongong, Australia: CRC Press.

Jowkar, M., Parsons, R. , and Han, J. (2013). "*Performance of geogrid reinforced ballast under dynamic loading."* (CD-ROM), Transportation Research Board, Washington, DC.

Leng. Z, and I. Al-Qadi. 2010. "Railroad ballast evaluation using ground penetrating radar: Laboratory investigation and field evaluation." *Transportation Research Record: Journal of the Transportation Research Board*, 2159: 110-117.

Raymond, G. P. 1978. "Design for railroad ballast and subgrade support." *Journal of the Geotechnical Engineering Division*,105, no. 1: 45-60.

Roberts, R., and J. Rudy. 2006. “Railroad ballast fouling detection using ground penetrating radar. A new approach based on scattering from voids.” *ECNDT 2006 – Th.4.5.1*. http://www.ndt.net/article/ecndt2006/doc/Th.4.5.1.pdf

Samouelian, A., I. Cousin, A. Tabbagh, and Richard G. Bruand. 2005. “Electrical resistivity survey in soil science.” *Soil & Tillage Research*, 83: 173-193.

Selig, E.T, and J. Waters. 1994. *Track geotechnology and substructure management*. London: Thomas Telford.

Tagg, G. F. 1964. *Earth resistances*. Great Britain: Pitman Publishing Corporation.

Wallace, A. J. 2003. “Permeability of fouled rail ballast.” UG Thesis, School of Civil, Mining and Environmental Engineering, University of Wollongong, New South Wales, Australia.